2021

PREFORMULATION STUDIES FOR THE PREPARATION OF AMORPHOUS SOLID DISPERSIONS

Hemanth Kumar Mamidi

PREFORMULATION STUDIES FOR THE PREPARATION OF AMORPHOUS SOLID DISPERSIONS

A dissertation submitted in partial fulfillment of the

requirements for the degree of

DOCTOR OF PHILOSOPHY

to the faculty of the

DEPARTMENT OF PHARMACEUTICAL SCIENCES

of

COLLEGE OF PHARMACY AND HEALTH SCIENCES

at

ST. JOHN'S UNIVERSITY

New York

by

HEMANTH K. MAMIDI

Date Submitted: _____ Date Approved: _____

_____ _____

Hemanth K. Mamidi Bhagwan D. Rohera, Ph.D.

ABSTRACT

PREFORMULATION STUDIES FOR THE PREPARATION OF AMORPHOUS SOLID DISPERSIONS

Hemanth K. Mamidi

The major challenges in the formulation of amorphous solid dispersions (ASDs) using hot-melt extrusion (HME) are the selection of an ideal polymeric carrier, optimization of HME processing conditions, and screening of the physical stability of the ASDs. Addressing these challenges using traditional approaches require extensive experimentation and large amounts of active pharmaceutical ingredients (API) which may not be feasible during the initial stages of product development. Therefore, there is a need to develop material-sparing techniques for the successful formulation of ASDs. The objective of the present study was to develop material-sparing techniques that can be used as pre-formulation tool during the formulation of ASDs. For this purpose, mefenamic acid (MFA) was used as a model drug and four chemically distinct polymers with close values of the solubility parameters, *viz.* Kollidon® VA64, Soluplus®, Pluronic® F68, and Eudragit® EPO, were used as polymeric carriers. The selection of an ideal polymer was carried out based on the solubility parameter approach, melting point depression method, thermodynamic phase diagrams, and Gibbs free energy plots. Then the HME processing conditions were determined based on a material-sparing technique using differential scanning calorimeter (DSC). The physical stability of the ASDs was estimated using the modified Avarami equation. Based on the results of the melting point depression, thermodynamic phase diagrams and Gibbs free energy plots, Eudragit® EPO

was found to be an ideal polymer for the preparation of amorphous solid dispersion formulation of mefenamic acid. The design space for HME determined using DSC method showed that when 20% drug loaded MFA-EPO blends was heated at a rate of 5.5 °C/min to a temperature of 146 °C, the resulting ASD contained a residual crystallinity of 13.6% and drug degradation of 3.8%. The physical stability of the MFA-EPO ASDs determined using a modified Avarami equation showed that the rate of recrystallization changed significantly with the change in process temperature as compared to the change in the relative humidity. The study results show that the time frame and experiments required in the formulation of ASDs can be significantly reduced by using the material-sparing techniques developed based on the theoretical and experimental approaches.

ACKNOWLEDGEMENTS

I wish to express my sincere gratitude to my supervisor Prof. Dr. Bhagwan D. Rohera, for providing me this precious study opportunity as a MS student in his laboratory. His unconditional support and guidance during my thesis research was invaluable. It was he who taught me that research is the ability to think, plan, design, and troubleshoot, rather than just learn the laboratory techniques. My research approach, problem-solving skills, systematic and meticulous style of working has grown under him. I could not have imagined having a better supervisor for my MS and PhD research study.

Besides my supervisor, I would like to thank the rest of my thesis committee: Dr. Vikas Dukhande, Dr. Sebesan Yoganathan, Dr. Ketan Patel and Dr. Nitesh Kunda for providing their advice, knowledge, insightful discussions and suggestions for my thesis. I would also like to thank other faculty members of the department who helped me develop other skills through course work and assignments.

I thank the Department of Pharmaceutical Sciences at College of Pharmacy and Allied Health Sciences, St. John's University for providing me the financial aid throughout my MS and PhD study and also for providing the facilities to carry out this research work.

I would also like to thank my fellow lab mates and friends at St. John's University for their perpetual help and support. I also wish to thank everyone who helped me during my thesis research.

I would like to express utmost gratitude to my parents (Manmadha Rao and Dhana Laxmi) and brother (Ramesh Naidu) for their blessings, love and support. It is those endless moments that they sacrificed to harbor and culminate the principles that make me the person I am. I faithfully owe my gratitude to them for their invaluable place in my life.

Last but not least, I would like to thank ***Lord Shiva*** for giving me this wonderful life and the sole reason for my very existence.

TABLE OF CONTENTS

LIST OF TABLES

LIST OF FIGURES

LIST OF ABBREVIATIONS

i. ASD: Amorphous Solid Dispersion

ii. DSC: Differential Scanning Calorimeter

iii. CED: Cohesive Energy Density

iv. EPO: Eudragit® EPO

v. SLP: Soluplus®

vi. VA64: Kollidon® VA64

vii. F68: Pluronic® F68

viii. MPa: Mega pascal

ix. HME: Hot Melt Extrusion

x. L/D: Length to Diameter Ratio

xi. VCM: Vaccum Compression Molding

xii. MTM: Minimum Temperature of Miscibility

xiii. pXRD: Powder X-ray Diffraction

xiv. ESI-MS: Electron Spin Resonance Mass Spectroscopy

xv. QbD: Quality by Design

xvi. CQA: Critical Quality Attribute

xvii. TPP: Target Product Profile

xviii. MLRA: Multiple Linear Regression Analysis

xix. CMA: Critical Material Attributes

LIST OF SYMBOLS

i. ϕ_{drug}: Volume fraction of drug

ii. $\phi_{polymer}$: Volume fraction of polymer

iii. χ: Interaction parameter

iv. T_g: Glass transition temperature

v. T_m: Melting temperature

vi. T_d: Degradation temperature

vii. T_c: Critical temperature

viii. δ: Hildebrand solubility parameter

ix. δ_t: Hansen solubility parameter

x. δ_v: Combined solubility parameter

xi. δ_d: Dispersion forces

xii. δ_p: Polar forces

xiii. δ_h: Hydrogen bonding forces

xiv. M_w: Molecular weight

xv. ρ: True density

xvi. γ_{drug}: Activity coefficient of drug

xvii. ΔE_A: Activation energy

xviii. V: Molecular volume

xix. ΔH_f: Heat of fusion

xx. A: Entropic constant to Gibbs free energy of mixing

xxi. B: Enthalpic constant to Gibbs free energy of mixing

xxii. R: Universal gas constant

xxiii. m: Ratio of molecular volume of polymer to that of drug

xxiv. ΔG_{mix}: Gibbs free energy of mixing

xxv. k: Recrystallization rate constant

xxvi. $\alpha(t)$: Relative crystallinity

xxvii. x_{drug}: Mole fraction of drug soluble in polymer

xxviii. n: Dimensionality of recrystallization

1. Introduction

Poor aqueous solubility of drugs is one of the major challenges in the pharmaceutical industry. Enhancing the oral bioavailability of poorly aqueous soluble drugs by improving their solubility remains one of most challenging aspects of drug development process. Various traditional and newer approaches have been developed to improve the solubility of poory water soluble drugs. The traditional methods include solid dispersion, complexation and pH adjustment while newer methods include liquisolid technology, hydrotropy, lipid-based system, etc. The choice of technique is selected based on the properties of drug, nature of excipients and the intended dosage form. Out of all the techniques to improve solubility, solid dispersion formulation remains one of the widely used technique due to its simplicity and ease of commercialization.

1.1. Solid Dispersions

Sekiguchi and Obi in 1961 first proposed the concept of solid dispersions (1). They described solid dispersions as the biphasic systems of drug particles dispersed in a polymeric carrier. Over the decades, various other definitions of solid dispersions were proposed. Most recently, Janssens *et al*. defined solid dispersions as, “Formulations of poorly-soluble compounds which might lead to particle size reduction, improved wetting, reduced agglomeration, changes in the physical state of the drug and possibly dispersion on a molecular level, according to the physical state of the solid dispersions that depends on the physicochemical properties of carrier and the drug, the drug-carrier interaction and the method of preparation” (2). Solid dispersions are divided into various types on the

basis of the crystalline nature of the drug molecules and their distribution in the carrier matrix as shown in Table 1. Type I solid dispersions are eutectic mixtures in a specific ratio and have a single melting point which is lower than the melting point of the individual components. Type II solid dispersions are amorphous precipitates in crystalline matrix where the drug is present in amorphous form dispersed in crystalline polymeric matrix. Type III solid solutions are similar to Type II but the drug is molecularly dispersed in the polymeric carrier. It can be either monophasic or biphasic. In type IV, V and VI solid dispersions, the drug is either in crystalline, amorphous or molecularly dispersed form, respectively in an amorphous polymeric matrix. To obtain a glassy solution, the drug should be completely miscible in the polymeric matrix. Type IV, V and VI solid dispersions are prominent now a days and are prepared using spray-drying or hot-melt extrusion technique. Type IV is achieved if the drug is dispersed as crystals in the amorphous polymer phase. This is a two-phase system in which the melting endotherm of the drug and the glass transition temperature of the polymer are obtained when the drug-polymer blend is subjected to DSC analysis. In type V solid dispersions, the drug is transformed into amorphous state but is not molecularly dispersed in the polymer matrix. In case of type VI, the solid dispersion of the drug is molecularly dispersed in the polymer phase. This results in a single-phase system showing only one glass transition temperature.

To better understand the difference in the thermodynamic properties of a crystalline and an amorphous form, consider a crystalline drug that is heated to ceratin temperature where it melts completely. Upon slowly cooling, the drug molecules form an orderly system which is thermodynamically stable point on crystal lattice (3). However, if

the cooling rate is high, then the drug molecules may attain a supercooled liquid state without undergoing crystallization. On further cooling, a glass transition temperature (T_g) is reached below which it converts into a frozen glassy state. A material in a glassy state behaves like a brittle solid but without crystalline structure (4). The amorphous state of a drug has a higher enthalpy, entropy and Gibbs free energy as compared with the crystalline form. This is the reason why amorphous drug has higher apparent solubility. When an amorphous drug is added to the dissolution media, the drug solubilizes rapidly forming a supersaturated solution followed by a decrease in solubility due to devitrification. This phenomenon is known as “spring and parachute effect” and creates considerable challenges during dissolution. The choice of the polymeric carrier plays a major role in maintaining the supersaturated solution and preventing the spring and parachute effect during dissolution. Therefore, the selection of a polymeric carrier plays a major role in the formulation of amorphous solid dispersions.

Table 1: Various types of solid dispersions based on the physicochemical properties of the drug and the carrier

Type of solid dispersion	**Matrix**	**Drug**	**Phases**
I. Eutectic	C	C	2
II. Amorphous precipitates in crystalline matrix	C	A	2
III. Solid solutions	C	M	1 or 2
IV. Glassy suspensions	A	C	2
V. Glassy suspensions	A	A	2
VI. Glassy solutions	A	M	1

**C – Crystalline; A – Amorphous; M – Molecularly dispersed

1.2. Various Polymeric Carriers for ASDs

Polymers are repetitive structural units of monomers which are linked with each other. They can be classified on the basis of their origin as natural, semisynthetic or synthetic polymers (5). Polymers are classified as homopolymers (one type of monomer) or a copolymer (two monomers). Polymers can be amorphous, semicrystalline or crystalline. Since polymers have a complex 3-dimensional structure, incorporation of amorphous drugs into the polymeric matrix hinders the molecular mobility of amorphous drug, thereby preventing recrystallization over the shelf life of the product (6). The physical and chemical stability of ASDs depend on various factors like molecular mobility, thermodynamic properties, environmental stress, and method of preparation. The polymeric carriers will effects these factors and stabilize the ASDs by four main mechanisms:

- Crystallization inhibition
- Antiplastisization
- Intermolecular interactions
- Reduction of molecular mobility

1.2.1. Crystallization Inhibition

The crystallization of an amorphous drug is a 2-step process that occur simultaneously. The first step is nucleation and occurs at a lower temperature, and the second step is the crystal growth that requires higher temperatures (2). Thus, nucleation may not start until a certain degree of supersaturation is reached to overcome the energy barrier. The supersaturated concentrations where no nucleation occurs is known as the

metastable zone. An ideal polymeric excipient increases the degree of supersaturation, thus expands the metastable region. Polymeric excipients that increase aqueous solubility can retard the nucleation rate by decreasing the free drug concentration available for nuclei/ seed formation (7). Since polymeric carriers have sufficiently high configurational entropy due to their large, complex, and flexible structures, they significantly reduce the chance of drug recrystallization as it lowers the total Gibbs free energy of the amorphous drug.

1.2.2. Antiplasticization

Antiplasticization is described as a phenomenon which leads to an increase in glass transition temperature, T_g of the material. This results in an increase in the free energy required by the amorphous drug to convert into the crystalline form (8). When two materials having different T_g are mixed together, the final T_g of the mixture will be somewhere between the T_g of both the materials. Mixing a low T_g amorphous drug with a high T_g polymer at the molecular level leads to the formation of ASDs with a T_g intermediate of these two components. In other words, the polymer undergoes plasticization whereas the T_g of the drug increases, and it undergoes antiplasticization. Sathigari *et al.* have studied the stabilization of amorphous efavirenz in Plasdone S-630 carrier (9). They have reported that the stability of the amorphous efavirenz in the solid dispersion is due to the antiplasticizing effect of the polymer which increased the viscosity of the system and decreased the diffusion of drug molecules.

1.2.3. Intermolecular Interaction

The drug molecules may interact with polymers by several weak forces such as hydrogen bonding, van der Waals forces, electrostatic, ionic, or hydrophobic interactions (10). These intermolecular bonds restrict the molecular mobility of the drug molecules in the polymer matrix and increases the physical stability of the drug-polymer system (11). Meng *et al*. highlighted the importance of drug-polymer interactions in the stability of amorphous curcumin as a model drug (12). They examined the ability of different polymers, such as PVP K90, Eudragit EPO®, HPMC, and PEG 8000, to interact with the model drug through stable bond formation. It was concluded that a certain degree of interaction between a drug and a polymer is important for successful formulation of ASDs. Maniruzzaman *et al.* have reported that the drug polymer ratio and miscibility defines the magnitude of the intermolecular interactions (13).

1.2.4. Reduction of Molecular Mobility

The molecular mobility of amorphous materials determines their physical stability. Polymeric carriers have the capacity to restrict the molecular mobility of the amorphous API which can be determined using certain analytical techniques like differential scanning calorimeter (DSC), solid-state nuclear magnetic resonance (ssNMR), and dielectric spectroscopy. Knapik *et al.* have shown that the physical stability and water solubility of the amorphous ezetimibe was improved over 6 times when mixed within a ASD using Soluplus® as carrier (14). DSC and dielectric spectroscopy analysis of amorphous ezetimibe have led to the conclusion that the high molecular mobility, reflected in structural relaxation, is mainly responsible for its high

crystallization tendency. This indicates that formation of ASDs in the Soluplus® matrix acts as physical barrier to the molecular motions of glass ezetimibe leading to improved stability. In another study, Kothari *et al.* reported that the relaxation time of the drug increases with an increase in polymer concentration (15).

1.3. Preparation of ASDs using Hot Melt Extruion

The pharmaceutical industry is shifting from the traditional spray drying process towards hot-melt extrusion for the preparation of solid dispersions. This is to reduce the use of solvents and also to achieve the goal of continuous manufacturing. Hot-melt extrusion (HME) has been revealed as a viable technology for variety of applications in the pharmaceutical industry (16). The enhancement of solubility and bioavailability through the manufacturing of ASDs is the primary use of HME, as indicated by the multiple papers and patents. Current, interest in the formulation of ASDs using HME is growing rapidly with a number of papers published in the scientific literature during the past two decade (9, 17-19). Although there is a huge potential for formulating poorly soluble drugs into ASDs, only a few commercial formulatiosn are available in the market (Table 2).

Table 2: List of marketed formulations of solid dispersions manufactured using HME

Product	**API**	**Manufacturer**	**Indication**	**Polymer**
Norvir®	Ritonavir	Abbott	HIV	PEG-glyceride
Rezulin®	Troglitazone	Parke-Davis	Diabetes	PVP
Noxafil®	Posaconazole	Merck	Antifungal	HPMCAS
Onmel®	Itraconazole	Merz	Onychomycosis	HPMC
Kaletra®	Lopinavir/ Ritonavir	Abbott Labs.	HIV	Copovidone
Belsomra®	Suvorexant	Merck	Insomnia	Copovidone
Technivie®/ Viekirax®	Ombitasvir,paritaprevirand ritonavir	AbbVie	Hepatitis C virus	Copovidone/vitamin E-polyethylene glycolsuccinate
Viekira Pak®	Dasabuvir, Ombitasvir, Paritaprevir, Ritonavir	AbbVie	Hepatitis C virus	Copovidone
Venclexta®	Venetoclax	AbbVie	Chronic lymphocyticleukemia	Copovidone/polysorbate80
Mavyret®	Glecaprevir/pibrentasvir	AbbVie	Hepatitis C virus	Copovidone/vitamin Epolyethyleneglycol succinate

This can be attributed to the poor understanding of the ASD formulations at the molecular level and also the trial and error approach employed for HME (Fig. 1). However, with an increase in the number of some high quality research in the field of ASDs, more and more scientific data is available to understand the drug-polymer interactions and the effect of the HME process on the performance of ASDs. This is evident as more and more HME-based drug products appear in the pipeline of many pharmaceutical companies. Lately, there have been new product submissions to the FDA and to the European Medicines Agency (EMA) (19). In HME-based drug products, a robust preformulation assessment is the key to a successful development. A step-by-step approach, starting with the thermodynamic evaluation of several systems, followed by a polymer screening test is useful to rapidly identify optimized HME formulations. The three main aspects of developing ASDs are:

- Rationale selection of polymer
- Process design and optimization
- Stability testing

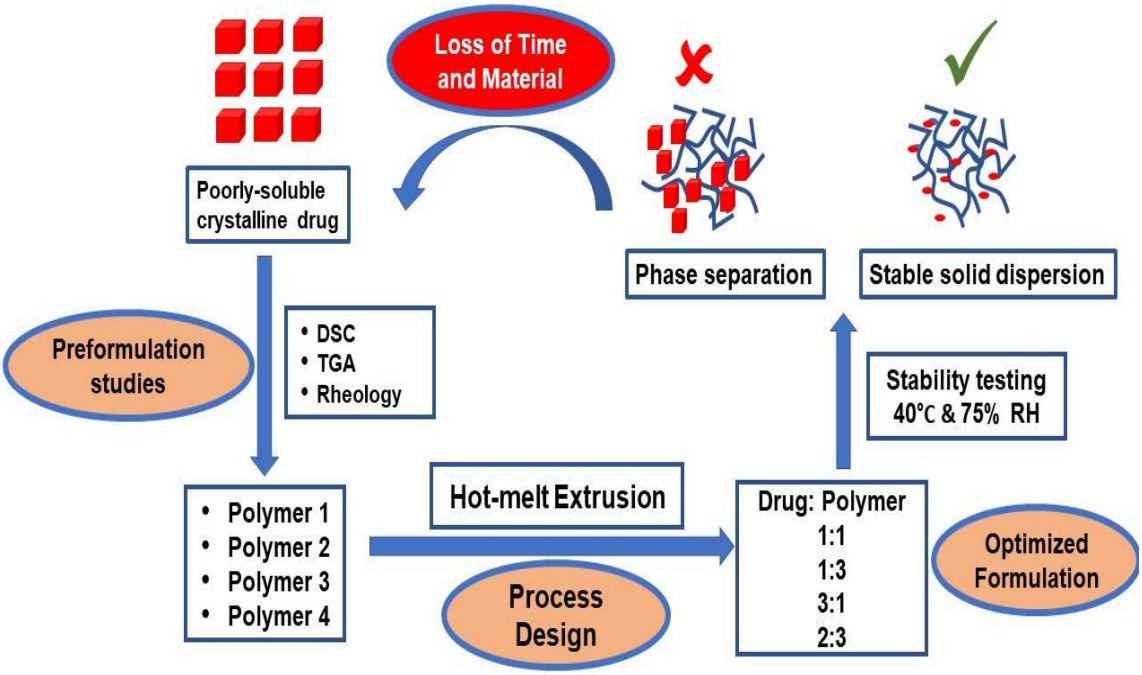

Figure 1: Current approach in the formulation of amorphous solid dispersions and its drawback

1.4. Rationale Selection of Polymeric carrier

The rationale for the selection of polymer has been largely its glass transition temperature (T_g), melt viscosity and dissolution rate. Polymers with high glass transition temperature T_g are generally used to prepare ASDs owing to their antiplasticizing effect that reduces the molecular mobility of amorphous drug. However, when there is no T_g differences between amorphous drug and the solid dispersion, then the drug-polymer interactions will determine the shelf life of ASDs (20). Increasing the molecular weight raises the T_g of polymers which favors antiplasticization of amorphous drugs. Whereas, at high molecular weight, the rise in T_g becomes insignificant as other factors such as viscosity come into play during the dissolution process. Viscosity of polymers increases with molecular weight which has significant effect on the dissolution properties. Once the polymers are selected, they are further screened based on the miscibility with the drug which is determined by film-casting method. It involves mixing the drug and polymer in a common solvent and then applying the solution as a film. Once the solvent is evaporated, the film is then analyzed under hot-stage microscopy to observe the presence of phase separation. However, this approach is applicable only in processes such as spray drying where a solvent is used. In the case of hot melt extrusion, the drug and polymer are directly in physical contact with each other without the presence of a solvent. Their molecular mobility is less and depends on the processing temperature. Therefore, results obtained from film-casting method are often overestimated compared to the actual results obtained from hot-melt extrusion. This shows that there is a need to develop a robust methodology with the use of minimum material to successfully formulate solid dispersions. Different methods such as solubility parameter approach, Flory-Huggins

theory and melting enthalpy approach as preformulation tools for the rational selection of polymers have been reported in the literature.

1.4.1. Solubility Parameter Approach

Solubility parameters are the numerical values that represent the dispersive, polar and hydrogen bonding forces in a molecule. They are calculated based on the functional groups present in the chemical structure of a molecule and they contribution to various intermolecular forces. These intermolecular forces were calculated using various group contribution methods, *viz*. Hoftyzer and Van Krevelen, Hoy, Small, Dunkel, Hayes, and Di Benedetto (21). Generally, drug polymer systems with similar solubility parameter values are predicted to be more miscible. Drug-polymer mixtures with the solubility parameter difference, $\Delta\delta < 7.0$ $MPa^{1/2}$ are found to be miscible whereas systems with $\Delta\delta > 10.0$ $MPa^{1/2}$ are likely to be immiscible (22). Estimation of drug-polymer miscibility based on the difference in the solubility parameter values is still one of the most applied approaches in the academia and pharmaceutical industry owing to its relative simplicity. Just *et al*. discussed about various attempts to improve group contribution parameters and to develop new values based on solids (23). Wlodarski *et al*. reported the use of the solubility parameters for the prediction of miscibility between itraconazole and two polymers, polyvinyl alcohol and copovidone (24). Pawar and co-workers used Hansen solubility parameters to predict the miscibility of efavirenz in polymers for the preparation of ASDs using HME (25). Although the solubility parameter can be useful for the fast screening of polymers, it often leads to the exclusion of good polymeric candidates. Therefore, additional experimental work is required to confirm the

interpretations obtained using solubility parameter approach. Recently, Turpin *et al*. experimentally determined the miscibility of various model drugs and the results were compared with that of the results predicted using Hansen solubility parameters approach. (26). The study showed that the predicted results from the solubility parameters did not match the experimental data. The authors attributed this to the negligence of not considering the intermolecular interactions in the solubility parameter approach. To address these drawbacks, more complex methods were introduced to predict the drug-polymer miscibility. One of these methods is the calculation of the Flory–Huggins interaction parameter ($\chi_{d\text{-}p}$), usually through the application of the melting point depression (MPD) theory.

1.4.2. Melting Point Depression Theory

The most widely used method for the estimation of drug solubility in a polymer is by using the melting enthalpy of the crystalline drug in a drug-polymer system measured by DSC. This method is based on a simple principle that the fraction of drug dissolved in the polymer does not contribute to the melting endotherm. Therefore, by measuring the melting enthalpy of a series of drug concentrations in drug-polymer mixtures and extrapolating the plot to zero enthalpy, the solubility of a given drug in selected polymers can be estimated from the x-intercept of the plotted line.

1.4.3. Flory-Huggins Theory

Flory-Huggins (F-H) theory is a well-known lattice-based theory which describes polymer-solvent miscibility on the basis of the Gibbs free energy change associated with the mixing of a polymer in a solvent (27). Recently, this theory was applied for assessing drug-polymer miscibility using the melting point depression method to obtain F-H interaction parameter, $\chi_{d\text{-}p}$ (22). A negative value of $\chi_{d\text{-}p}$ indicates stronger drug-polymer interaction than individual drug-drug or polymer-polymer interaction which predicts drug-polymer miscibility, whereas a positive value indicates that homonuclear interactions are preferred over heteronuclear interactions which may lead to phase separation (28). This method is also used by the pharmaceutical industry and is probably the most popular approach, with research work published by many reputed pharmaceutical companies. Earlier, the assessment of acetaminophen and naproxen solubility in polymeric excipients, such as povidone and co-povidone, calculated with three models including F-H equation, was published by Lehmkemper and co-workers (29). The results were in line with the experimental solubility data. However, the F-H theory underestimated the effect of acetaminophen miscibility on stability.

1.4.4. Thermodynamic Phase Diagrams

Another common tool within the industry is the construction of phase diagrams which are usually based on the F-H theory. Phase diagrams depict the relationship between the free energy and drug loading. The use of phase diagrams have been described extensively in the literature (27,28,30,31). Still, phase diagrams are

temperature dependent, and an immiscible system can, therefore, become miscible if the temperature increases.

1.5. Hot Melt Extrusion Process Optimization

Once a suitable polymer is selected for the formulaton of ASDs, the next challenge is to determine the optimum formulation and process parameters. When choosing a commercial ASDs manufacturing process, there are two leading choices: spray drying or hot melt extrusion (HME). Although solvent-based processes are more common because they are applicable to a wide range of compounds, HME offers several advantages for thermally stable systems. It is solvent-free, continuous, high-throughput, easily scalable and inexpensive. Avoidance of thermal degradation and an absence of residual crystallinity are two critical quality attributes of hot melt extruded ASDs (36, 37). To avoid thermal degradation of drug and/or polymer, lower processing temperatures are desirable, although accompanied by a risk of residual crystalline content if the crystals do not fully melt or dissolve during the process. Various studies have reported the HME processing at temperatures below the drug's melting point utilizing melting point depression phenomenon (38, 39). Studies providing strategies to mitigate the corresponding risk of crystallinity have thus far been limited to equipment setup like screw configuration and drug particle size reduction (18). Physical instability and dissolution performance are affected by many parameters, such as drug loading, polymer type, miscibility, T_g and the inherent crystallization tendency of the drug and may be accelerated by the presence of seed crystals (36–39). Therefore it is considered critical to design the ASD manufacturing process to generate a fully amorphous system. In light of

the FDA encouraging Quality by Design (QbD) practice for all the formulations, applying it in the case of ASDs seems challenging (40). This is due to various factors that effect the characteristics of ASDs. However, once the maximum drug loading was determined using preformulation studies, the process parameters can then be optimized using a suitable experimental design. Since fully amorphous systems are considered stable, it is significant to determine the maximum solubility of the drug in the polymeric carrier. The thermodynamic phase diagram has been conceptually proposed in the literature as a methodology for identifying the maximum solubility of the drug in the polymeric carrier as well as the processing temperature (36, 39). A typical thermodynamic phase diagram shown in Figure 2 consists of a solubility curve, a miscibility curve and a glass trasition curve.

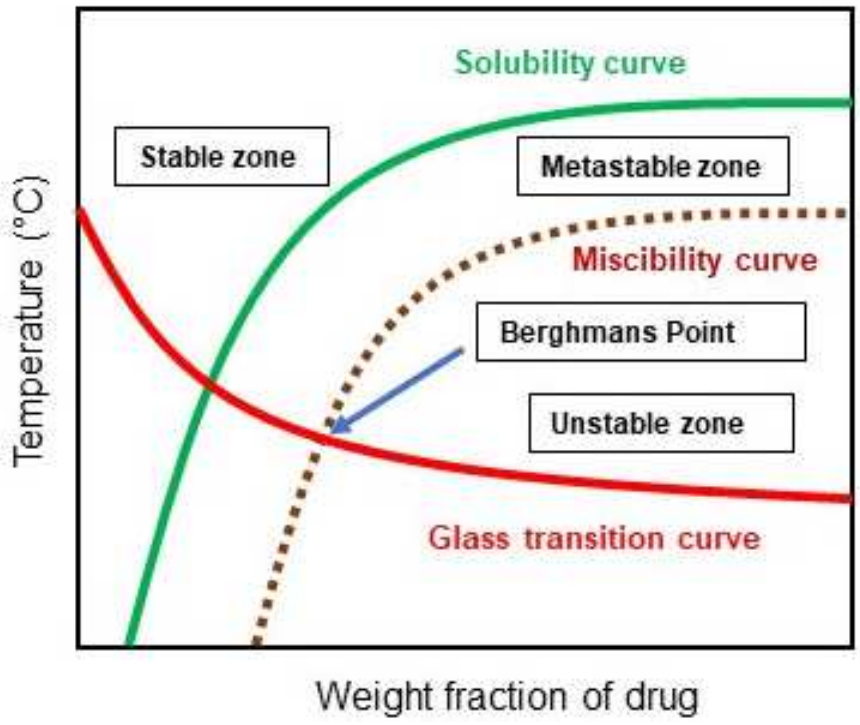

Figure 2: Typical thermodynamic phase diagram consisting of a solubility curve, a miscibility curve and a glass transition curve

Most of the research in the field of HME is limited to a simple experimental design which fails to determine the interaction effect between the CMAs and the CQAs on the CMAs. Since HME is a complex process with various interaction effects, it is ideal to study the process using a design that better helps understand the effect of various CQAs and CPPs on the CMAs. However, it is challenging to perform enough experimental runs using HME, especially during initial phase of development due to limited availability of the drug. Therefore, material sparing techniques are necessary to speed up the formulation development process using HME. One such technique is DSC, a commonly used thermal analysis instrument. It is similar to HME in the case of heat conduction except the absence of mechanical stress. However, when the particle size of drug and polymer blend is reduced significantly, then the thermal events in the DSC and HME are comparable. Apart from that, DSC requires small quantity of material and the samples subjected to thermal analysis can be retrived and analyzed. Phase diagrams coupled with DoE could provide useful information regarding formulation and process optimization.

1.6. Physical Stability of ASDs

The amorphous drug–polymer dispersion is commonly characterized in terms of physical properties such as glass transition temperature (T_g), heat capacity, and miscibility (45, 46). Though it is widely regarded that an increase in T_g indicates the improvement of physical stability, there is no direct evidence disclosed to relate T_g to recrystallization activation energy, the critical parameter evaluating stability. T_g is not an intrinsic property and contingent to prior thermal history. Methods involving T_g

measurement therefore are ambiguous. Some studies experimentally proved the surprising occurrence of nucleation below T_g indicating that T_g is not a reliable indicator of physical stability (41, 47). Recrystallization kinetics is a mathematical model which has a potential to estimate the physical stability of ASDs. The model is based on the approximation of the nucleation and crystal growth contributions which are inherently essential to an accurate prediction of the physical stability of ASDs. This approach was first introduced by Avrami and is the commonly used model to estimate the crystallization kinetics for decades (48, 49). However, the reliability and accuracy of this equation is compromised because of its critical oversimplifications, most notably that the nucleation rate is constant throughout the recrystallization process. Other models also have been developed based on solid state reaction kinetics (46–49), however, there has been little progress in their application to stability prediction of pharmaceutical solid dispersion. Most recently, a new kinetics model was developed by Yang *et al*. by correcting the critical oversimplification on nucleation rate in the Avrami equation (50). However, further studies need to be done to validate the applicability of the kinetic model to determine the shelf life of ASDs.

1.7. Need to Restructure the Formulation Approach for ASDs

A systematization of a rational approach to design solid dispersions is crucial for a successful, fast and low-cost development, which avoids promising formulations being prematurely eliminated from experimental studies. The most common approaches for screening excipients for HME formulations are based on solvent evaporation methods, DSC analysis, hot stage microscopy (HSM) and melt-based methods. Solvent-

evaporation methods are probably the most common in the industry setting, because of their simplicity and low cost. Some studies have been published, describing ways of automating and miniaturizing the screening of excipients in a high-throughput manner (51–53). However, DSC studies, HSM or melt-based methods have the advantage of applying heat which can be beneficial when the manufacturing process under study is HME. Auch and co-workers noticed discrepancies between a solvent-based screening method and experimental results for ASDs (54). Based on the literature a structured screening approach for the formulation of ASDs is presented in Figure 3. This methodology reflects the usual techniques, based on physicochemical principles and thermodynamic assessment of the drug and the polymer, with the aim of maximizing success rates and reducing risks. One of the main advantages is including the assessment of physical stability at the early stages during product development. This approach is divided into four stages. During the first stage, an in-depth evaluation of physicochemical properties of the drug and potential polymers is performed. Then, in the second stage, excipients are assessed through solubility parameters, melting point depression and Flory-Huggins interaction parameter. This preliminary evaluation can be complemented with experimental tests, such as DSC, where depression of the melting point evaluated and, eventually, the interaction parameter can be calculated. As an outcome, excipients with a high probability of miscibility and chemical interaction are taken to the third stage where the process optimization is done using the thermodynamic phase diagrams and a material sparing DSC method. The results from the DSC method is validated using samples prepared by vaccum compression molding (VCM) and HME. In the final stage, the kinetic stability of the ASDs is predicted using a kinetic model.

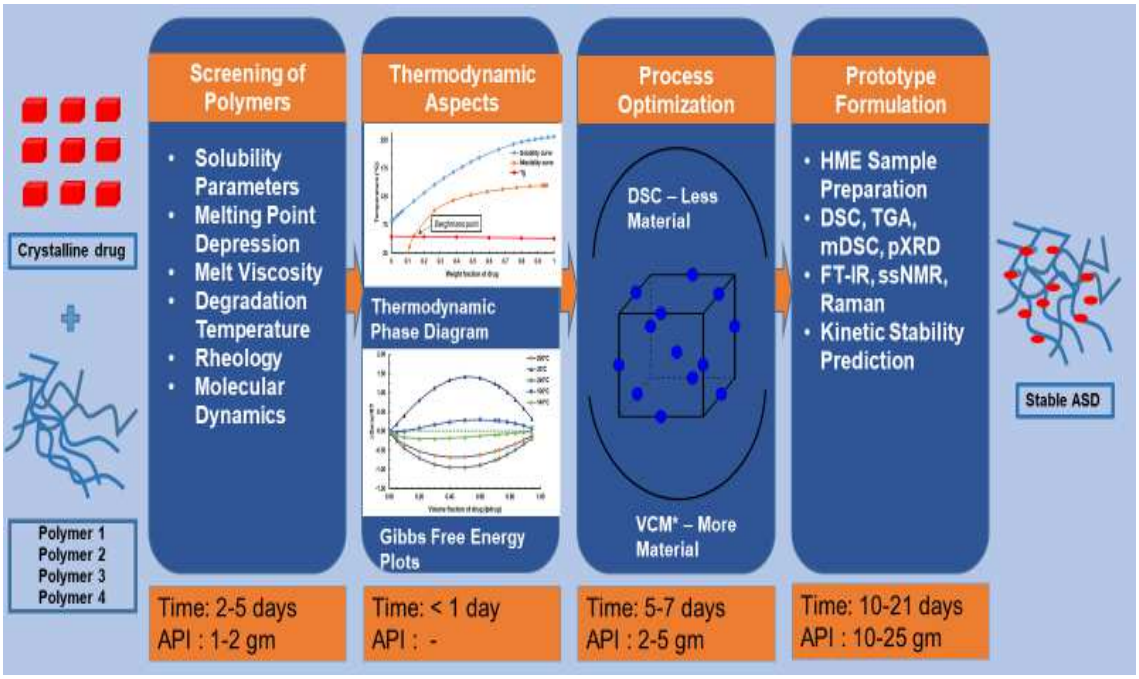

Figure 3: Proposed approach for early formulation development of ASDs by HME

2. Study Objectives

The objective of the present study was to develop various material-sparing pre-formulation tools for rapid formulation development of ASDs. To achieve this, various specific objectives were proposed which are as follows:

1. To estimate the drug-polymer miscibility using solubility parameter approach and melting point depression method and to compare the results from both the approaches.
2. To estimate the ideal drug loading and ideal processing temperature for HME using thermodynamic phase diagrams and Gibbs free energy plots.
3. To develop a material-sparing method based on differential scanning calorimeter (DSC) to determine the design space for hot melt extrusion.
4. To predict the physical stability of ASDs at various temperature and relative humidity conditions using modified Avarami equation.

3. Materials and Methods

3.1. Model Drug: Mefenamic acid

Mefenamic acid was selected as a model drug based on its physicochemical properties. It is a BCS class II drug with poor water-solubility and high permeability. It has a pKa value of 4.2 making it a weakly acidic drug. The rationale for the selection of mefenamic acid was its high melting point of 230 - 231 °C and its tendency to degrade upon melting. This makes it a challenging drug to process using thermal techniques, i.e. hot-melt extrusion. There are three polymorphic forms reported for mefenamic acid. Form III is the metastable form which transforms into form I at ambient conditions and into form II at elevated temperatures (55). The saturated solubility of form II is more than form I, however, in the dissolution media, form II rapidly converts into form I. Therefore, the rate of conversion of form II into form I is the rate-limiting step in the dissolution of mefenamic acid. For the current study, mefenamic acid was purchased from Alfa Aesar (Haverhill, MA)

3.2. Model Polymers

Four model polymers, i.e. Eudragit® EPO (EPO), Kollidon® VA 64 (VA 64), Soluplus® (SLP) and Pluronic® F68 (F 68) were used as polymeric carrier materials. Eudragit® EPO was a kind gift from Evonik Corp. (Parsippany, NJ). Soluplus®, Pluronic® F68 and Kollidon® VA64 were kind gifts from BASF Corp. (Florham Park, NJ). These polymers were selected based on their glass transition temperature, T_g, solubilization capacity, hygroscopicity and toxicity profile. These four polymers differ in

their chemical composition and ionic nature; F68 is a non-ionic, EPO is a cationic, and SLP and VA64 are amphoteric polymers in nature. These polymers have similar solubility parameters to that of the drug MFA but differ in their chemical structure. This helps to understand the role of solubility parameter in predicting the drug-polymer miscibility.

3.3. Physicochemical Evaluation of Drug and Polymers

3.3.1. Determination of Melting Temperature, T_m

The melting temperature of drug and polymers were determined using a differential scanning calorimetry (DSC 6000, Perkin Elmer, USA) which was calibrated using indium standard prior to analysis. During analysis, accurately weighed, approximately 10 mg of material was taken in an aluminum sample pan and thermal runs were conducted over a temperature ranges of 30° to 250 °C, depending on the melting point of the material reported in the literature. A heating rate of 5 °C/min and nitrogen gas flow rate of 50 mL/min were maintained. The endpoint of the melting endotherm was taken as the melting point of the material.

3.3.2. Determination of Degradation Temperature, T_d

The degradation temperature of the drug and the polymers were determined using a thermogravimetric analyzer (Pyris^{TM} 1 TGA, Perkin Elmer, USA). The temperature calibration of the instrument was performed using nickel Cure point method before analysis. Accurately weighed, approximately 10 mg of material was placed on a

platinum sample pan and thermal run was conducted over a temperature range of 30° to 270 °C. A heating rate of 5 °C/min and nitrogen gas flow rate of 50 mL/min were maintained during analysis. The percent degradation was calculated from the difference in the initial and the final weight of the sample.

3.3.3. Determination of Glass Transition Temperature, T_g

The glass transition temperatures, T_g, of the drug and the polymers were determined using differential scanning calorimetry (DSC 6000, Perkin Elmer, USA). Accurately weighed, approximately 10 mg of material was placed and sealed in an aluminum sample pan. The sample pan was equilibrated at 30°C for 1 min and heated to 240°C at 5°C/min rate and modulation of 1°C/min. The T_g of the drug and the polymers were determined using Pyris™ Manager software (Perkin Elmer, USA).

3.3.4. Determination of True Density, ρ

True density of the powder materials was determined using a gas pycnometer (AccuPyc® II 1340, Micromeritics Instruments Corp., Norcross, GA). Prior to analysis, the pycnometer was calibrated with an iron sphere of known mass prior to each measurement. During analysis, a known weight of powder sample was transferred into an aluminum sample container of 3.5 cm^3 volume, and helium gas was passed through the sample from the reservoir. The determinations were carried out at room temperature. The instrument automatically purges moisture and volatile materials from powder sample and repeats the analysis until successive measurements yield consistent results. The

determination of sample density was repeated for up to 10 cycles. The average reading of 10 cycles was recorded as the true density of the material (56–59).

3.4. Solubility Parameter Approach

3.4.1. Calculation of Hildebrand Solubility Parameter, δ

The calculation of the Hildebrand solubility parameter of a chemical is based on the cohesive energy density of the functional groups in its molecule. Cohesive energy density is expressed as the cohesive energy, ΔE_v, of the molecules per unit volume, V. The Hildebrand solubility parameter is then calculated as the square root of the cohesive energy density of the molecule according to eq. (1). The values of the ΔE_v and V of the functional groups were adapted from Fedors (60).

$$\delta = \mathrm{CED}^{0.5} = (\Delta E_v / V)^{0.5} \quad (1)$$

3.4.2. Calculation of Hansen Solubility Parameters, δ_t

The Hansen solubility parameter is a modification of the Hildebrand method in which the cohesive energy is divided in three different forces, i.e. dispersion, polar and hydrogen bonding forces. The Hansen solubility parameter is expressed as δ_t, and its value is calculated using the following equation (Eq. 2):

$$\delta_t = \sqrt{\delta_d^2 + \delta_p^2 + \delta_h^2} \quad (2)$$

Where δ_d, δ_p and δ_h are the dispersion forces, polar forces, and hydrogen bonding forces, respectively, in a molecule that are calculated using the following relationships:

$$\delta_d = \frac{\sum F_{di}}{V}; \quad \delta_p = \frac{\sqrt{\sum F_{pi}^2}}{V}; \quad \delta_h = \sqrt{\frac{\sum E_{hi}}{V}} \tag{3}$$

The chemical structure of a molecule was divided in different functional groups and the values of F_{di}, F_{pi} and E_{hi} were calculated according to the group contribution method by Van Krevelen-Hoftyzer for each functional groups in a molecule (61). The value of molar volume, V was calculated according to Fedors (60).

3.4.3. Construction of Bagley's Plot

Bagley *et al.* introduced the combined solubility parameter, δ_v, based on the thermodynamic considerations that dispersion forces, δ_d, and polar forces, δ_p, show similar effect, whereas the effect of δ_h is different (62). The combined value of the solubility parameter, δ_v was calculated according to eq. (4):

$$\delta_v = \sqrt{\delta_d^2 + \delta_p^2} \tag{4}$$

Bagley's plot was constructed using the relationship between δ_v and δ_h which helps to project the three-dimensional solubility parameters into a two-dimensional plot.

3.4.4. Estimation of F-H interaction parameter, χ

The Flory–Huggins interaction parameter between the drug and the polymers, $\chi_{d\text{-}p}$ was estimated using the solubility parameters of drug, δ_{drug} and polymer, $\delta_{polymer}$ according to the following equation:

$$\chi_{d-p} = V\frac{(\delta_{drug} - \delta_{polymer})^2}{RT} \quad (5)$$

Where $\chi_{d\text{-}p}$ represents the F-H interaction parameter between the drug and the polymer, V is the molar volume calculated according to the group contribution method from Fedors (60). R is the universal gas constant (8.314 J/mol.K); T is the temperature in Kelvin (293.1 K).

3.5. Melting Point Depression Method

3.5.1. Preparation of Drug-Polymer Physical Mixtures

The drug-polymer physical mixtures were prepared by accurately weighing various ratios of drug and polymer and then gently mixing them together to form a homogenous mixture using a mortar and pestle. Care was taken not to apply excessive mechanical stress on the mixture that could result in the amorphization of the drug.

3.5.2. Determination of Melting Point of MFA

The melting point of the mefenamic acid in drug-polymer mixtures was determined using a differential scanning calorimetry (DSC 6000, Perkin Elmer, USA).

Accurately weighed, approximately 10 mg of the drug-polymer mixture was taken in an aluminum sample pan and thermal runs were conducted over a temperature range of 30° to 250 °C at a heating rate of 5 °C/min under nitrogen gas flowing at the rate of 50 ml/min. The endpoint of the melting endotherm was taken as the melting point of the drug. To ensure content uniformity, several samples were analyzed for each drug-polymer ratio and only three samples (n=3) with the heat of fusion, ΔH_f, values of less than ±5% variation from the theoretical value were used for analysis.

3.5.3. Estimation of Drug-Polymer Interaction Parameter

The drug-polymer interaction parameter, χ, was estimated using the melting point depression using the following equation (Eq. 6):

$$\frac{1}{T_m} - \frac{1}{T_{m0}} = -\frac{R}{\Delta H_f}\left[\ln\phi_d + \left(1 - \frac{1}{m}\right)\phi_p + \chi\phi_p^2\right] \quad (6)$$

Where T_m is the melting point of drug-polymer mixture (K); T_{mo} is the melting point of pure drug crystal (K); R is the real gas constant (8.314 J/mole K); ΔH_f is the heat of fusion of the drug (kJ/mol), ϕ_d is the volume fraction of the drug, ϕ_p is the volume fraction of the polymer, χ is the drug-polymer interaction parameter, and m is the degree of polymerization of the polymer which is the ratio of the volume of a polymer chain to drug molecular volume. It was calculated using the following equation (Eq. 7):

$$m = \frac{\frac{M_{w(polymer)}}{\rho_{polymer}}}{\frac{M_{w(drug)}}{\rho_{drug}}} \quad (7)$$

where the $M_{w(polymer)}$ and $M_{w(drug)}$ are the molecular weight of polymer and drug, respectively, and the $\rho_{polymer}$ and ρ_{drug} are the density of polymer and drug, respectively.

3.5.4. Establishing Relationship Between Interaction Parameter, χ and Temperatures

The interaction parameter, χ between drug and polymer is temperature dependent. The value of χ estimated using the melting point depression method is clost to the melting temperature of the drug. To estimate the Gibbs free energy of mixing at various temperatures, the value of χ at various temperatures was estimated. This was done by determining the temperature dependence of the interaction parameter, χ using the following equation:

$$\chi = A + \frac{B}{T} \quad (8)$$

Where A is the entropic contributions, and B is the enthalpic contributions for mixing. These constants are used to theoretically calculate the value of χ at any specific temperature.

3.6. Construction of Gibbs Free Energy Plots

The Flory-Huggins theory relates the Gibbs free energy of mixing the drug-polymer mixtures with the drug-polymer interaction parameter (χ) according to the following equation:

$$\Delta G_{mix} = RT\left(\phi_{drug} \ln \phi_{drug} + \frac{\phi_{poly}}{m} \ln \phi_{poly} + \chi_{d-p}\phi_{drug}\phi_{poly}\right) \quad (9)$$

The value of the interaction parameter, χ at various temperatures was determined from eq. (8). These values were then used to estimate the Gibbs free energy of mixing (ΔG_{mix}) at various temperatures.

3.6.1. Validation of Gibbs Free Energy Plots

The Gibbs free energy plots constructed using the Flory-Huggins theory were validated using a hot stage microscope (FP82HT, Mettler-Toledo, Greifensee, Switzerland) equipped with a Nikon Eclipse 50i microscope (Nikon Inc., Tokyo, Japan) with a 10x cross-polarized lens. A 1:1 ratio of the drug and the polymer was dispersed in acetone and transferred onto a glass slide. This step ensured that the drug and the polymer were mixed thoroughly. After evaporation of the organic solvent, the samples were heated on the hot stage microscope from 30° to 230 °C at 10 °C/min rate and the changes in the drug crystal morphology as a function of temperature were recorded using a Nikon digital single-lens reflex camera attached to the microscope. The onset temperature where the drug crystals were completely miscible in the polymeric matrix was recorded and compared with the results obtained from the Gibbs free energy plots.

3.7. Construction of Thermodynamic Phase Diagrams

A binary phase diagram depicts the maximum solubility and miscibility of an amorphous drug in the polymeric carrier as a function of temperature. It consists of a

drug-polymer solubility curve, drug-polymer miscibility curve and the glass transition curve of the drug-polymer system.

3.7.1. Estimation of Solubility Curve

The solubility curve refers to the temperature at which the crystalline drug is in equilibrium with the dissolved or dispersed drug in the polymeric matrix. Marsac *et al*. proposed an approach for the estimation of the drug-polymer solubility that was based on the Flory-Huggins lattice theory (42). According to the authors, the mole fraction solubility of a drug in the polymer is related to the activity coefficient of the drug and the interaction parameter between the drug and the polymer as expressed by the following equation (Eq. 10):

$$\ln \gamma_{drug}\, x_{drug} = \ln \phi_{drug} + \left(1 - \frac{1}{m}\right) \phi_{polymer} + \chi\, \phi_{polymer}^{2} \qquad (10)$$

Where x_{drug} is the mole fraction of the drug dissolved or dispersed in the polymer, γ_{drug} is the activity coefficient of the drug in the polymer, ϕ_{drug} is the volume fraction of the drug, $\phi_{polymer}$ is the volume fraction of the polymer, and m is the ratio of the volume of the polymer to the volume of the drug.

Another approach to determine the temperature at which the crystalline drug is in equilibrium with the dissolved or dispersed drug in the polymeric matrix is using the following solid-liquid equilibrium (SLE) equation (Eq. 11):

$$\ln x_{drug} = \frac{\Delta H_f}{R T_m}\left(1 - \frac{T_{m0}}{T}\right) - \ln \gamma_{drug} \qquad (11)$$

Where x_{drug} is the mole fraction of the dissolved drug, γ_{drug} is the activity coefficient of the drug, T is the temperature of the two phases of the drug in equilibrium (K), T_{m0} is the melting point of pure drug crystal (K), R is the real gas constant (8.314 J/mol.K), and ΔH_f is the heat of fusion of the drug (kJ/mol).

The value of activity coefficient, γ_{drug}, of the drug can be calculated using the extended Hansen solubility model (Eq. 12):

$$\ln \gamma_{drug} = \frac{V_{drug}}{RT}\left\{\left(\delta_d^{drug} - \overline{\delta}d\right)^2 + 0.25\left[\left(\delta_p^{drug} - \overline{\delta}p\right)^2 + \left(\delta_h^{drug} - \overline{\delta}h\right)^2\right]\right\} + \ln\frac{V_{drug}}{\overline{V}} + 1 - \frac{V_{drug}}{\overline{V}} \quad (12)$$

Where V is the molar volume of the drug, δ is the Hansen solubility parameter, $\overline{\delta}$ is the molar volume-weighted Hansen solubility parameter, and $\bar{V}$ is the mixture volume. The subscripts, d, p and h, stand for dispersion, polar and hydrogen-bonding forces, respectively.

The values of mixture volume and molar volume-weighted Hansen solubility parameter can be calculated using the following equations:

$$\bar{\delta} = \sum_{k=1}^{n} \phi_k \delta_k \quad (13)$$

$$\phi_k = \frac{x_k V_k}{\bar{V}} \quad (14)$$

$$\bar{V} = \sum_{k=1}^{n} x_k V_k \quad (15)$$

Where ϕ is the volume fraction, x is the mole fraction, M is the molecular weight, ρ is the density, and the subscript k denotes the different components of the mixture.

3.7.2. Estimation of Miscibility Curve

The drug-polymer miscibility curve is also called as the spinodal decomposition curve that defines the boundary between the unstable zone and the metastable zone in the drug-polymer mixture. It is plotted by equating the second derivative of the free energy to zero as expressed below (Eq. 16):

$$T_s = \frac{2B}{\left(1/\phi\right)+\left(1/_{(m(1-\phi))}\right)-2A} \quad (16)$$

Where, ϕ is the volume fraction of the drug calculated using the true density of the drug and polymer, 1-ϕ is the volume fraction of the polymer, and m is the degree of polymerization of the polymer which is the ratio of the volume of a polymer chain to drug molecular volume. The constants A and B are obtained by the melting point depression data obtained using eq. (8).

3.7.3. Estimation of Glass Transition Curve

The glass transition temperatures, T_g, of the drug and the polymers were determined using differential scanning calorimetry (DSC 6000, Perkin Elmer, USA). Accurately weighed, approximately 10 mg of material was placed and sealed in an aluminum sample pan. The sample pan was equilibrated at 30°C for 1 min and heated to 240°C at 5°C/min rate and modulation of 1°C/min. The T_g of the drug and the polymers were determined using Pyris™ Manager software (Perkin Elmer, USA). The glass transition temperature, T_g, of drug-polymer mixtures was predicted using the following Gordan-Taylor equation (Eq. 17) .

$$T_{gmix} = \frac{\{(w_1 T_{g,1}) + (K w_2 T_{g,2})\}}{(w_1 + K w_2)} \qquad K = \frac{\rho_1 T_{g1}}{\rho_2 T_{g2}} \tag{17}$$

Where, w_1, T_g and ρ are the weight fraction, the glass transition temperature, and true density of drug and polymer, respectively.

3.8. Material Sparing DSC Method for Process Optimization of HME

3.8.1. Analytical Techniques

3.8.1.1. Differential Scanning Calorimeter

A differential scanning calorimeter (DSC 6000, Perkin Elmer, USA) was used to determine the melting endotherm of crystalline drug, MFA. The instrument was calibrated using indium standard before analysis. Accurately weighed, approximately 15 mg of MFA was placed and sealed in an aluminum sample pan (50 µL) and heated over a temperature range of 30° to 250 °C at a heating rate of 1 °C/min to 10 °C/min under nitrogen gas flowing at the rate of 50 ml/min. The final heating temperature and the heating rate were changed according to the experimental design. The changes in the melting endotherm of MFA was recorded using Pyris™ Manager software (Perkin Elmer, USA).

3.8.1.2. Thermo Gravimetric Analysis

The thermal degradation of MFA was determined using a thermogravimetric analyzer (Pyris™ 1 TGA, Perkin Elmer, USA). The temperature calibration of the instrument was performed using the nickel Curie point measurement method before

analysis. Accurately weighed, approximately 10 mg of pure MFA was placed in a platinum sample pan and a thermal run was conducted over a temperature range of 30° to 250 °C at various heating rates from 0.5 °C/min to 15 °C/min under nitrogen gas flowing at the rate of 50 ml/min. The heating rate was changed according to the experimental design. The percent weight loss was calculated from the difference in the initial and final weight of the sample using Pyris™ Manager software (Perkin Elmer, USA).

3.8.1.3. High Performance Liquid Chromatography

The amount of MFA in the samples was determined by carefully diluting them with mobile phase consisting of 46:40:14 ratio of acetonitrile, buffer solution (50 mM solution of monobasic ammonium phosphate adjusted with 3 M ammonium hydroxide to a pH of 5.0) and tetrahydrofuran. The diluted samples were then analyzed using a high-performance liquid chromatography (HPLC) system (Agilent Corporation, USA) equipped with an autosampler (AS2055 Plus, intelligent sampler, JASCO Corp, Japan) and photodiode array detector (JASCO Corp., Japan). A Phenomenex Luna® reversed phase C18 column (150 × 4.6 mm; 5 μm particles) was used as a stationary phase. The flow rate was 1.5 mL/min. with an injection volume of 20 μL and the detection wavelength of 224 nm.

3.8.1.4. X-Ray Powder Diffraction (pXRD)

The presence of MFA crystals in the samples was determined by powder X-ray diffraction (pXRD) analysis using X-ray diffractometer (Shimadzu 6000, Shimadzu Corporation, Kyoto, Japan) which was calibrated using a quartz standard prior to

analysis. During analysis, the drug-polymer dispersions were placed uniformly on a glass sample holder to obtain a smooth and uniform surface. The samples were analyzed through a CuKa, monochromatic radiation source emitting X-ray radiation with generated voltage of 40 kV and current of 30 mA at room temperature. The diffraction patterns of samples were obtained by scanning over a continuous 2θ range of 10–50° at a rate of 2 degree/min using a scan step size of 0.02 degree (63).

3.8.2. Initial Screening to Set up Experimental Design

Initial screening was performed to determine the study range for the experimental design. Film casting method was used to determine the maximum drug-polymer miscibility. Then, the minimum temperature at which the drug-polymer blends were completely miscible was determined using hot stage microscopy. Later, TGA analysis was performed at various heating rates to determine the temperature at which complete degradation of MFA occurs in the drug-polymer powder blends.

3.8.2.1. Determination of Maximum Drug-Polymer Miscibility Using Film Casting Method

The maximum miscibility of MFA in EPO was determined using film casting method. Various powder blends with MFA:EPO ratios from 1:1 to 1:4 was dissolved in enough quantity of acetone to form a clear solution. The resulting solutions were poured in aluminum pans and the solvent was evaporated at 50 °C. Once the solvent evaporated, the drug-polymer films were observed under a Nikon Eclipse 50i Microscope (Nikon

Inc., Tokyo, Japan) using 10x cross polarized lens to detect the presence of any crystalline MFA. The maximum drug loading at which no crystalline MFA was observed in the films was used for further analysis.

3.8.2.2. Determination of Minimum Temperature of Miscibility (MTM) Using Hot Stage Microscopy

The minimum temperature of miscibility (MTM) is the minimum temperature at which the drug crystal completely gets miscible in the polymeric carrier. To determine MTM, the powder blends of MFA and EPO corresponding to the maximum drug-polymer miscibility (determined from film casting method) were prepared using a mortar and pestle. The powder blend was then heated on a hot stage (Mettler-Toledo FP82HT, Greifensee, Switzerland) equipped with a Nikon Eclipse 50i Microscope (Nikon Inc., Tokyo, Japan) using 10x cross polarized lens. A small amount (2-4 mg) of sample was placed on a glass slide with a cover glass and heated from 30 to 250 °C at 10 °C/min. Changes in the samples morphology were recorded as a function of temperature using a Nikon digital single-lens reflex camera attached to the microscope which were then analyzed to determine the minimum temperature at which the MFA crystals got completely miscible in the EPO matrix.

3.8.2.3. Determination of the Relationship Between Heating Rate and Drug Degradation Using Thermogravimetric Analysis (TGA)

The heating rate and the final heating temperature for the experimental design was determined using TGA analysis. The powder blends of MFA and EPO corresponding to

the maximum drug-polymer miscibility were heated in TGA. Briefly, 10 mg of drug-polymer physical mixture was placed in a platinum sample pan and heated from 30° C to 250° C at various heating rates from 0.5 °C/min to 15 °C/min. The percent weight change in the samples were analyzed using Pyris^{TM} software V 8.0 (Perkin Elmer, USA). A relationship between the % weight loss and the TGA heating rate was established to determine the ideal heating rate for the experimental design.

3.8.3. Box-Behnken Experimental Design

In the present study, a Box-Behnken experimental design was used to study the effects of independent factors on the dependent factors (responses). The experimental design consisted of three independent factors, viz. drug loading (X_1), heating rate (X_2), and processing temperature (X_3). These factors were studied at three levels, i.e. low, medium and high (-1, 0, +1). Out of the three factors, two factors were varied through the four possible combinations of low-high, while one factor was kept constant resulting in twelve experiments. The center point consisted of all the three factors at medium level and was peformed in triplicate to identify any manual errors during experimentation. In total, the Box-Behnken experimental design consisted of fifteen experimental runs (twelve blocks and three center point). The levels of independent factors for the experimental design were determined from the initial screening experiments using film casting method, hot stage microscopy and TGA.

As per the applied design, the relationship between controlled input variables with the responses was quantified and the true functional relationship was established. Usually

a second order polynomial equation is used in response surface methodology to describe the model which is as follows (Eq. 18) (64):

$$Y = B_0 + B_1X_1 + B_2X_2 + B_3X_3 + B_{11}X_{21} + B_{22}X_{22} + B_{33}X_{23} + B_{12}X_1X_2 + B_{23}X_2X_3 + B_{13}X_1X_3 \quad \text{(Eq. 18)}$$

where Y is the level of predicted or measured response, B_0 is the model constant or intercept, X_1, X_2 and X_3 are independent variables, B_1, B_2 and B_3 are linear coefficients, B_{12}, B_{23} and B_{13} are interaction terms between independent variables or cross-product coefficients, and B_{11}, B_{22} and B_{33} are quadratic coefficients.

The dependent or response parameters selected for the study were residual crystallinity (Y_1) and drug loss degradation (Y_2). This design allowed estimation of the main factors and the interaction effects between the considerable independent parameters (40). The relationship of between the independent parameters on the dependent parameters was demonstrated by response surface plots with regions of maxima (red) and minima (blue). A commercial software (Design Expert, version 11, Stat-Ease Inc., Minneapolis, MN) was used to generate the Box-Behnken design matrix and to analyze the experimental data.

3.8.4. Preparation of Drug-Polymer Dispersions Using DSC

The drug-polymer physical mixtures were prepared according to the experimental design using a mortar and a pestle. Around 20 mg of the physical mixture was heated using a differential scanning calorimeter (DSC 6000, Perkin Elmer, USA) in a 50 µL

aluminum sample pan. The heating rates and final heating temperatures were maintained according to the experimental design. In order to ensure the content uniformity in the physical mixtures, the heat of fusion, ΔH_f, of the melting endotherm of MFA was compared to that of the pure crystalline drug. All the samples were stored in a desiccator for 24 hrs before characterization. A total of six samples were prepared at each experimental condition (n=6).

3.8.5. Determination of Residual Crystallinity of Drug using DSC

The residual crystallinity represents the percent of the total drug which remained in the crystalline form in a sample. It was calculated according to the heat of fusion values using following equation (Eq. 19):

$$\text{Residual crystallinity (\%)} = \frac{\Delta H_{f(\text{Observed})}}{\Delta H_{f(\text{Theoritical})}} \times 100 \quad (19)$$

The observed heat of fusion value, $\Delta H_{f\,(observed)}$, was experimentally determined by heating the drug-polymer samples in a DSC at a rate of 5 °C/min from 30 °C to 230 °C. The ΔH_f value was then computed as the area under the melting endotherm using Pyris software. The theoretical value of heat of fusion, $\Delta H_{f\,(Theoretical)}$ (J/g) depends on the drug load and the heat of fusion of pure mefenamic acid, $\Delta H_{f\,(Pure\ drug)}$, (134.0 J/g) was calculated using the following equation (Eq. 20):

$$\Delta H_{f\,(\text{Theoritical})} = \frac{\text{Drug load (\%)}}{100} \times \Delta H_{f\,(\text{Pure drug})} \quad (20)$$

3.8.6. Determination of Drug Degradation Using HPLC

The drug degradation indicates the percent of the drug that degraded during heating cycle. It was determined by carefully diluting the drug-polymer dispersions from the DSC sample pans with the HPLC mobile phase. The diluted samples were then analyzed using HPLC and the area under the curve (AUC) values of the degradation peak and the drug peak were calculated using Agilent software (Agilent Corporation, USA). The percent degradation was then calculated using the following equation (Eq. 21):

$$\text{Drug degradation (\%)} = \frac{(\text{AUC})_{\text{Degradation}}}{(\text{AUC})_{\text{Degradation}} + (\text{AUC})_{\text{Drug}}} \text{X } 100 \quad (21)$$

3.8.7. Statistical Analysis

Multiple regression analysis of the experimental data was performed using Design Expert software, version 11 (Stat-Ease Inc., Minneapolis, MN). The experimental data were fitted in the second-order quadratic polynomial model along with added interaction terms. The model was analyzed based on the values of R^2, adjusted R^2 (Adj. R^2), predicted R^2 (Pred. R^2), standard deviation (SD) and coefficient of variation (% CV). ANOVA was performed to determine if the independent parameters had significant effect on the response variables. The sum of squares (SS) and the mean square values of the model and the residuals were calculated and the significance of the independent parameters on the response variables was determined based on the F-value and P value.

The ability of the model to predict all the response variables was determined by calculating the values of lack of fit and the pure error.

3.8.8. Selection of Optimum Experimental Conditions

The selection of the optimum experimental conditions was carried out using both numerical and the graphical optimization. The target values of residual crystallinity and drug degradation were set at 15% and 5%, respectively to determine the optimum experimental conditions. The numerical optimization was performed to determine all the possible combinations of the independent parameters that result in the response variables within the target value. The optimum combination of the independent parameters was selected based on the desirability values. Graphical optimization was also perfomed to determined the optimum experimental conditions to obtain the target values for residual crystallinity and drug degradation. An overlay plot was constructed to determine design space of the independent parameters. Within the design space, any combination of the independent parameters results in a target residual crystallinity of less than 15% and a drug degradation of less than 5%.

3.8.9. Validation of the Experimental Design

The experimental design was validated using the linear correlation plots, the residual plots and the values of bias. The experimental design was validated to quantify the agreement between the predicted values and the experimentally determined values. Six different drug-polymer dispersions were prepared at various drug loadings, heating rate and processing temperature using DSC. The residual crystallinity and drug

degradation of the six drug-polymer dispersions were experimentally determined. The predicted values from the experimental design were compared with the experimentally determined values using linear correlation plots and residual plots. The mean percentage prediction error (percentage bias) was also calculated to determine the ability of the experimental model to predict the response variables. A lower value of percentage bias indicates that the model is not biased and can effectively predict the response variables.

3.8.10. Preparation of Drug-Polymer Dispersions Using Hot Melt Extrusion

Hot Melt extrusion was carried out using an 11-mm parallel twin screw melt extruder (Process 11, Thermo Fisher Scientific, Waltham, MA) comprising of 8 electric heating zones with an L/D ratio of 40. The feed zone (Zone 1) was maintained at room temperature and the subsequent zones (Zone 2, Zone 3, Zone 4, Zone 5, Zone 6 and Zone 7) were setup at increasing temperature gradient as shown in Figure 2. Two high kneading elements (at zone 3 and between zone 6 and 7) and one low kneading element (between zone 4 and 5) were used. An extrusion element was used at the end of the barrel for the formation of extrudates (65). The screw speed was varied between 50 and 150 rpm and the maximum temperature of the heating zones was set at 150 °C. The extrudates were collected and cooled down until further analysis.

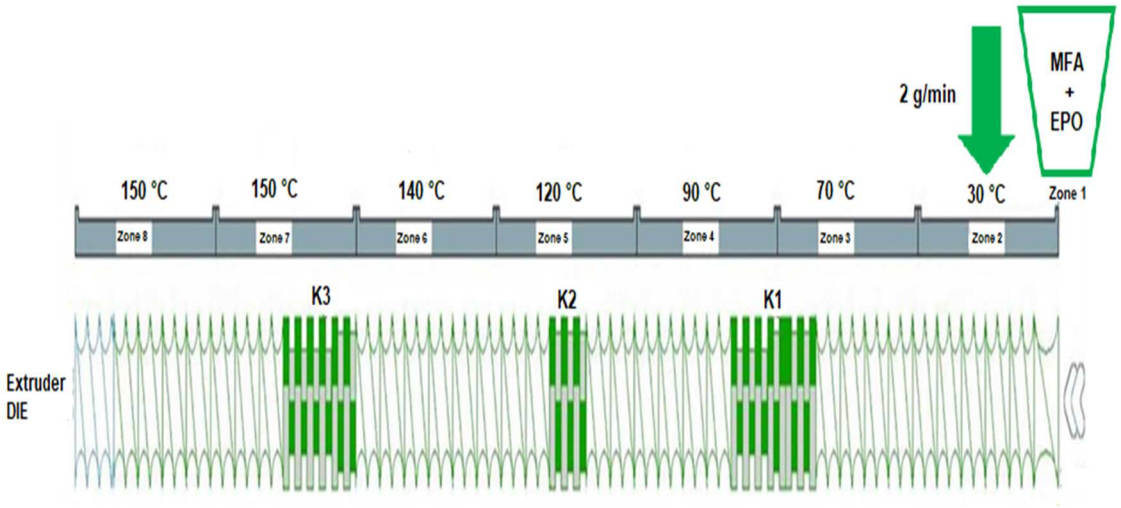

Figure 4: Screw design for HME used for processing MFA-EPO powder blends. K1, K2 and K3 represent the kneading elements.

3.8.11. Preparation of Drug-Polymer Dispersions Using Vacuum Compression Molding

A novel vacuum compression molding (VCM) tool was used to prepare the drug-polymer dispersions and compare them with HME filaments. The VCM tool has a cylindrical design and consists of a main body, a base plate, a lid, a piston and separation foils. The lid and the base plate have O-ring seals that provide a gas-tight closure when connected to the main body (66). Since the particle size difference between the drug and the polymer was high, the sample was prepared by dissolving the drug and the polymer in acetone prior to sample preparation. The solvent was evaporated until a molten mixture was observed. This molten mixture was then enclosed between two Teflon foils and loaded into the sample chamber. The tool was then placed on a pre-heated hot plate at 150 °C. The heat was transferred across the base plate to the sample forming a homogeneous bubble-free specimen. The samples were heated for a total of three minutes then the tool was subsequently cooled down and disassembled. The samples obtained were stored in an airtight container until further analysis.

3.8.12. Characterization of Drug-Polymer Dispersions Prepared Using HME and VCM

The drug-polymer dispersions prepared using HME and VCM were characterized to determine the total degradation and residual crystallinity of MFA according to the procedure mentioned earlier. Additionally, solid state characterization of the samples was performed using pXRD and DSC analysis to determine the crystalline state of MFA and the glass transition temperature (T_g) of the drug-polymer dispersions, respectively.

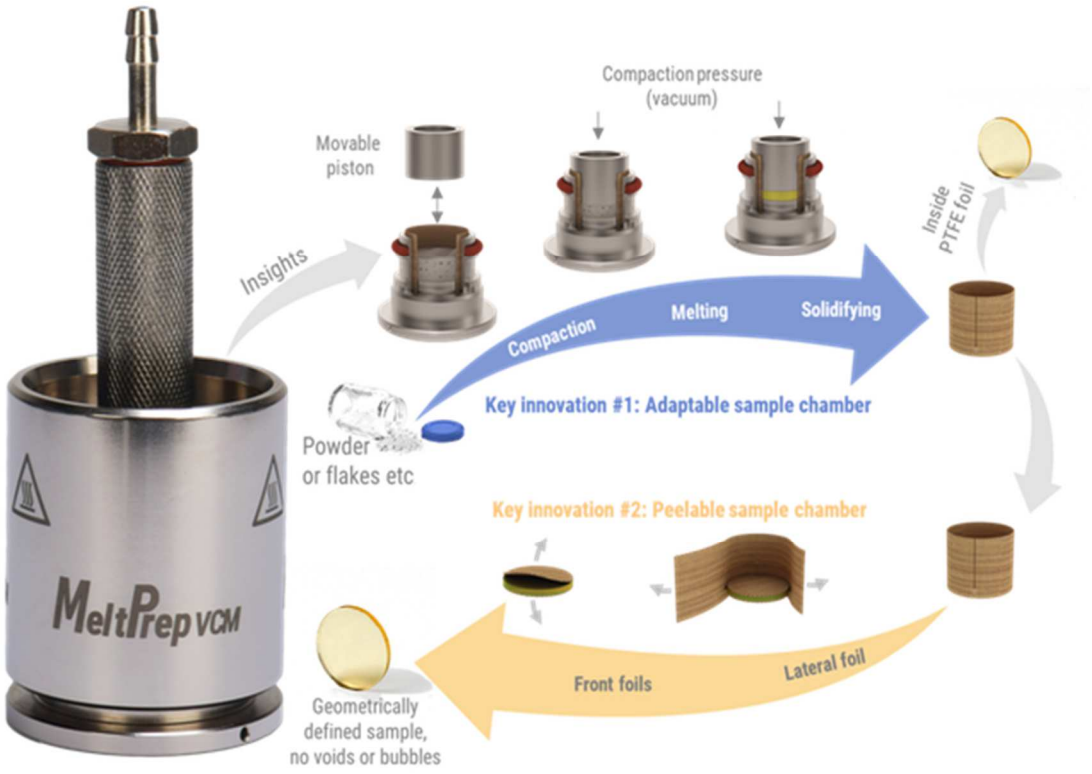

Figure 5: Parts of Vaccum compression molding (VCM) tool used to prepare drug-polymer samples

3.9. Estimation of Physical Stability of ASDs Using Modified Avarami Equation

3.9.1. Preparation of MFA Seed Crystals

Seed crystals of MFA were prepared by dissolving 1 g MFA in 40 ml of acetone using a sonicating water bath (Elmasonic S 50R, USA). After the drug was completely dissolved in the acetonic solution, the sonicator was turned off and samples were left in the water bath overnight for slow cooling. The crystals were collected after all the solvent was evaporated and stored until further analysis.

3.9.2. Preparation of Drug-Polymer Dispersions Using Heat Molding

The ASDs of MFA-EPO were prepared using a heat molding system developed in-house. The drug and the polymer were size reduced in a mortar and pestle and then sieved using #270 sieve (53 μm opening). Approximately, 2 g of MFA-EPO mixture (4:6) was prepared by properly weighing on a weighing balance and then transferred on to a hot plate. A 2 cm diameter cylindrical mold was placed on the hot plate and the drug-polymer mixture was placed in between two PTFE films. The drug-polymer mixture was evenly distributed inside the mold using a 2 cm die and the mixture was heated until 160 °C for 15 min. The samples were carefully transferred into a cooling chamber and flash cooled using nitrogen gas. After the samples were cooled, they were milled in a cryogenic mill to obtain a fine powder. The samples were taken out and stored at room temperature until further analysis.

3.9.3. Modified Avarami Equation to Estimate the Physical Stability of ASDs

The modified Avarami equation contains of two essential assumptions – (i) nucleation rate is proportional to amorphous fraction, and (ii) crystal size grows linearly with respect to crystallization time from t = 0 to the final crystal size. These assumptions can be mathematically expressed as:

$$J(t) = J_0(1 - \alpha(t)) \tag{22}$$

where J_o is the initial nucleation rate and 1- α(t) is a function of crystallization time.

$$r = \beta t \tag{23}$$

where r is the radius for spherical crystal, and β is crystal growth rate. During the time interval τ to dτ, the number of nuclei generated is:

$$N = J_0\big(1 - \alpha(\tau)\big)d\tau \tag{24}$$

Since each nuclei will grow into a sphere of radius β(t-τ), the increased volume due to nuclei appearing in the time interval will be:

$$d(V)t = \frac{4\pi}{3}\beta^3(t - \tau)^3 J_0\big(1 - \alpha(\tau)\big)d\tau \tag{25}$$

where V(t) is the volume transformed into the crystalline state. It is also related to the relative crystallinity by the Avrami phase transition theory:

$$1 - \alpha(t) = exp^{(-V(t))} \tag{26}$$

The derivative of the above equation provides an expression for the created crystalline volume in differential form:

$$dV(t) = \frac{1}{1-\alpha(t)} d\alpha(t) \tag{27}$$

A relationship between (t) and τ is established by solving Eqs. (25) and (27):

$$\frac{1}{[1-\alpha(t)]^2} d\alpha(t) = \frac{4\pi}{3} \beta^3 J_0 (t-\tau)^3 d\tau \tag{28}$$

Integration of eq. (28) gives the final model equation for spherical crystal growth:

$$\alpha(t) = 1 - \frac{1}{1+kt^4} \tag{29}$$

where k is crystallization rate constant, expressed as the production of nucleation rate constant, J_o, and crystal growth rate constant, β.

$$k = \frac{1}{3} \pi \beta^3 J_0 \tag{30}$$

A more general form for relative crystallinity can be presented as:

$$\alpha(t) = 1 - \frac{1}{1+kt^n} \tag{31}$$

Where the exponent, n, describes the dimensionality of crystal growth, and equals 2, 3 and 4 for rod, plate, and spherical geometry, respectively for homogeneous nucleation. A general form of k can be expressed in terms of activation energy, ΔE_A, and T according to the Arrhenius equation (Eq. 32). (Yoshioka *et al*., 1994):

$$k = k_0 \exp\left(-\frac{\Delta E_A}{RT}\right) \tag{32}$$

Where k_o is the pre-exponential factor, R is the universal gas constant, and T is the absolute temperature in the unit of kelvin. By correlating the crystallization rate constant, *k*, as a function of relative humidity and temperature, the optimum stability conditions of amorphous solid dispersions can be determined.

3.9.4. Preparation of Stability Chambers Using Saturated Salt Solutions

The drug-polymer samples were stored at various relative humidity (% RH) and temperatures as shown in Table 3. The ASD samples were stored in glass humidity chambers with different saturated salt solutions. The humidity chambers were kept in laboratory oven (VWR International, USA) at different temperatures. The relative humidity and temperature of the humidity chambers were monitored using humidity/temperature monitor (Sper Scientific, China).

3.9.5. Determination of Relative Degree of Crystallinity

The ASD samples stored at various storage conditions were taken out periodically at predetermined time points, and the extent of recrystallization was determined using a DSC by heating the samples from 30 °C to 240 °C at 20 °C/min. The relative degree of crystallinity, α(t), was calculated using the following equation (Eq. 33):

$$\alpha(t) = \frac{\Delta H(t)}{\Delta H_{\infty}} \tag{33}$$

Where $\Delta H_{(t)}$ is the heat of fusion of the drug at a time, t, and ΔH_{∞} is the heat of fusion of the drug after complete recrystallization.

3.9.6. Estimation of Recrystallization Rate Constant, *k*

The recrystallization rate constant, *k*, was estimated using the mathematical model according to eq. (33). A non-linear regression analysis was performed between the relative degree of crystallinity, α(t), with respect to time, t, using Origin Pro V.8.5 (Massachusetts, USA). The dimensionality of crystal growth, n, was set as n = 2 and n > 0.

Table 3: Various storage conditions used to study the recrystallization kinetics of drug from the polymeric carrier

Purpose	Saturated Salt Solution	Temperature (°C)	Relative Humidity (%)
To study the effect of temperature on the crystallization rate constant, k	Sodium Chloride	25	75
	Sodium Chloride	40	75
	Sodium Chloride	60	75
	Sodium Chloride	80	75
	Sodium Chloride	100	75
To study the effect of relative humidity on the crystallization rate constant, k	Lithium chloride	60	11
	Potassium Fluoride	60	22
	Magnesium chloride	60	32
	Potassium Iodide	60	57
	Sodium Chloride	60	75

4. Results and Discussion

4.1. Thermal analysis of Mefenamic acid (MFA) and Polymers

The physicochemical evaluation of the drug (MFA) and the thermoplastic polymers was conducted using DSC and TGA. The plots of thermogravimetric analysis of MFA is shown in Figure 6a. The weight loss of MFA when heated between 180 °C and 230 °C was found to be 4.3%. This indicates that mefenamic acid undergoes degradation before its melting point. Beyond 230 °C, rapid degradation of MFA was observed until 270 °C with a total weight loss of 68.5%. This was possibly due to increased molecular mobility of MFA after melting thereby exposing the carboxylic acid group (-COOH) of the molecule. The results obtained by thermo-gravimetric analysis are in accordance with the thermal decomposition of MFA observed by rapid ESI-MS method as reported by Zhou and Gilpin (67). The authors reported that when MFA was dissolved in a mobile phase consisting of methanol-water (80:20 v/v) and subjected to thermal degradation between 130 °C and 230 °C, MFA was converted to MFA-H^+, which is completely converted to the final decomposition fragment with an m/z value of 224 at a temperature of 230 °C. In the present study, only 4.3% degradation was observed at 230 °C. This was possibly due to the nature of the sample where MFA was present in solid form rather than molecularly dispersed form. Also, the time scale of thermo-gravimetric analysis was a magnitude of minutes in the case of rapid ESI-MS, it was hours which provides sufficient time and energy for degradation of MFA.

The DSC thermogram of MFA showed two endotherms, a shallow endotherm at 170 °C indicating polymorphic change of MFA from form I to form II followed by a

sharp endotherm at 231 °C indicating melting of form II (Fig. 6b). The melting of MFA is followed by its degradation due to decarboxylation. The cooling cycle showed an exothermic peak with a low intensity at 110 °C which indicates that mefenamic acid is not a glass former and undergoes recrystallization during cooling. An endothermic peak was observed in the second heating cycle which indicated the melting of the residual crystalline MFA from the cooling cycle. The results from the thermal analysis demonstrated the thermal degradation and recrystallization potential of MFA making it a challenging molecule to process using hot-melt extrusion.

The DSC scans of the polymers is shown in Figure 7. The glass transition temperature, T_g of the polymers was found to be in between the range of 55 to 101 °C. The absence of any other thermal event during the scans showed that the polymers were amorphous.

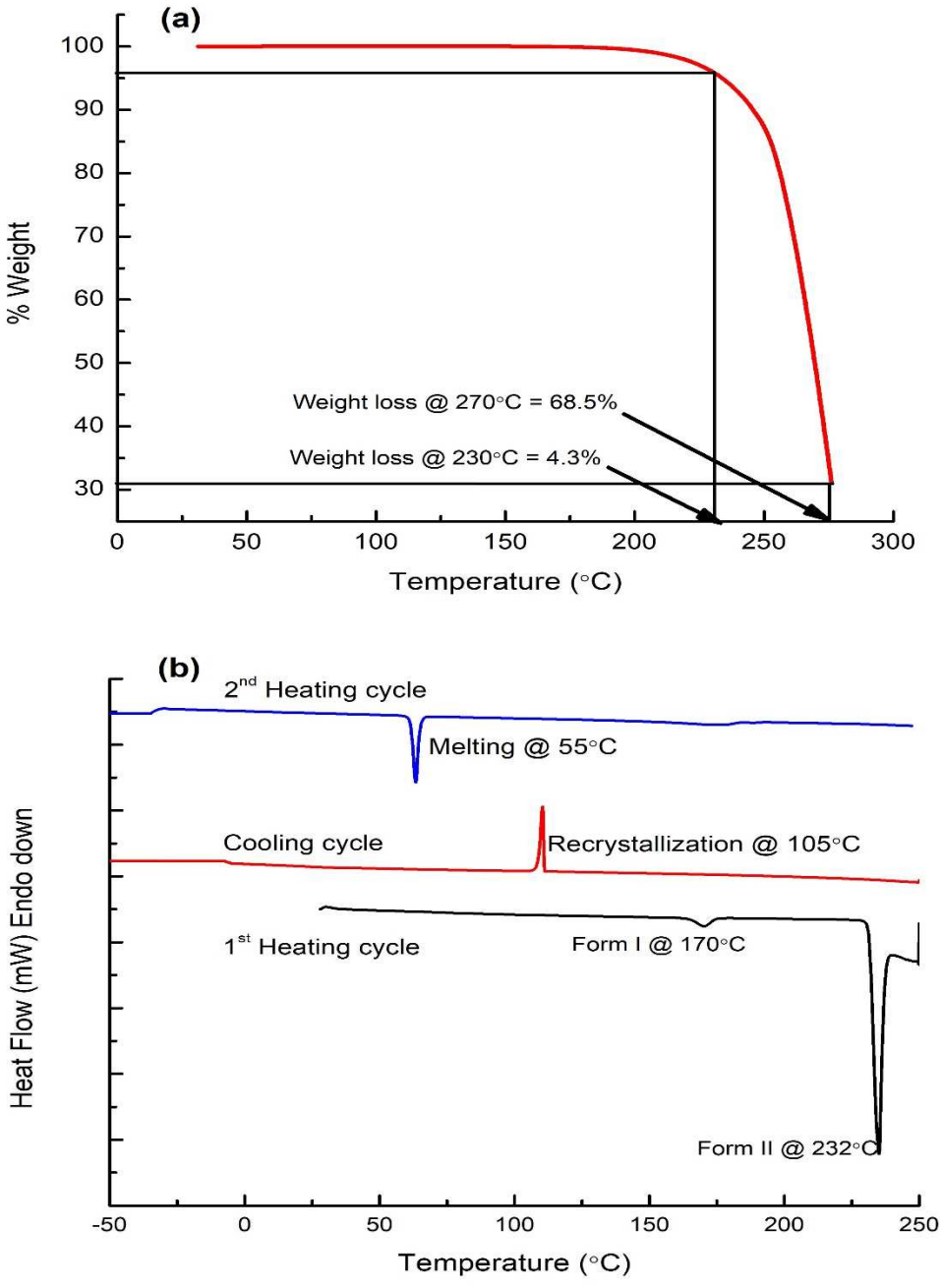

Figure 6: (a) TGA thermogram showing degradation of MFA in the temperature range between 180 °C and 270 °C, (b) DSC thermogram showing recrystallization of MFA during heat-cool-heat cycle

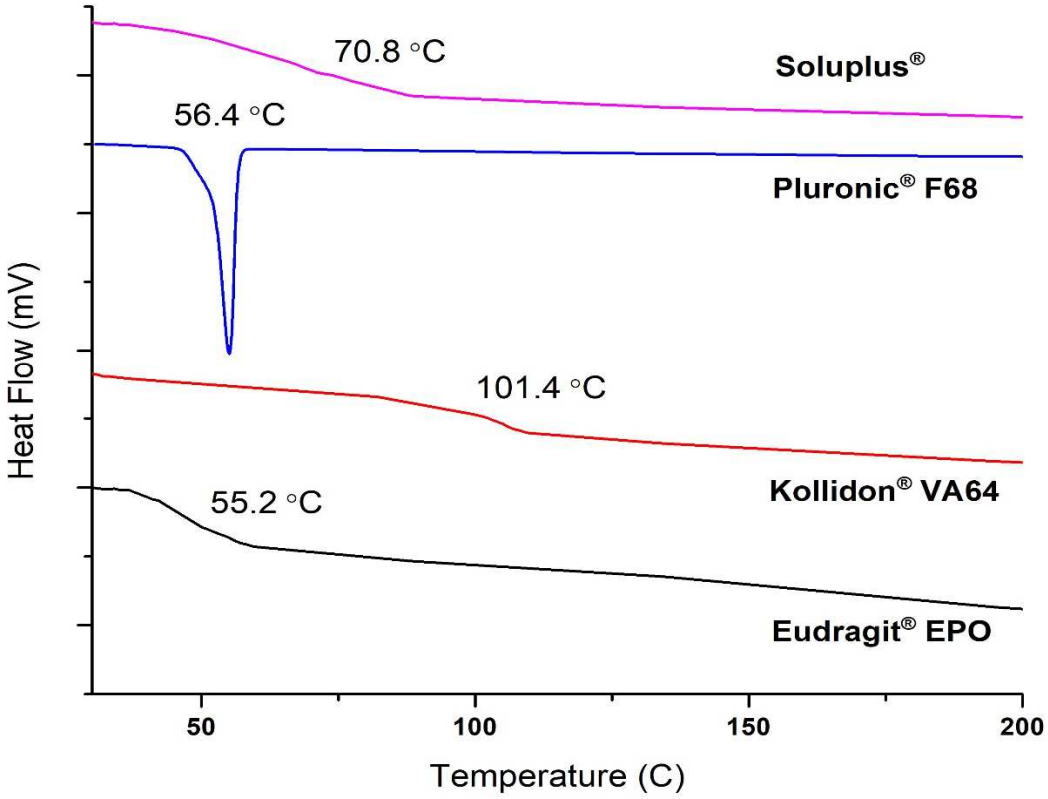

Figure 7: DSC curves of polymers showing their glass transition temperature

4.2. Calculation of Solubility Parameters

4.2.1. Hildebrand and Hansen Solubility Parameters

The values of the solubility parameters of MFA and the polymers estimated according to Hildebrand and Hansen method have been summarized in Table 4. It was observed that the values of the solubility parameter of the polymers were very similar according to both Hildebrand and Hansen method. However, the value of Hildebrand solubility parameter for MFA was found to be 20.40 $MPa^{0.5}$ whereas that of Hansen solubility parameter was 23.59 $MPa^{0.5}$. The difference between the two values was mainly due to the fundamental difference between Hildebrand and Hansen methods. In the Hildebrand method, the solubility parameter was calculated using only the cohesive energy density of the molecules whereas in Hansen method, the solubility parameter is dependent on the dispersive, polar and hydrogen bonding forces in a molecule. Irrespective of the method used, both Hildebrand and Hansen approach demonstrated that the difference in the solubility parameter between MFA and the polymers was < 7 $MPa^{0.5}$ that indicates a good miscibility between MFA and the polymers according to Greenhalgh (68). Upon comparing the values of Hildebrand solubility parameters of MFA and the polymers, it can be inferred that MFA would have good miscibility with F68 due to a very small difference in the values of solubility parameters of the two ($\Delta\delta$ = 0.04 $MPa^{0.5}$). Based on the solubility parameters of MFA and the polymers, it can be predicted that the order of miscibility of MFA in the four polymers according to the Hildebrand solubility parameter will be F68> EPO> SLP> VA64. The values of the Hansen solubility parameter of the drug and the polymers also indicated that MFA would exhibit the highest miscibility with F68 with the order of its miscibility in the four

polymers being F68> SLP> VA64> EPO. To further understand the effect of solubility parameters on drug-polymer miscibility, Bagley plot was constructed using the Hansen solubility parameters.

Table 4: Physicochemical properties and the calculated values of Hildebrand and Hansen solubility parameters of mefenamic acid (MFA) and Eudragit® EPO, Soluplus®, Kollidon® VA64, and Pluronic® F68

Material	F_{di} $(J/cc)^{0.5}.mol^{-1}$	F^2_{pi} $(J/cc)^{0.5}.mol^{-1}$	E_{hi} (J/mol)	V (cc/mol)	Hildebrand solubility, δ	Hansen solubility, δ_t	Interaction parameter, χ	
							Hildebrand	Hansen
MFA	4390	220720	13100	185.8	20.40	23.59	-	-
EPO	6010	2270	26000	350.2	20.17	19.47	0.0040	1.268
SLP	4300	2690	56000	238.7	25.16	20.22	1.6970	0.849
F68	2470	1800	46000	140.6	26.19	19.81	2.5085	1.071
VA64	1700	490	40500	97.7	20.36	21.52	0.0002	0.320

4.2.2. Construction of Bagley Plot

The Bagley plot (Fig. 8) represents the three-dimensional solubility parameters determined using the three intermolecular forces (δ_d, δ_p , δ_h) in a two-dimensional plot (δ_v, δ_h) according to Bagley *et al.* (62). It was observed from the plot that MFA was close to EPO indicating good miscibility between MFA and EPO. The distance between the drug and the polymer in the Bagley plot referred as $R_{a,v}$ was calculated according to the following equation:

$$R_{a,v} = \sqrt{(\delta_{v2} - \delta_{v1})^2 + (\delta_{h2} - \delta_{h1})^2} \quad (34)$$

According to Bagley *et al.*, when the $R_{a,v}$ value is <5.6 $MPa^{0.5}$, the drug and the polymer are miscible and when the $R_{a,v}$ values is > 5.6 $MPa^{0.5}$, it indicates that the drug and the polymer are immiscible. The $R_{a,v}$ values were found to be 4.70 $MPa^{0.5}$, 1.73 $MPa^{0.5}$, 1.09 $MPa^{0.5}$ and 1.08 $MPa^{0.5}$ for MFA-EPO, MFA-SLP, MFA-VA64 and MFA-F68, respectively. Based on the $R_{a,v}$ values, one can therefore conclude that MFA will be miscible in all the four ploymers. By comparing the values of Hildebrand solubility parameters and Hansen solubility parameters, and the Bagley plots, it can be seen that three methods predicted the miscibility of MFA differently in different polymers. The Hildebrand approach predicted that MFA would have a good miscibility with EPO whereas the Hansen approach predicted that MFA would have good miscibility with VA64. The Bagley plots predicted that MFA would have a good miscibility with SLP. This discrepancy between the three approaches was possibly due to the fundamental difference in the calculation of the solubility parameters and the methodology used to

predict the miscibility. While the Hildebrand approach is based on the calculation of the cohesive energy density of the molecules, the Hansen approach is based on calculating different intermolecular forces in a molecule. However, it should be noted that all the theoretical approaches indicated that the drug MFA will be miscible in all the four polymers. This shows that the assumption that a difference in the solubility parameter, $\Delta\delta$, of < 7 $MPa^{0.5}$ between the drug and the polymer does not always indicate miscibility. However, since these are theoretical estimates, these results were, therefore, validated using the melting point depression method which is an experimental approach.

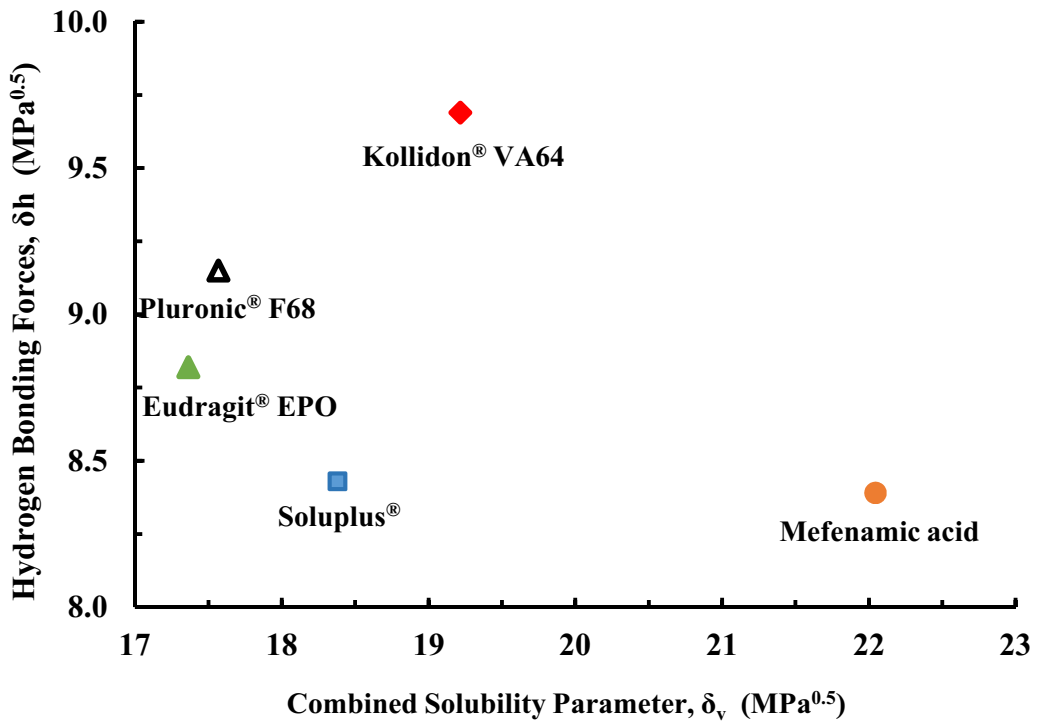

Figure 8: Bagley plots of hydrogen bonding forces as a function of combined solubility parameter for mefenamic acid, Eudragit® EPO, Soluplus®, Kollidon® VA64, and Pluronic® F68

4.3. Melting Point Depression of Mefenamic acid in Various Polymers

The plots of melting point depression of MFA as a function of polymer fraction in various polymers are shown in Figure 9 and the numerical data are given in Table 5. From Figure 9, it can be seen that the melting point of MFA decreased rapidly in the presence of SLP, followed by EPO, VA64, and F68. The melting endotherm of MFA was not observed after 60%, 75%, 75% and 50% concentration of MFA-EPO, MFA-SLP, MFA-VA64 and MFA-F68, respectively. This indicates concentration-dependent miscibility of MFA with the four polymers. It was interesting to observe that the melting temperature of MFA changed with the polymer. This was possibly due to difference in the thermal conductivity and melt viscosity of the polymers. The absence of melting endotherm in the case of MFA-SLP and MFA-VA64 below 75% MFA may be due to the presence of MFA in microcrystalline form at the melting temperature. In that case, the value of heat of fusion, ΔH_f, of these crystals was too low to be detected by DSC. However, based on the results from melting point depression, it can be concluded that MFA had concentration-dependent miscibility with both EPO and SLP. To further understand the miscibility of MFA in the four polymers, mathematical models were used to estimate the value of drug-polymer interaction parameter, χ, and the mole fraction of MFA dissolved in the polymer, x_{drug}.

Table 5: Depression in the melting point of mefenamic acid (MFA) with increasing concentration of Eudragit® EPO, Soluplus®, Kollidon® VA64, and Pluronic® F68

MFA (% w/w)	Melting Temperature of Mefenamic acid (ºC)			
	Eudragit® EPO	**Soluplus®**	**Kollidon® VA64**	**Pluronic® F68**
95	230.30±0.46	231.10±0.22	230.68±0.72	230.15±0.95
90	228.64±0.26	229.50±0.21	229.64±0.34	229.95±0.68
85	226.81±0.32	227.11±0.16	228.21±0.51	229.64±1.22
80	224.71±0.85	223.41±0.58	227.28±0.56	229.13±0.94
75	221.98±0.65	218.93±0.42	225.04±0.87	228.57±0.86
70	218.20±0.97	-	-	227.64±0.75
60	208.86±1.32	-	-	225.40±1.06
55	-	-	-	223.87±0.65
50	-	-	-	221.85±1.33

* The data are presented as mean ± standard deviation (n=3).

**The blank spaces in columns indicate that no melting endotherm was observed for these drug-polymer concentrations.

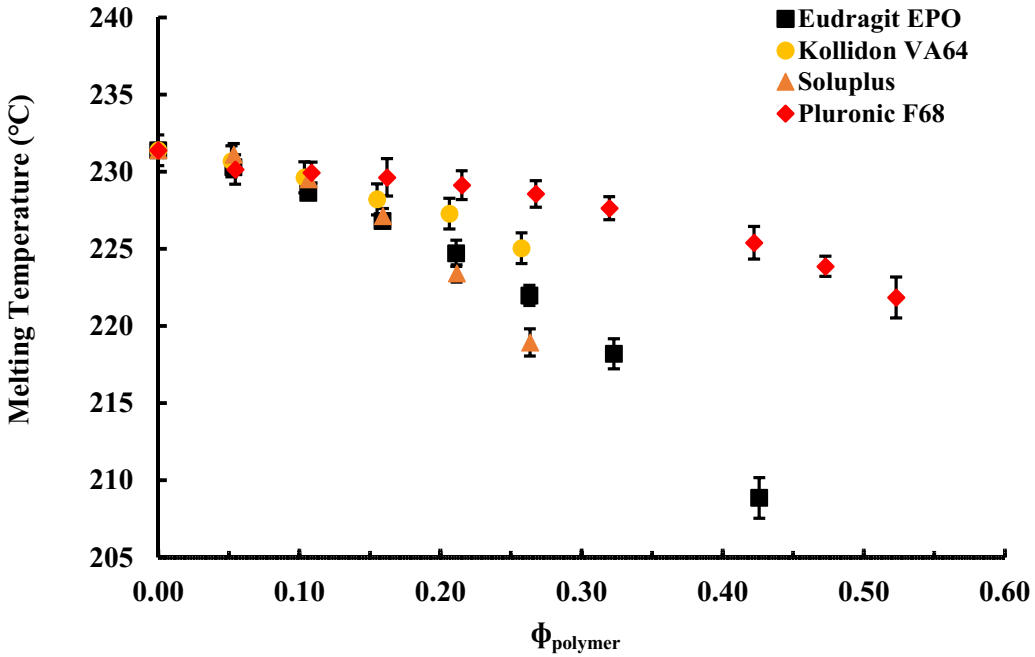

Figure 9: Plot showing depression in the melting point of MFA as a function of polymer fraction (by volume) in the drug-polymer mixture. The error bars represent mean ± standard deviation (n=3).

4.4. Estimation of Drug-Polymer Interaction Parameter from Melting Point Depression Data

The melting point depression of MFA resulting because of polymers may be used to estimate the value of drug-polymer interaction parameter, χ. In the present investigations, the relationship between an increase in the polymer concentration in the drug-polymer mixture resulting in a decrease in the melting point of MFA was plotted according to eq. (6) (Fig. 10). A linear relationship was observed for all the drug-polymer mixtures which allowed for the estimation of the value of interaction parameter, χ, from the slope of the fitted line. A negative value of the interaction parameter was observed for MFA-EPO, MFA-SLP and MFA-VA64 mixtures indicating good drug-polymer miscibility. A positive value of the interaction parameter was observed in MFA-F68 mixtures indicating that they were immiscible or poorly miscible. Also, a closer look at the MFA-EPO plot shows a lack of linearity at higher concentration of MFA (Fig. 10). This suggests a dependence of the interaction parameter, χ, on the composition of the MFA-EPO mixture. This observation is in agreement with the previously reported studies involving mixtures of carbamazepine and Soluplus® (69) and nifedipine and poly(vinyl pyrrolidone) (70). Also, the value of interaction parameter, χ, for MFA-SLP mixture was found to be -3.05 which according to Marsac *et al.* indicates adhesive enthalpic interaction of favorable miscibility between MFA and SLP (42).

The temperature dependence of the interaction parameter exhibits first-order kinetic relationship according to eq. (8). The plot of values of interaction parameter, χ, as a function of 1/T for various drug-polymer mixtures is shown in Figure 11. In the case of MFA-F68 system, a linear relationship between the values of χ and 1/T was observed

across the experimental composition of 80% to 50% MFA in the composition with an R^2 value of 0.7747. In the case of MFA-EPO system, a linear relationship was observed from 80% to 60% MFA composition with an R^2 value of 0.9703. For the MFA-SLP system, a linear relationship was observed from 85% MFA to 75% MFA with an R^2 value of 0.9896. Similarly, for the MFA-VA64 system, a linear relationship was observed from 85% to 75% MFA with an R^2-value of 0.9859. A non-linear relationship was observed at lower values of 1/T that corresponds to higher temperature and high drug loading. This is in line with previously reported studies where non-linearity was observed at high drug loading in the case of indomethacin-PVP-VA64 system (70) and felodipine-Soluplus® and felodipine-HPMCAS systems (28). The regression equation from the linear region in Figure 6 was used to estimate the entropic (A) and enthalpic (B) constants of corresponding drug-polymer mixtures. These values were used to obtain the value of interaction parameter at various temperatures which were subsequently used to estimate the mole fraction of MFA dispersed in the polymeric carrier according to eq. (16).

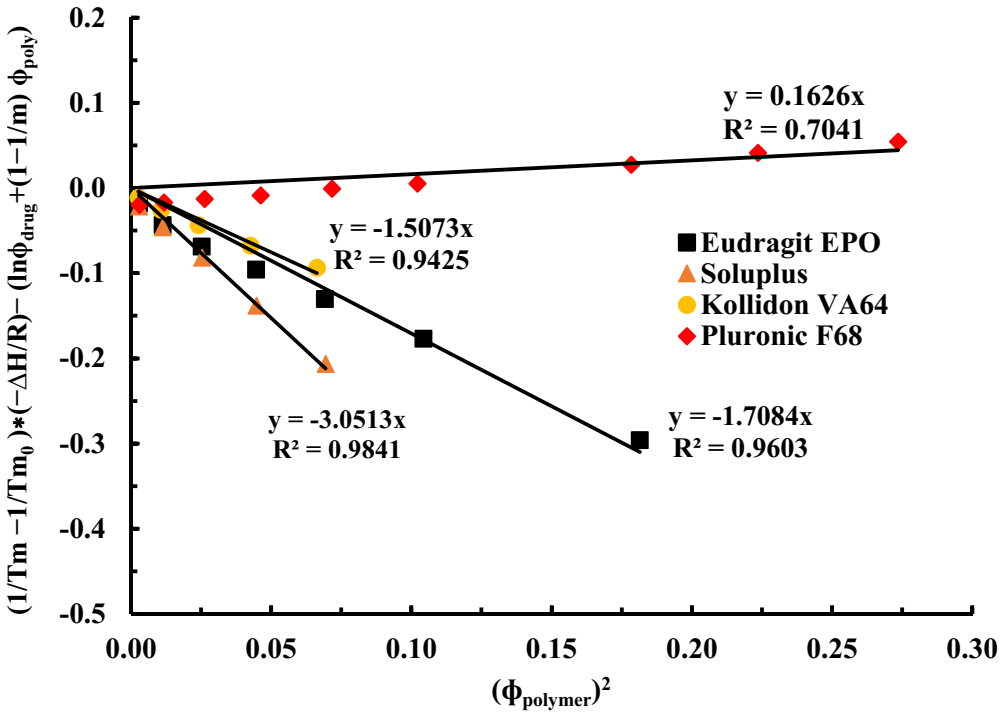

Figure 10: Estimation of interaction parameter of mefenamic acid in various polymers

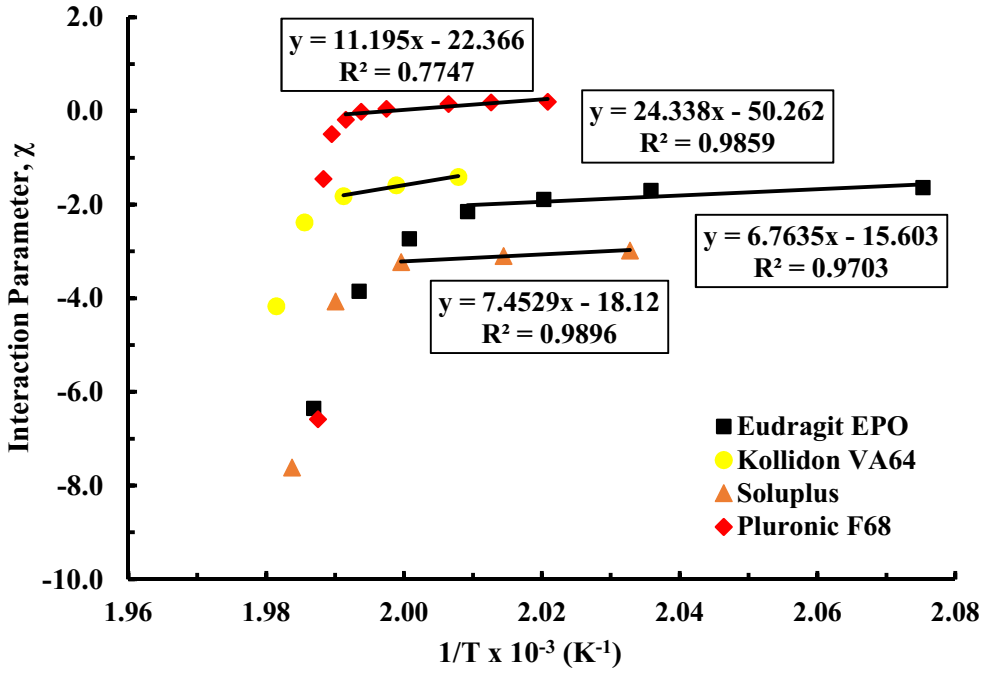

Figure 11: Plot of the value of the drug-polymer interaction parameter, χ, as a function of temperature.

4.5. Estimation of Gibbs Free Energy of Mixing

The Gibbs free energy of mixing, ΔG_{mix} indicates the energy change (enthalpy) and the disorderliness (entropy) in a drug-polymer mixture. A negative value of ΔG_{mix} indicates miscibility and a positive value indicates immiscibility between drug and the polymer. Since the drug-polymer mixtures are non-ideal systems, the total Gibbs free energy of mixing is expressed as $\Delta G_{mix}/RT$. Estimation of $\Delta G_{mix}/RT$ at various temperatures helps to determine the critical processing temperature required for complete mixing of the drug and the polymer. The plot of Gibbs free energy of mixing, $\Delta G_{mix}/RT$, as a function of volume fraction of MFA in the four polymers at various temperatures is shown in Figure 12. It was observed that the interaction parameter significantly affected the Gibbs free energy of mixing of MFA in all the four polymers. At room temperature (25 °C), the Gibbs free energy of mixing, $\Delta G_{mix}/RT$, was positive for all the drug-polymer mixtures, indicating immiscibility. As the temperature increased, the values of Gibbs free energy of mixing, $\Delta G_{mix}/RT$, decreased and eventually became negative, indicating miscibility. In the case of the MFA-VA64 system, the effect of temperature on the Gibbs free energy of mixing was found to be significant compared to other drug-polymer mixtures.

The temperature at which the Gibbs free energy becomes negative depended on the polymer. In the case of MFA-F68 and MFA-VA64 system, the Gibbs free energy was negative at 200 °C, and in the case of MFA-SLP and MFA-EPO, it was at 140 °C. These temperatures indicate the formation of a homogeneous mixture that was thermodynamically stable at all drug-polymer compositions. The information from these plots is helpful in setting up the processing conditions in hot-melt extrusion.

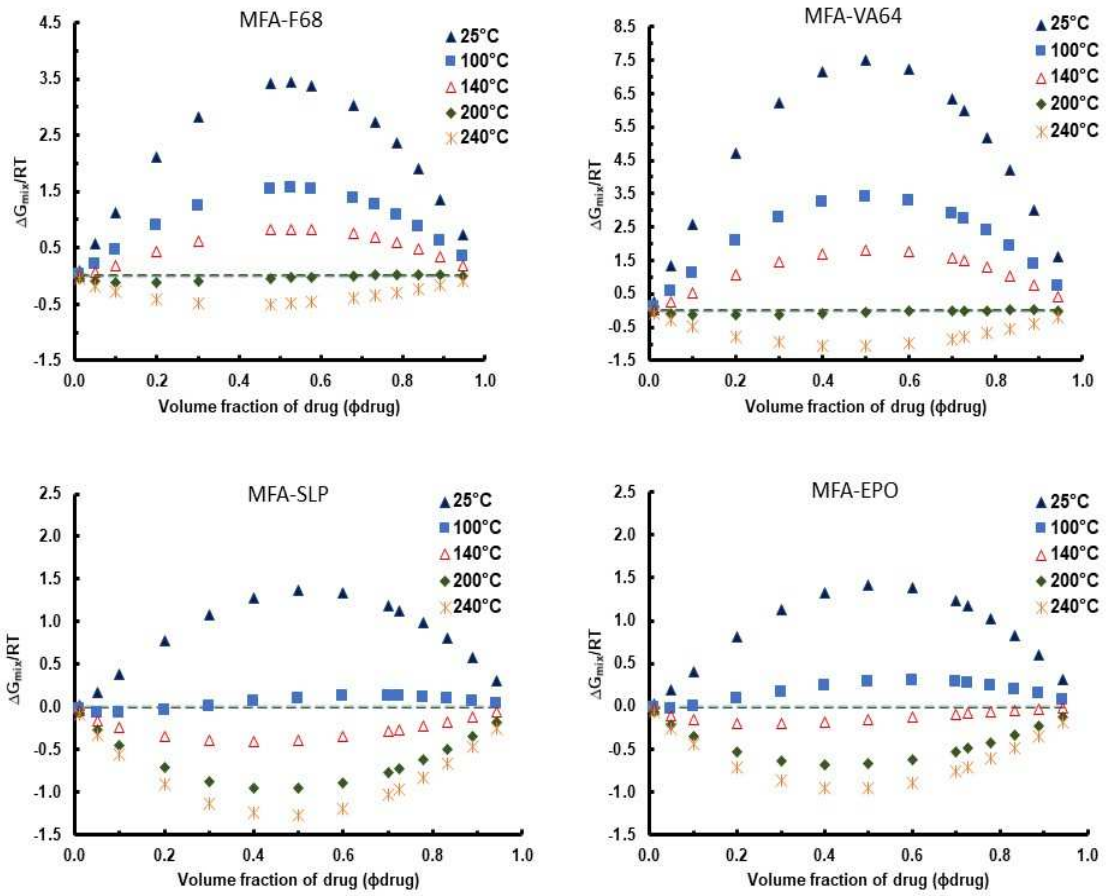

Figure 12: Plots of the values of Gibbs free energy, ΔGmix/RT, versus volume fraction of the drug, ϕdrug, for drug-polymer mixtures at 25 °C, 100 °C, 140 °C, 200 °C, and 240 °C

4.6. Validation of Gibbs Free Energy Plots

The polarized light microscopy images of MFA in various polymers at different temperatures are shown in Figure 13. The morphology of the MFA crystals at 50 °C was distinct in different polymers. While sharp needle like crystals were observed in case of MFA-VA64 (Fig. 13(j)), small rod like crystals were observed in case of MFA-F68 (Fig. 13(d)). In the case of MFA-EPO and MFA-SLP, the drug crystals were present as small aggregates along with the polymer (Figs. 13a and 13g). The morphology of the crystals at room temperature itself indicated that MFA had good miscibility with EPO and SLP. The onset temperature is the point where the MFA crystals just start to melt and dissolve in the polymeric matrix. In case of MFA-EPO system, the onset temperature was observed at around 130 °C (Fig. 13)) and almost all the MFA crystals were dissolved in EPO by 150 °C (Fig. 13c). These results were in accordance with the Gibbs free energy plots which predicted that the upper solution critical temperature (USCT) of MFA in EPO in between 100 - 140 °C. Similarly, the USCT of MFA-F68 and MFA-VA64 were found to be in between 180 °C - 200 °C (Figs. 13f and 13l)) and for MFA-SLP it was found to be in between 130 °C - 150 °C (Fig. 13i). These results were in accordance with the predicted values of the Gibbs energy plots (Fig. 12) which establishes the validity between the theoretically predicted and the experimentally observed values. These values can be further used in establishing the processing temperatures for hot melt extrusion.

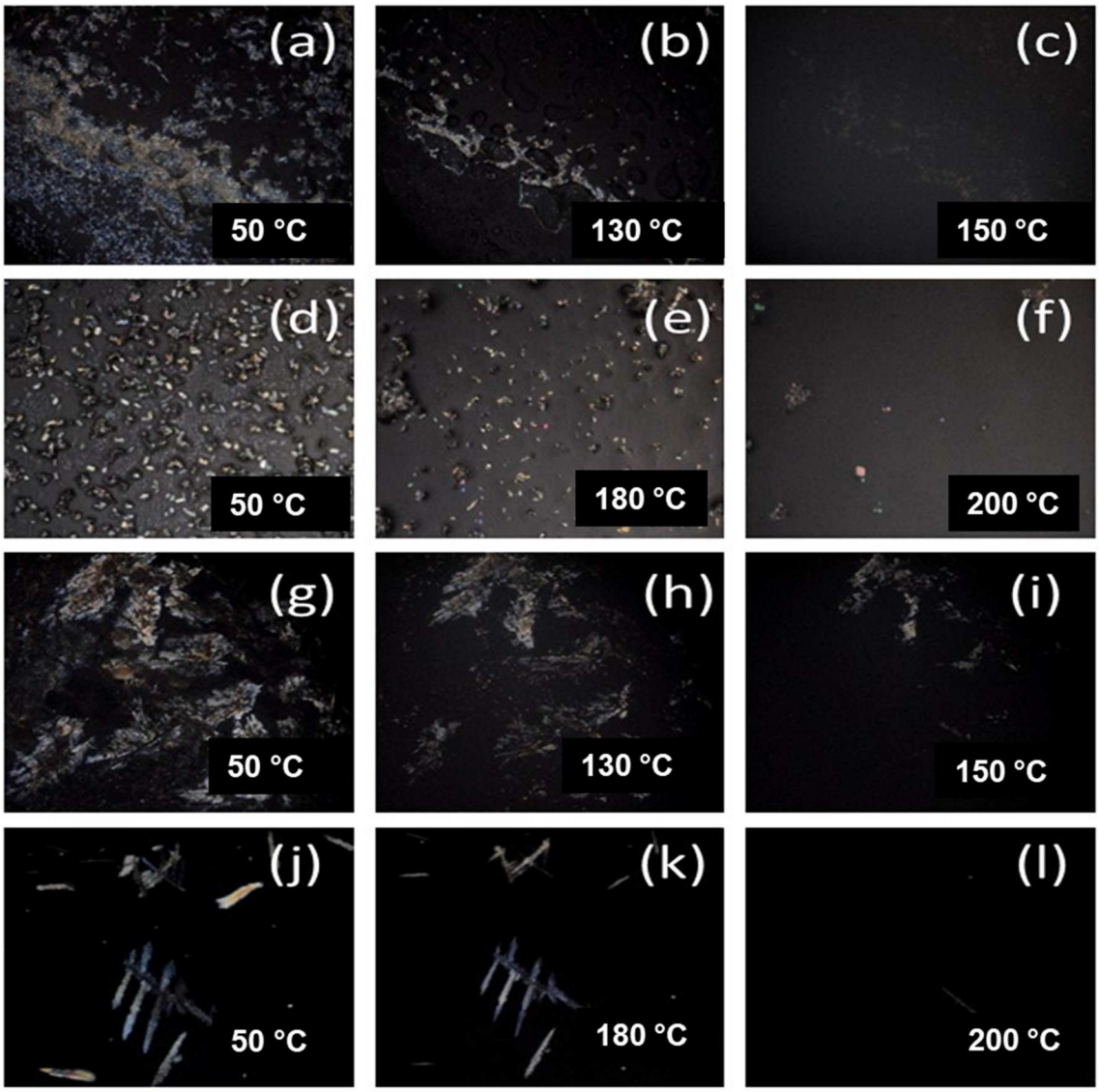

Figure 13: Polarized light micrographs of 1:1 ratio of MFA-EPO at 50 °C (a), 130 °C (b), and 150 °C (C); MFA-F68 at 50 °C (d), 180 °C (e), and 200 °C (f); MFA-SLP at 50 °C (g), 130 °C (h), and 150 °C (i); and MFA-VA64 at 50 °C (j), 180 °C (k), and 200 °C (l)

4.7. Determination of Solubility, Miscibility and Glass Transition Curves

A typical thermodynamic phase diagram consists of a solubility curve, a miscibility curve and a glass transition curve. Initially, the activity coefficient, γ_{drug} of MFA in the polymers was estimated using Hansen solubility parameter. Later, these values were used to estimate the value of x_{drug} which is mole fraction of molecularly dispersed drug in the polymer using solid-liquid equilibrium (SLE) equation. This information was used to construct the solubility curve according to F-H lattice theory.

4.7.1. Estimation of Activity Coefficient of Mefenamic acid in Various Polymers

The value of activity coefficient of MFA in various polymers was calculated using to eq. (12) for various drug-polymer mixtures with MFA concentration in the mixture ranging from 2.5% w/w to 50% w/w. Figure 14 shows plots of temperature dependence of the values of activity coefficient, γ_{drug}, for various drug-polymer mixtures. The drug-polymer miscibility is expected to increase with an increase in the temperature due to an increase in the mobility of the drug and the polymeric molecules. The dotted lines in the plots shown in Figure 14 indicate the ideal mixing in which case the value of activity coefficient is 1 (i.e., $\ln\gamma_{drug} = 0$). From the plots, it can be observed that the activity coefficient of MFA was dependent on the ratio of MFA in the drug-polymer mixture for all the four drug-polymer mixtures. An increase in the concentration of MFA in the mixture resulted in an increase in the value of activity coefficient of the drug, γ_{drug}. However, for all the drug-polymer mixtures, the value of activity coefficient was found to be <1 (i.e., $\ln\gamma_{drug} < 0$) for up to 25% w/w MFA at room temperature (25 °C). Frank *et al.* have reported that a solid solution is formed when the value of the activity coefficient,

γ_{drug} <1 (71). According to this, MFA should form a solid solution with all the four polymers at room temperature at a drug loading of 25% w/w and lower. However, in the present study, this was not the case as the results of the melting point depression showed that MFA was immiscible in all the four polymers at a drug loading of 25% at room temperature. This clearly shows that the value of the activity coefficient of MFA in the four polymers was underestimated due to its mathematical form. In eq. (12), it can be clearly seen that the difference in the magnitude of dispersion, hydrogen bonding and polar forces between the drug and the polymer determine the value of the activity coefficient. However, it does not consider the fact that even when the difference in the magnitude is lower for one of the three forces, the drug and polymer will be miscible in each other. While estimation of the value of activity coefficient using eq. (12) include contribution of all types of intermolecular forces equally which resulted in the values of activity coefficient of MFA obtained with the four polymers to be relatively low that resulted in overestimation of drug-polymer miscibility.

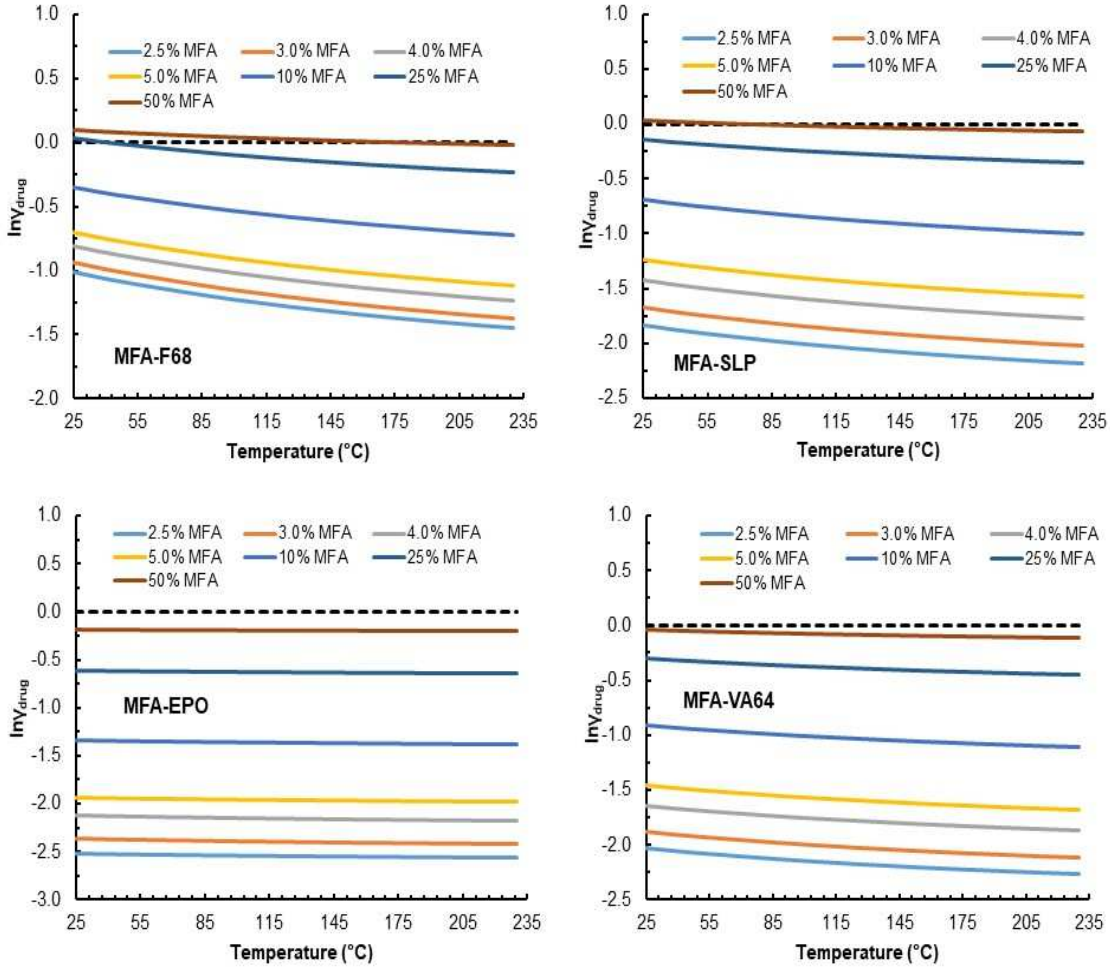

Figure 14:Plots demonstrating the change in the value of activity coefficient, γdrug, of MFA as a function of temperature. The figure legends indicate % weight fraction of the drug (MFA) in the drug-polymer mixture.

4.7.2. Estimation of Mole Fraction Solubility of Mefenamic acid in Various Polymers

The mole fraction of MFA dispersed in the four polymers studied as a function of temperature was estimated according to eq. (10) and the results are plotted in Figure 15. The horizontal dotted line in the plots indicates the ideal case of complete dissolution of MFA in the polymers. It can be observed from the plots that the mole fraction solubility of MFA in all the polymers was composition-dependent at room temperature whereas it was found to be independent of drug composition (up to 5% w/w) at higher temperatures. In the case of the MFA-SLP mixture, the complete dissolution of MFA in SLP was observed at ~125 °C. In the case of MFA-EPO, it was observed at ~150 °C, for MFA-F68 it was observed at ~200 °C, and for MFA-VA64 it was observed at ~205 °C. The temperature at which the mole fraction of MFA dispersed in the polymers was less than 0 ($x_{drug} = 0$) is termed as the critical temperature (T_c). At this critical temperature, MFA starts to disperse in the polymer. For MFA-SLP and MFA-EPO system, the critical temperature was found to be dependent on the composition of MFA in the mixture whereas in the case of MFA-F68 and MFA-VA64, it was found to be independent of the composition. The critical temperature was found to be in between 85-95 °C for MFA-SLP, 90-110 °C for MFA-EPO, 175-185 °C for MFA-F68, and 195-200 °C for MFA-VA64. This information will be helpful to fix the processing conditions during hot-melt extrusion.

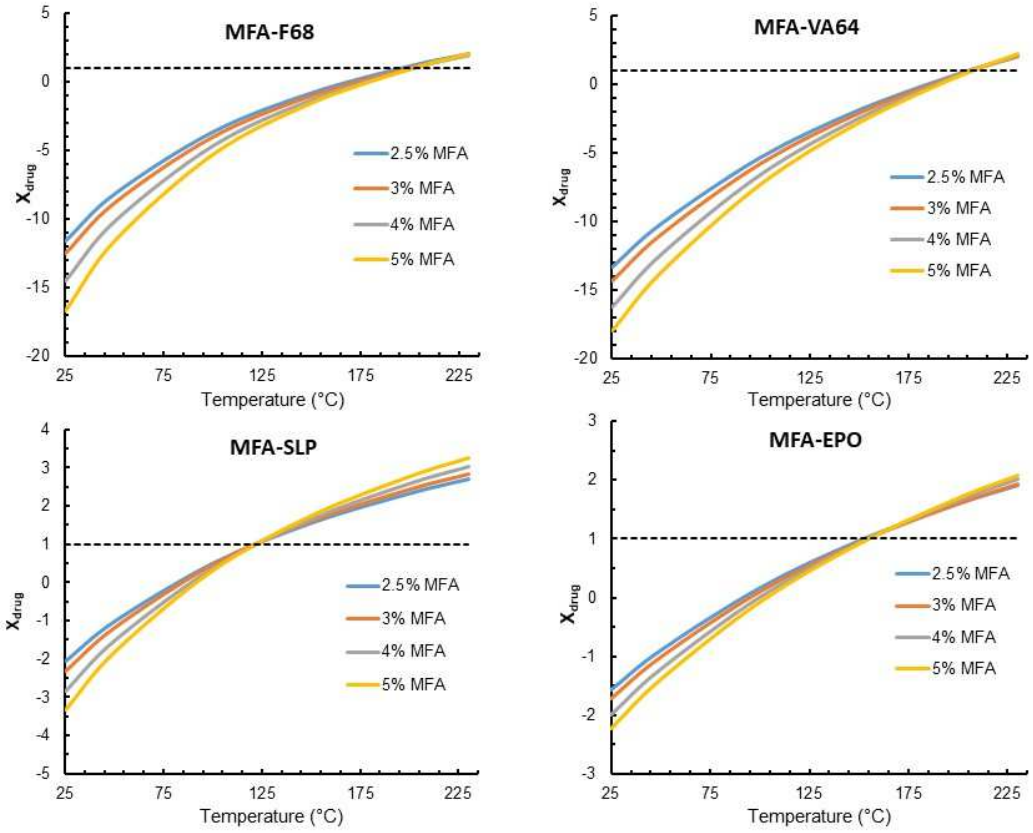

Figure 15: Plots demonstrating the change in the mole fraction of dispersed MFA as a function of temperature estimated using Flory-Huggins theory. The figure legends indicate % weight fraction of the drug (MFA) in the drug-polymer mixture.

Another approach to estimate the mole fraction of MFA dispersed in the polymeric carrier is by use of solid-liquid equilibrium (SLE) equation. According to eq. (11), the mole fraction of MFA dispersed in the polymers was estimated using the values of the activity coefficient of MFA in the polymers obtained using eq. (12). The mole fraction, x_{drug}, of MFA dispersed in the polymers as a function of temperature is presented in Figure 16. The results demonstrated that the mole fraction of MFA dispersed in the polymer increased as a function of temperature, however, an increase in the concentration of MFA in drug-polymer mixture led to the decrease in the miscibility of MFA in the polymer. At lower temperatures (i.e., < 75 °C), the drug-polymer miscibility was found to be independent of drug-polymer composition, however, at higher temperatures, the miscibility was composition-dependent and decreased with an increase in the concentration of MFA in the mixture. Ideal mixing was observed for up to 5% w/w concentration of MFA in the mixture which indicates complete molecular dispersion of MFA in all the four polymers. Unlike the results obtained from Flory-Huggins theory, no negative values were obtained for x_{drug} using the solid-liquid equilibrium (SLE) equation. A closer look at the plots in Figure 16 shows that the mole fraction, x_{drug}, of MFA dispersed in the polymers is both dependent on temperature and drug loading, making it difficult to determine the solubility curve using the theoretical approach. Therefore, a simple and novel approach was used in the current study to determine the solubility of MFA in the polymers.

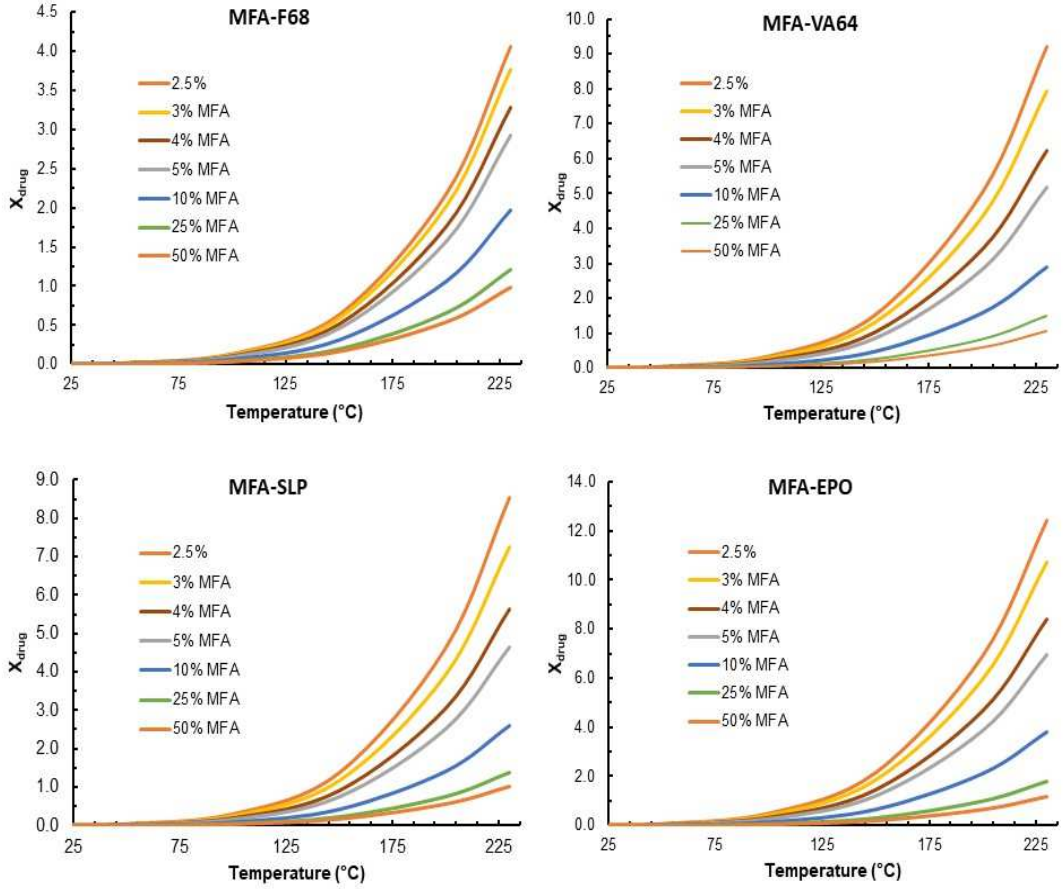

Figure 16: Plots demonstrating the change in the mole fraction of dispersed MFA as a function of temperature estimated using the solid-liquid equilibrium (SLE) equation. The figure legends indicate % weight fraction of the drug (MFA) in the drug-polymer mixture.

4.7.3. Determination of Solubility Curve Using Melting Point Depression Data

A melting point is the temperature at which the drug crystal overcomes the lattice energy and gets dissolved in the polymeric matrix. While it is easy to determine the melting point of MFA in drug-polymer blends with higher drug loading, it is challenging to estimate the melting point of MFA at lower drug loading. However, it was indirectly estimated using the melting point depression data. A relationship was established between the weight fraction of the drug and melting temperature using a polynomial equation. This relationship was used to estimate the melting temperature of the drug at lower drug loadings. The plots between the melting temperature and weight fraction of MFA in various polymers is shown in Figure 17. In all the drug-polymer blends, the melting point data fitted well with the weight fraction of MFA using a polynomial equation with R^2 values of > 0.99. Based on the polynomial equation, the melting point of MFA at various drug loadings was determined and this data was used to estimate the solubility curve.

4.7.4. Determination of Miscibility Curve and Glass Transition Curve

A miscibility curve represents the boundary above which the drug is present at a supersaturated state and undergoes spontaneous phase separation. Unlike solubility curve, there are no reported experimental techniques in the literature to estimate the miscibility of drug and polymer with respect to drug loading and temperature. Therefore, in the current study, miscibility of MFA in the polymers was estimated according to eq. (16) using the enthalpic and entropic constants obtained from the melting point depression

data. The glass transition curve was plotted according to the Gordan Taylor equation using the glass transition temperature of MFA and the polymers.

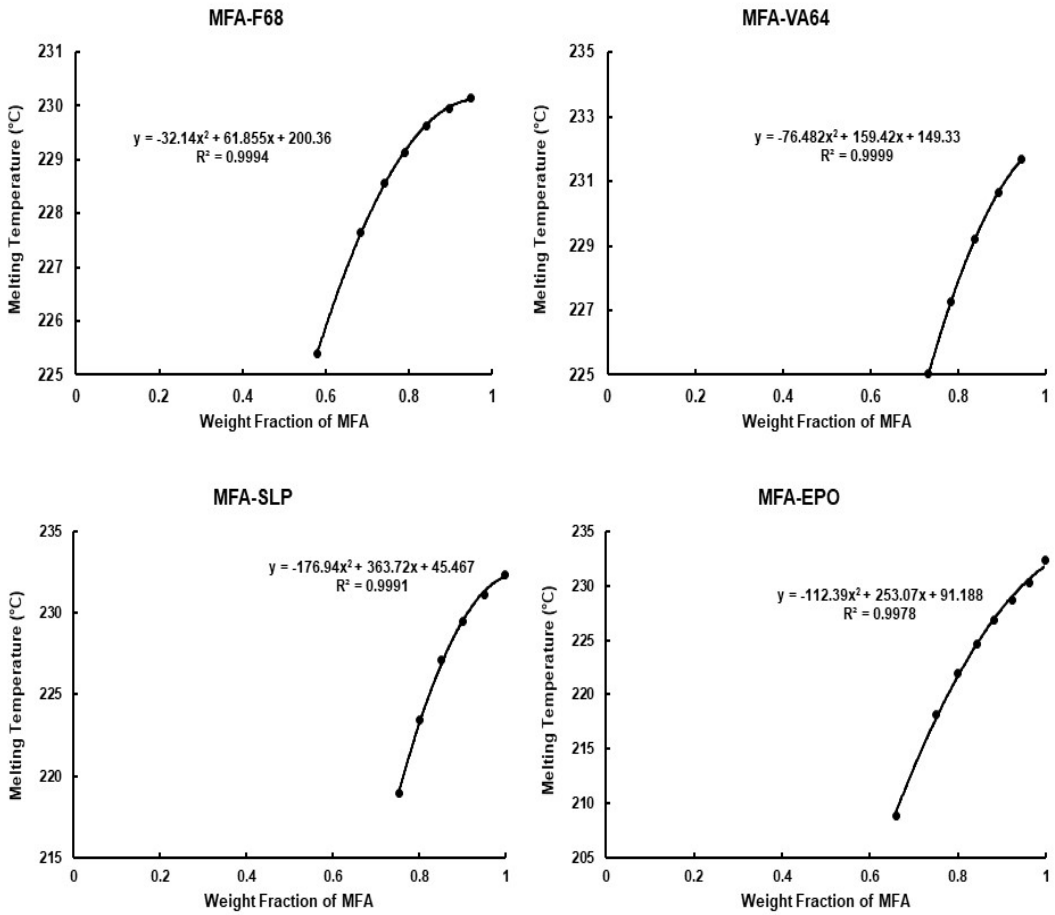

Figure 17: The plots showing a polynomial relationship between the melting temperature and the weight fraction of MFA in various polymers

4.7.5. Construction of Thermodynamic Phase Diagrams

The thermodynamic phase diagrams of MFA in the four polymers are shown in Figure 18. The solubility curve represents the boundary where the fraction of MFA is dissolved into the polymeric matrix. A miscibility curve represents the boundary above which the drug is present at a supersaturated state and undergoes spontaneous phase separation. The glass transition curve, T_g predicted using the Gordan-Taylor equation indicates the molecular mobility of the drug and the polymer within the amorphous solid dispersion system. In the region above the T_g curve, phase separation is thermodynamically favored due to increase in the mobility of the polymeric strands, which reduces the activation energy for nucleation and subsequently, crystal growth. Below the T_g curve, the system remains stable due to the kinetic hinderance caused by the polymeric strands. The region between the miscibility curve and the solubility curve indicate the metastable zone where the drug-polymer system remains stable at temperatures below T_g but can undergo phase separation at temperatures above T_g. The point where the miscibility curve intercepts the glass transition curve is called Berghmans point (72). It theoretically defines the maximum drug concentration that will be stable without undergoing phase separation until the temperature reaches the T_g of the drug-polymer mixture. By comparing the thermodynamic phase diagrams of MFA in the four polymers, the miscibility of MFA is higher in case of EPO, followed by SLP, F68 and VA64. The Berghmans point was found to be around 13% w/w of MFA in both MFA-EPO and MFA-SLP systems. However, the metastable zone is narrow in case of MFA-SLP system, indicating that a small fluctuation in the formulation can lead to phase separation.

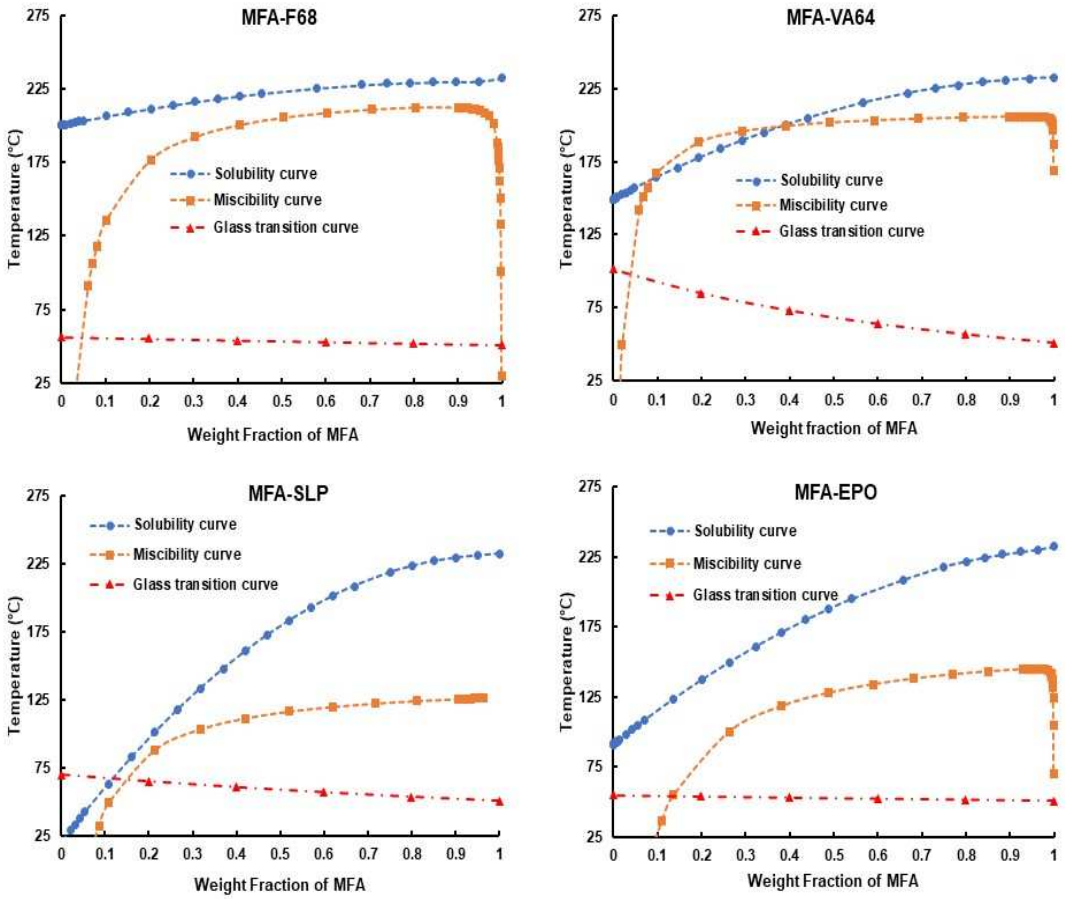

Figure 18: Thermodynamic phase diagrams of MFA in the four polymers showing the solubility curve, miscibility curve, and the glass transition curve. The arrows represent the Berghmans point of MFA in each polymer.

4.8. Process Optimization of HME Using Material Sparing DSC Method

The critical elements in preparing ASDs using HME are the drug loading, temperature of the heating zones, the screw design, the screw speed (residence time) and the feeding rate of the input material. If the processing temperature is high, it can result in degradation of certain drugs which is detrimental if the degradant is toxic. If the processing temperature is low, insufficient heat energy is available for the crystalline drug to convert into amorphous form, resulting in residual crystallinity. Therefore, it is important to optimize the processing conditions so that minimum drug degradation and minimum residual crystallinity is present in the ASDs. This can be done by understanding the interdependency of drug load, processing temperature and the HME screw speed on the residual crystallinity and drug degradation. However, it requires a lot of experiments and large amounts of drug to run these experiments. Therefore, there is a need to develop a material sparing method to determine the ideal processing conditions for HME, with minimum number of experiments. One such approach could be the use of differential scanning calorimeter (DSC), which is a commonly used analytical technique. Like HME, the thermal energy applied while heating the sample in a DSC breaks the crystal lattice of the drug then the drug becomes miscible in the polymeric matrix depending on its affinity with the polymer. Therefore, DSC has a potential to be a miniature, material sparing, screening tool to determine the optimum processing conditions in the preparation of ASDs using HME. The objective of the following work was to optimize the processing conditions of HME using DSC and response surface methodology. For this purpose, the effect of drug loading, heating rate and temperature on the residual crystallinity and degradation of MFA in EPO was studied using DSC. Initial screening was performed

using film casting method, hot-stage microscopy and TGA to determine the range of experimental conditions. Based on this information, a Box-Behnken experimental design was used to create a total of fifteen experimental runs with an ability to understand the main effect and the interaction effect between the independent parameters; drug loading (X_1), heating rate (X_2) and temperature (X_3), and the dependent variables residual crystallinity (Y_1) and drug degradation (Y_2).

4.8.1. Results of Initial Screening Experiments to Setup the Experimental Design

The initial screening was performed to determine the ideal conditions for the experimental design. The polarized light microscope images of various films prepared using the film casting method is shown in Figure 19. It was observed that at drug loading of less than 40% w/w drug loading (Fig. 19a) a homogeneous film with very traces of MFA crystals were observed. At 45% w/w drug loading (Fig. 19b), small amounts of MFA crystals were observed, indicating recrystallization. In case of 50% w/w drug loading (Fig. 19c), large drug rich regions were observed on the film indicating that MFA recrystallized from the polymeric matrix of EPO. Based on the results from film casting experiments, it could be concluded that a maximum of 40% w/w MFA was miscible with EPO without undergoing recrystallization at room temperature. Alshehri et al. reported that a maximum of 25% MFA was miscible with EPO when processed using HME (73). In another study, Kojima *et al*. reported that a maximum of 24% MFA was miscible with EPO when processed using cryo-milling (74). The higher drug loading achieved in the case of film casting can be attributed to its high mixing efficiency as compared to HME or cryo-milling. In the case of film casting, the drug and polymer are molecularly

dispersed in a common solvent resulting in higher mixing efficiency. In the case of HME and cryo-milling, the mixing efficiency was much lower resulting in drug-polymer dispersions with regions having higher drug concentration. These drug rich regions initiate nucleation, followed by crystal growth and recrystallization of drug. Therefore, it is safe to assume that the maximum drug loading achieved using HME or cryo-milling is always lower than the film casting method. Hence, 40% w/w drug loading was taken as the higher level of drug loading in the experimental design. The lower level of drug loading was taken as 20% w/w based on the published literature and to ensure that a wide range of responses were observed from the experimental design. Based on the results of film casting method, the powder blend containing 40% w/w drug loading was prepared in a mortar and pestle and analyzed under hot stage microscopy. Figure 19 shows the hot stage microscopy images of 40% drug loading at various temperatures. It was observed that at around 60 °C (Fig. 19d), EPO started to transform into rubbery state. At around 100 °C (Fig. 19e), EPO completely transformed into a rubbery state exposing the MFA crystals. At around 140 °C (Fig. 19f), a homogeneous mixture was observed indicating that MFA crystals dissolved into the polymeric matrix of EPO. Although MFA has a high melting point of 231° C, it was miscible in EPO at much lower temperature due to a phenomenon called melting point depression. Once the EPO molecules undergo glass transition, the higher mobility of EPO molecules reduces the chemical potential of MFA crystals, thereby reducing the total energy required to break the crystal lattice. This results in the melting of MFA at much lower temperatures than its melting point (75). The results of the hot stage microscopy (HSM) suggest that the minimum temperature at which MFA and EPO are miscible with each other (at 40% w/w drug loading) is around

140 °C. Therefore, it was taken as the lower level for temperature (X_3) in the experimental design.

The higher level for the temperature and the experimental level for heating rate were determined using TGA analysis. Initially, the % weight loss of pure EPO was determined for upto 250 °C to ensure that the polymer was stable at such high temperature. It was observed that less than 2% of EPO degraded at around 250 °C, which showed that EPO was stable at ahigh temperature. The powder blends containing 40% w/w MFA-EPO were analyzed using TGA at various heating rates. Based on the TGA data, it was observed that the rate of degradation of MFA was dependent on the heating rate of the TGA. Since EPO was proved to be stable at a high temperature, any weight loss observed during the TGA analysis could be attributed to the degradation of MFA. It was evident from the data that most of the MFA underwent degradation at around 220 °C. Therefore, the higher level for the heating temperature (X_3) was taken as 220 °C in the experimental design. The relationship between the TGA heating rate and the % weight loss of MFA at 220 °C is shown in Figure 20. It was observed that at heating rates of 0.1 °C/min to 1 °C/min, the % weight loss of MFA was more than 60%. As the heating rate increased from 1 °C/min to 10 °C/min, the % weight loss decreased exponentially. At higher heating rates of 10 °C/min to 20 °C/min, the % weight loss remained low at around 10%. Since a significant amount of weight loss took place between 1 °C/min to 10 °C/min, these values were taken as the lower lever and higher level for the heating rate (X_2), respectively, in the experimental design.

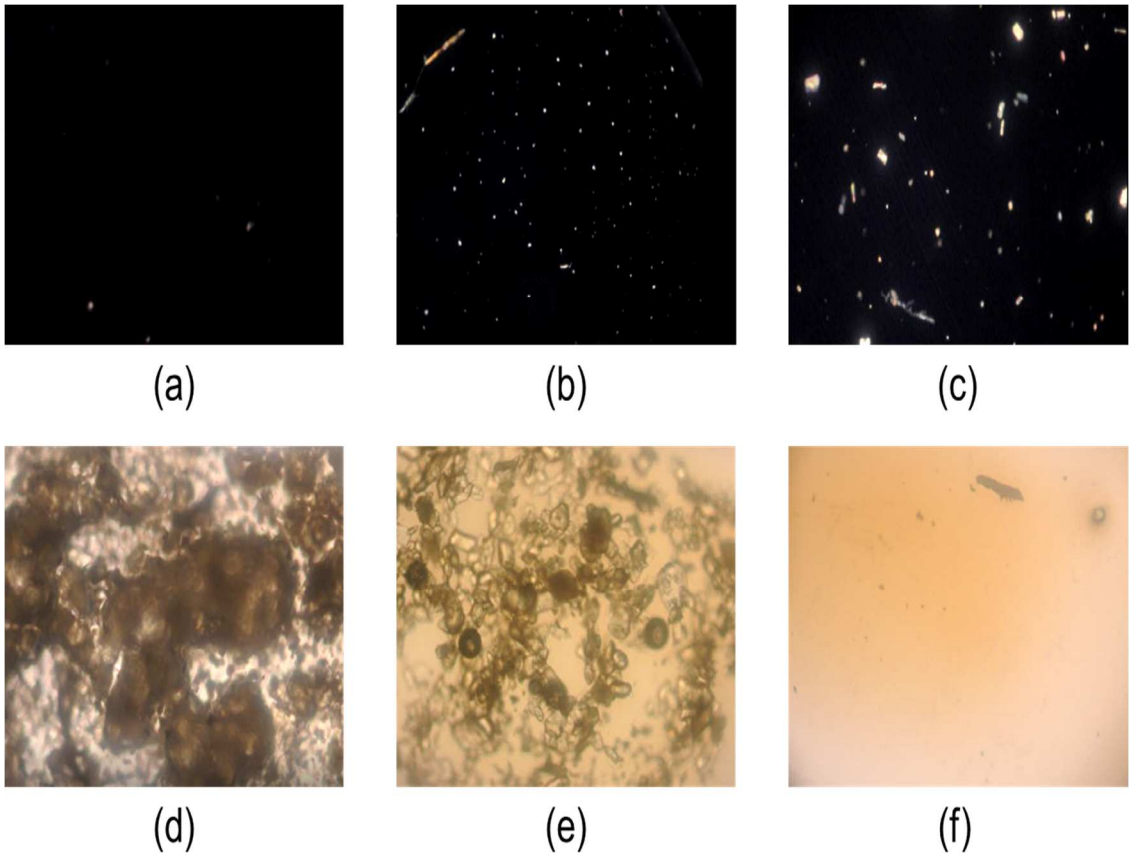

Figure 19: Polarized light microscopy images of films prepared by film casting method: 40% w/w drug loading (a), 45% w/w drug loading (b), 50% w/w drug loading (c). Hot stage microscopy images of 40% w/w MFA-EPO powder blends at 60 °C (d), 100 °C (e) and 140 °C (f).

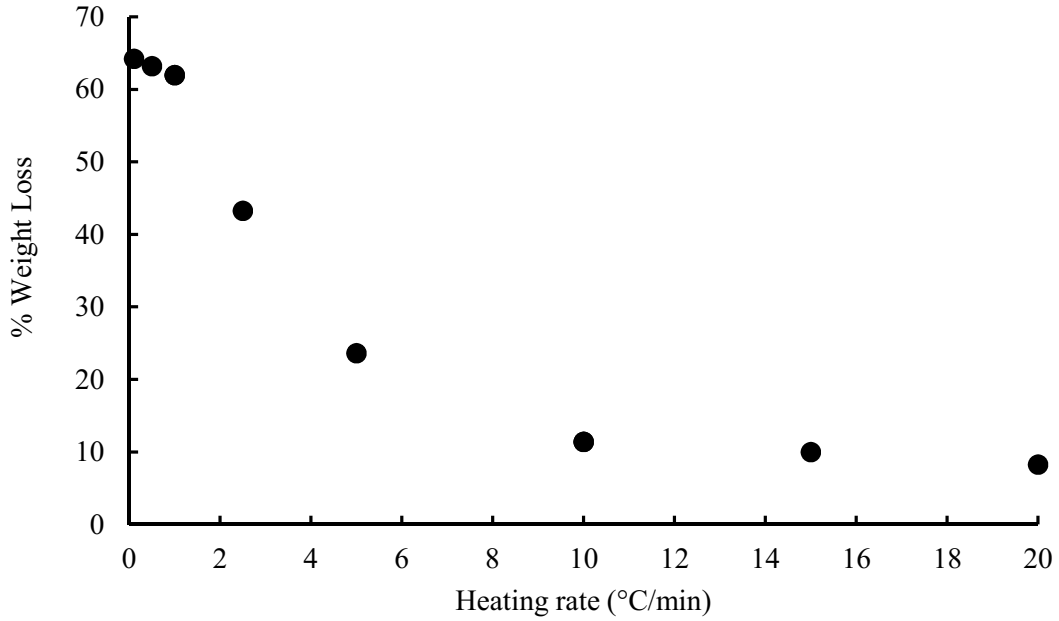

Figure 20: Relationship between % weight loss (drug degradation) at 220 °C and heating rate analyzed using TGA

4.8.2. Box-Behnken Design and Observed Responses

The fifteen experimental runs along with the observed responses are given in Table 6. Within the studied experimental domain, the minimum value of residual crystallinity (Y_1) was found to be 1.0 ± 0.3% and the maximum value was found to be 33.5 ± 4.1%. A minimum % drug degradation (Y_2) was found to be 3.5 ± 0.7% and the maximum value was found to be 26.8 ± 4.2%. Based on the obtained experimental data, it was difficult to determine the effect of each independent parameters on the dependent parameters. Therefore, the observed responses were fitted into various models (linear, cubic and quadratic) to obtain the best fit. It was found that all the responses were fitted into a second-order quadratic polynomial model. The model coefficients that were not significant were eliminated and the significant coefficients including the interaction terms were defined according to the following quadratic equations (Eqs. 35 and 36):

$$\text{Residual crystallinity } (Y_1) = 15.57 + 8.61X_1 + 3.28X_2 - 8.34X_3 + 2.48X_1X_2 - 1.16X_1X_3 - 3.93X_2X_3 + 0.34X_1^2 - 2.79X_2^2 + 0.19X_3^2 \quad \text{(Eq. 35)}$$

$$\text{Drug degradation } (Y_2) = 8.67 + 2.01X_1 - 3.89X_2 + 7.60X_3 - 0.005X_1X_2 + 2.68X_1X_3 - 1.22X_2X_3 - 0.56X_1^2 + 2.54X_2^2 + 2.72X_3^2 \quad \text{(Eq. 36)}$$

Table 6: Box-Behnken experimental design showing the fifteen experimental runs and the observed responses

Run	Drug Load (%)	Heating rate (°C/min)	Temperature (°C)	Residual Crystallinity (%)	Drug Degradation (%)
1	30	5.5	180	16.3 ± 2.3	8.5 ± 2.1
2	30	5.5	180	14.9 ± 1.8	7.1 ± 1.4
3	40	5.5	140	33.5 ± 4.1	3.7 ± 0.4
4	30	1	220	5.7 ± 0.9	26.8 ± 4.2
5	30	10	140	28.1 ± 4.8	3.5 ± 0.7
6	30	1	140	14.3 ± 2.2	8.4 ± 2.3
7	40	5.5	220	14.3 ± 5.1	23.5 ± 4.2
8	30	5.5	180	15.5 ± 2.2	10.4 ± 1.5
9	40	1	180	16.5 ± 3.1	16.0 ± 2.8
10	20	10	180	4.8 ± 1.2	5.3 ± 1.8
11	20	5.5	140	15.6 ± 3.3	3.5 ± 1.3
12	40	10	180	28.6 ± 4.5	7.8 ± 2.2
13	20	1	180	2.6 ± 0.4	13.5 ± 4.2
14	20	5.5	220	1.0 ± 0.3	12.6 ± 3.8
15	30	10	220	3.8 ± 0.7	17.0 ± 2.2

All the experiments were performed in triplicate and the results are expressed as mean±SD (n=3).

The summary of ANOVA results is shown in Tables 7 and 8. It was found that the model was significant for all the studied responses. The lack of fit was found to be not significant which shows that the experimental results had excellent goodness of fit. Based on the experimental coefficients (Eqs. 35 and 36), it can be observed that drug load (X_1) had a significant positive effect and temperature (X_3) had a significant negative effect on residual crystallinity (Y_1). It means, an increase in drug load (X_1) results in increase in residual crystallinity (Y_1) while increase in temperature (X_3) results in decrease in residual crystallinity (Y_1). Also, the combination of heating rate and temperature (X_2X_3) was found to have a negative effect on residual crystallinity (Y_1). In the case of % degradation, temperature (X_3) was found to have a positive effect and the heating rate (X_2) was found to have a negative effect. It indicates that an increase in the temperature and decrease in the heating rate increased the % drug degradation (Y_2). To exhibit the effect of independent factors on the dependent factors, response surface plots and contour plots were plotted using the observed responses.

Table 7: Summary of results from ANOVA showing the residual sum of squares, F statistics and the lack of fit test results

Parameters	**SS**	**DF**	**MS**	**F value**	**P Value**	**Significance**
Residual crystallinity (%)						
Model	1356.42	9	150.71	105.88	<0.0001	significant
Residual	7.12	5	1.42	-	-	
Lack of fit	6.13	3	2.04	4.14	0.2006	not significant
Pure error	0.9867	2	0.4933	-	-	
Total	1363.54	14	-	-	-	
Drug degradation (%)						
Model	700.98	9	77.89	33.57	0.0006	significant
Residual	11.60	5	2.32	-	-	
Lack of fit	6.12	3	2.04	0.7431	0.6137	not significant
Pure error	5.49	2	2.74	-	-	
Total	712.58	14	-	-	-	

Table 8: Statistical analysis of the observed responses showing the best-fit model, regression coefficient and coefficient of variation (% CV)

Responses	**Model**	**R^2**	**Adj R^2**	**Pred R^2**	**SD**	**% CV**
% Residual crystallinity (Y_1)	Quadratic	0.9948	0.9854	0.9264	1.19	8.30
% Drug degradation (Y_2)	Quadratic	0.9837	0.9544	0.8454	1.52	13.60

4.8.3. Response Surface Plots and Contour Plots

Response surface plots exhibit presence of cause and effect relationship among the studied factors for providing enhanced product and process understanding. The contour plots and response surface plots indicating the effect of the independent parameters on the residual crystallinity (Y_1) are shown in Figures 21 and 22.

4.8.4. Effect of Independent Parameters on Residual Crystallinity

The contour plot representing the effect of the final heating temperature of the DSC and the heating rate on the residual crystallinity is shown in Figure 21a. It can be observed that higher heating rate and lower temperature, increased the % residual crystallinity. When the heating rate is high, the total time and energy provided to the sample will be low. As a result, not enough energy is available to break the crystal lattice of the drug thereby resulting in higher % residual crystallinity. Interestingly, the 3D response surface plot (Fig. 21b) shows that at lower heating rate, the temperature did not have any effect on the % residual crystallinity. However, at higher heating rates, the % residual crystallinity decreased linearly with an increase in the temperature. The contour plot representing the effect of the temperature and the drug load on the residual crystallinity is shown in Figure 21c. It was observed that high residual crystallinity was obtained when the drug load was high, and the temperature was low. On the other hand, lower values of residual crystallinity were observed at low drug load and high temperature. When the drug load is high, higher amount of heat energy is required to break the crystal lattice of MFA. To provide such amount of heat, the MFA-EPO dispersions should be heated to higher temperature. When enough heat energy is not

provided, the MFA particles remain in the crystalline form resulting in higher % residual crystallinity. This shows the importance of the processing parameters on the residual crystallinity (76). The 3D response surface plot (Fig. 21d) shows that at low temperatures, the % residual crystallinity increased linearly with an increase in the drug loading. This shows that when an increase in the processing temperature is a limitation for HME processing, then the drug load should be decreased to lower the residual crystallinity. The contour plot representing the effect of the heating rate and the drug load on the residual crystallinity is shown in Figure 21e. At high drug load and high heating rate, high residual crystallinity was observed. The 3D response surface plot (Fig. 21f) shows that at low heating rate, the drug load did not show any significant increase in the residual crystallinity. However, at high heating rate, the drug load significantly increased the residual crystallinity. This is due to the lower amount of heat energy provided when the heating rate is high resulting in higher residual crystallinity.

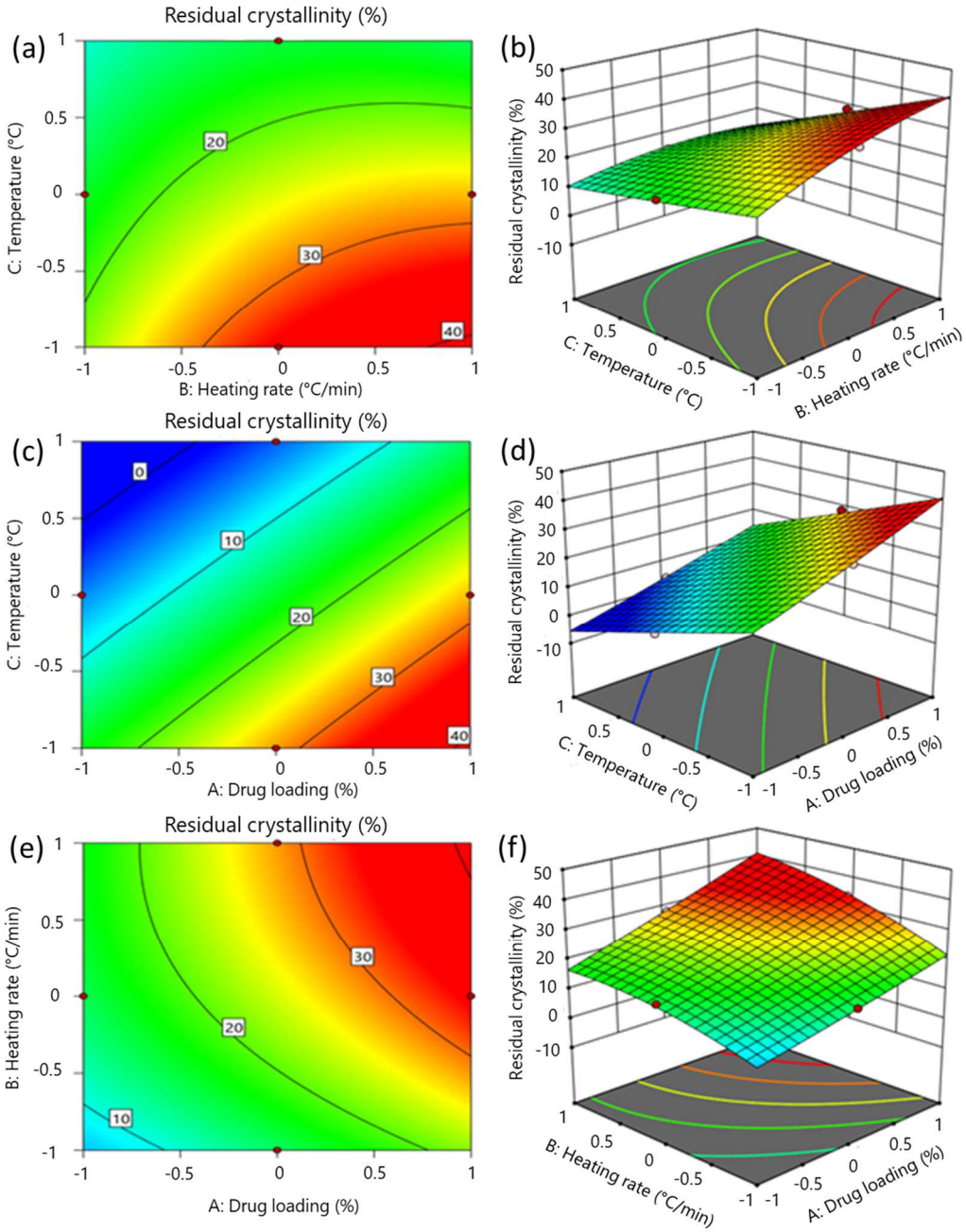

Figure 21: 2D-contour plots and 3D response surface plots showing the effect of independent parameters on the residual crystallinity (%)

4.8.5. Effect of Independent Parameters on Drug Degradation

The contour plot representing the effect of the temperature and the heating rate on the drug degradation is shown in Figure 22a. It was observed that at lower heating rate and high temperature, the drug degradation was high. This was due to the excess thermal energy provided to the drug-polymer dispersions which resulted in breakage of the crystal lattice of MFA and an increase in the molecular mobility. This exposed the carboxylic acid group (-COOH) of the molecule which underwent decarboxylation. The results were in accordance with the thermal decomposition of MFA observed by rapid ESI-MS method as reported by Zhou and Gilpin (67). The authors reported that when MFA was dissolved in a mobile phase consisting of methanol-water (80:20 v/v) and subjected to thermal degradation between 130 °C and 230 °C, MFA was converted to MFA-H^+ which was completely converted to the final decomposition fragment with an m/z value of 224 at a temperature of 230 °C. The 3D response surface plot (Fig. 22b) shows that at lower heating rate, the temperature has a significant effect on the drug degradation. On the other hand, at low temperatures, the % degradation remained constant with increase in the heating rate. The contour plot presenting the effect of the temperature and the drug load on the degradation is shown in Figure 22c. It was observed that high drug degradation was obtained when the drug load and the temperature were high. The 3D response surface plot (Fig. 22d) shows that at low temperature, the drug degradation was low and remained constant with an increase in the drug load. However, at high drug load, the degradation increased significantly with an increase in the temperature. The contour plot representing the effect of the heating rate and the drug load on the drug degradation is shown in Figure 22e. At high drug load and low heating rates, high drug degradation was

observed. The 3D response surface plot (Fig. 22f) also show that high drug load and low heating rate resulted in high drug degradation. However, at lower drug load, the drug degradation was low and did not change with an increase in the heating rate. Based on the response surface plots and the contour plots, it is evident that all the three independent parameters had significant effect on the two studied dependent parameters.

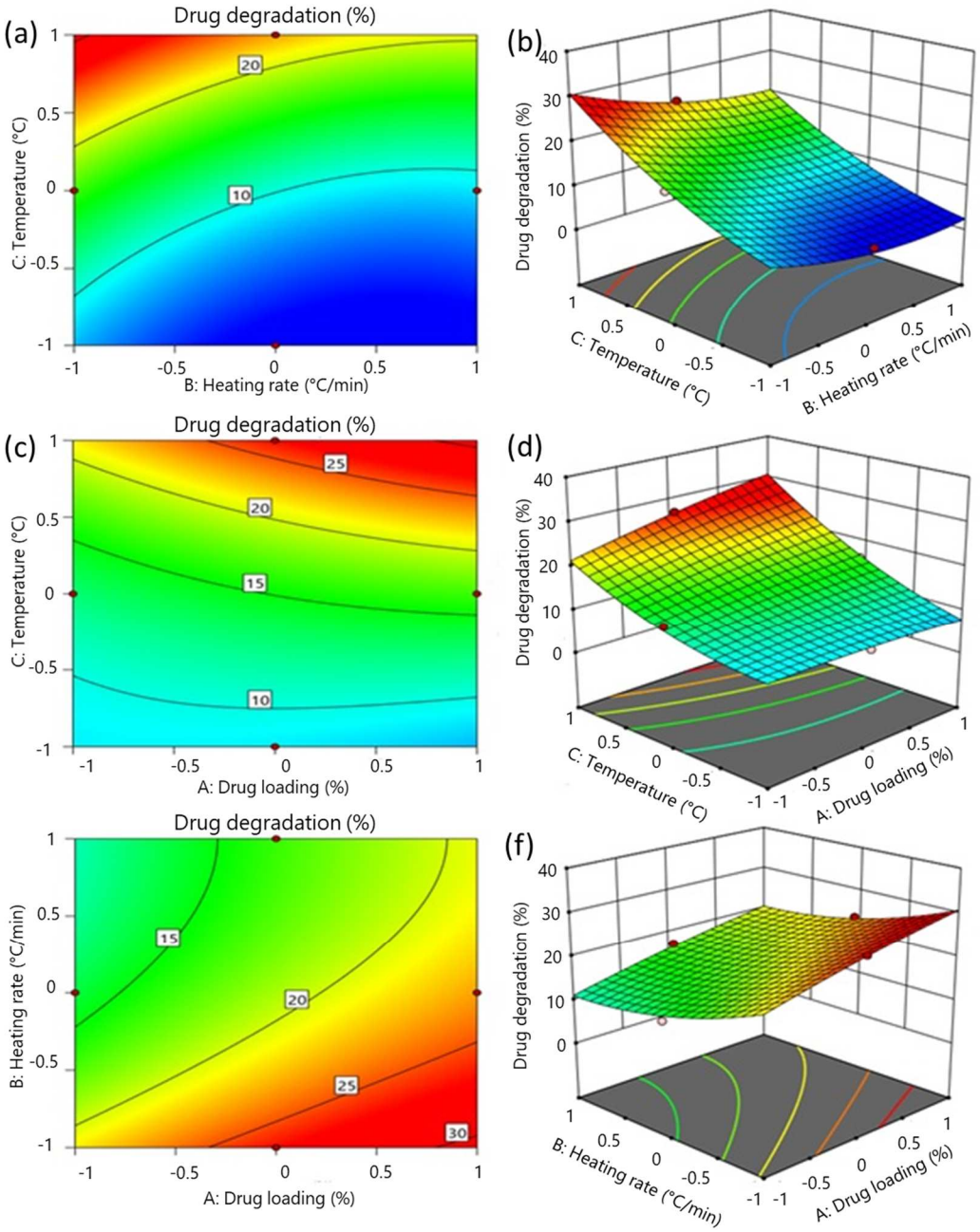

Figure 22: 2D-contour plots and RSA plots showing the effect of experimental variables on drug degradation (%)

4.8.6. Establishment of Design Space

The selection of the optimum formulation was carried out using the numerical and the graphical optimizations. Initially, the target values for residual crystallinity and drug degradation were assigned and the numerical optimization was performed to determine the possible solutions and the desirability values. The optimized batch was selected from among the solutions obtained for the criteria, i.e. maximu drug load, minimum % residual crystallinity, and minimum % drug degradation. The solutions with desirability close to one was considered as the optimum formulation. The results of the numerical optimization are shown in Table 9.

The optimum processing conditions were also selected using an overlay plot using the same constraints as that of numerical optimization. Figure 23 shows the overlay plot between the processing parameters with the design space indicated in yellow shade. The contour lines indicate the boundary lines set for each of the responses. According to the overlay plot, it was found that when powder blend containing 20% w/w drug load was heated at a rate of 5.5 °C/min to the heating temperature of 146 °C, the resulting drug-polymer dispersion contained residual crystallinity of 13.6% with drug degradation of 3.8%. Once the optimum processing conditions was determined, the experimental design was validated by preparing six checkpoint formulations. The experimentally observed values of the six checkpoint formulations were compared with the predicted values from the experimental design.

Table 9: Results of the numerical optimization performed using desirability function. The value of desirability close to 1 was selected.

No.	Drug loading	Heating rate	Processing temperature	Residual crystallinity (%)	Drug degradation (%)	Desirability	
1	-1.000	0.000	-0.858	13.605	3.867	0.698	Selected
2	-1.000	0.000	-0.850	13.541	3.869	0.698	
3	-1.000	0.000	-0.832	13.408	3.876	0.698	
4	-1.000	0.000	-0.915	14.030	3.861	0.695	
5	-1.000	0.000	-0.924	14.100	3.862	0.694	
6	-1.000	0.000	-0.980	14.526	3.876	0.683	
7	-1.000	0.000	-0.989	14.592	3.880	0.680	
8	-1.000	0.000	-0.991	14.603	3.880	0.680	
9	-1.000	0.000	-1.000	14.672	3.885	0.677	
10	0.147	0.000	-1.000	25.540	3.677	0.546	
11	0.348	0.000	-0.996	27.500	3.500	0.531	

* The values of the independent parameters are coded according to the experimental design

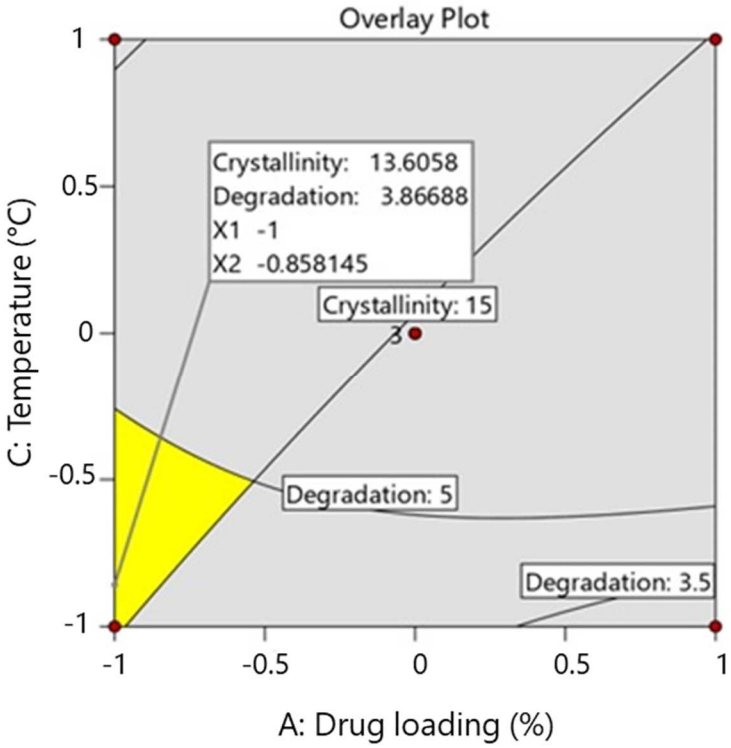

Figure 23: Overlay plot showing the design space established using graphical optimization for minimum residual crystallinity, minimum degradation and maximum drug loading.

4.8.7. Validation of Experimental Design

The design space was validated by preparing six confirmatory formulations within the experimental domain. The linear correlation plots and the residual plots of all the validation batches are shown in Figure 24. The values of bias were found to be 0.018 and -0.61 for residual crystallinity and drug degradation, respectively (Table 10). Low values of bias close to zero (‘0’) indicate that the model was unbiased. The prediction error was found to be 5.72 and 9.94 for residual crystallinity and drug degradation, respectively. Low values of bias and the prediction error indicate the high degree of predictability of the experimental design.

Table 10: The values of bias and percent error calculated from the validation batches

Drug loading (%)	Heating rate (°C/min)	Temp. (°C)	Residual crystallinity (%)			Degradation (%)		
			Pred.	Obs.	Residual	Pred.	Obs.	Residual
25	5	180	11.08	12.1±1.4	0.9815	7.98	8.86±0.28	16.1
25	10	200	4.80	5.4±0.69	0.6291	9.37	9.83±0.97	12.81
20	1	140	7.16	7.9±0.58	0.7333	9.09	10.53±0.78	-4.76
20	5	200	3.84	4.6±0.41	0.7885	9.77	10.46±1.48	-18.64
40	3	140	27.96	25.5±3.9	-2.3992	4.83	5.66±1.06	-15.04
40	10	180	27.48	26.9±2.31	-0.6208	8.78	9.73±1.93	5.83
Bias				**0.018**			**-0.61**	
Percent Error				**5.72**			**9.94**	

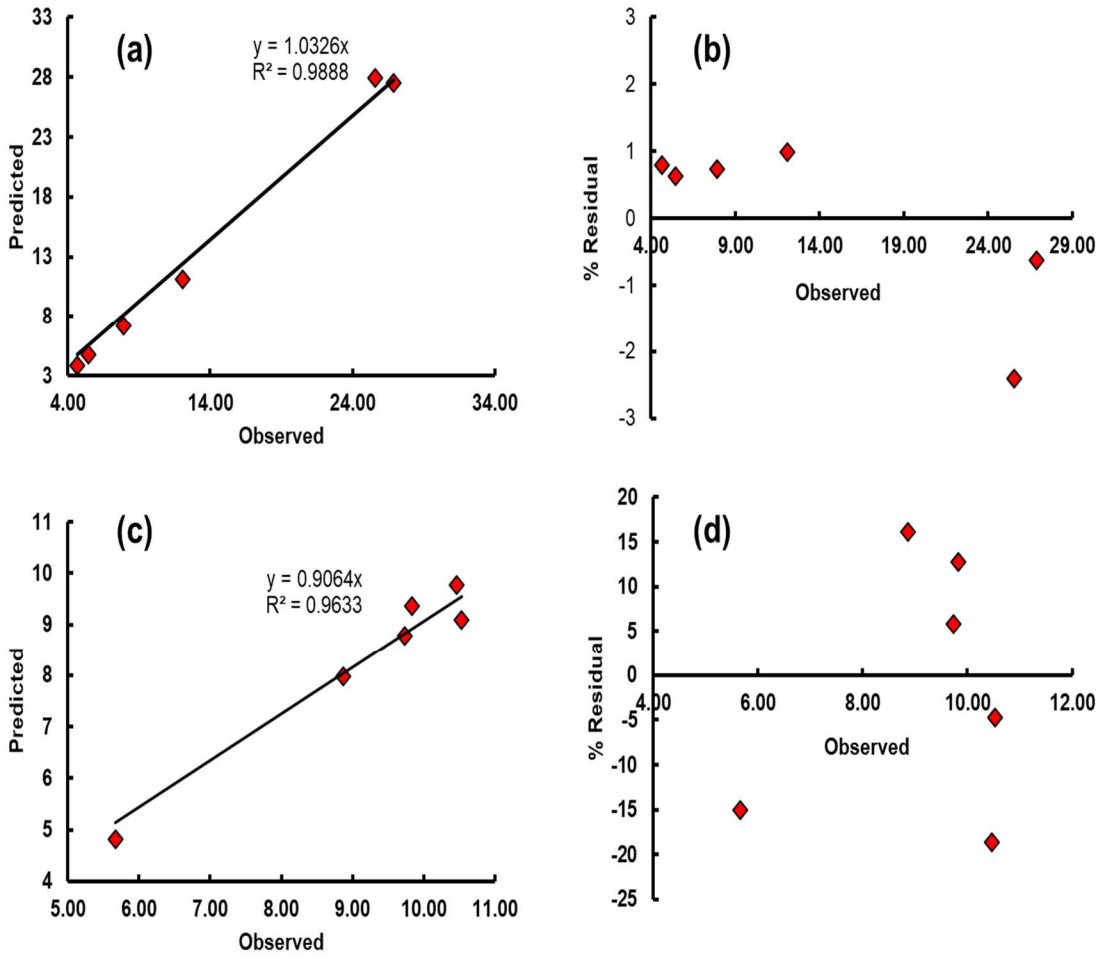

Figure 24: Linear and residual plots between the observed and the predicted values of residual crystallinity (a & b) and drug degradation (c & d), respectively.

4.8.8. Hot Melt Extrusion and Vacuum Compression Molding Samples

Based on the design space obtained from the DSC experiments, 20% w/w MFA-EPO dispersions were prepared using HME and VCM. The drug loading and final heating temperature can be correlated directly with the HME process parameters. However, the heating rate in DSC cannot be correlated to the screw speed in HME. Therefore, three different samples were prepared at three different screw speeds (i.e., 50 rpm, 100 rpm and 150 rpm) to see the effect of screw speed on residual crystallinity and % degradation. The HME filaments prepared at a screw speed of 100 rpm and 150 rpm along with the VCM sample prepared at 150 °C are shown in Figure 25. The drug-polymer dispersions processed in HME at a screw speed of 50 rpm had high torque and did not get extruded. The HME filaments obtained at a screw speed of 100 rpm and 150 rpm looked clear without any visible signs of MFA crystals. However, the filaments obtained at a screw speed of 100 rpm did show slight discoloration. This could be due to the degradation of drug or the polymer. The MFA-EPO dispersions processed in VCM at 150 °C for 3 minutes resulted in a clear dispersion with no evidence of phase separation. To further confirm that the MFA-EPO dispersions prepared using HME and VCM formed a homogeneous dispersion, DSC analysis was done, and the results are shown in Figure 26. In all the three samples, no endothermic peak of the drug was observed indicating that the MFA converted into amorphous form. Also, a single T_g was observed at around 50 °C which shows that MFA was molecularly dispersed in EPO and there was no phase separation. However, the HPLC analysis of the samples showed that 5% of MFA was degraded in the VCM samples. In the case of HME samples, no degradation was observed in filaments processed at 150 rpm as compared to 7.51% drug degradation

in samples processed at 100 rpm (Table 11). This marked increase in MFA degradation at 100 rpm can be attributed to an increase in the residence time as compared to the samples processed at 150 rpm. This shows the significance of the screw speed as an important process parameter in HME. Also, it should be noted that the samples processed in HME are subjected to both thermal and mechanical energy as compared to the samples processed in DSC where only thermal energy is provided. This is the reason why no residual crystallinity was observed in the HME filaments as compared to the samples prepared in DSC. To further confirm that there is no residual crystallinity in the HME and VCM samples, X-ray diffraction analysis was performed, and the results are shown in Figure 27. The X-ray diffractogram of pure MFA revealed characteristic crystalline peaks at 21.3° and 26.3° along with some crystalline peaks of lower intensity at 13.4°, 14.9°, 15.5°. These results suggest that pure MFA obtained from the vendor was a mixture of form I and form II (59, 77). The X-ray diffractograms of drug-polymer dispersions prepared using HME and VCM showed amorphous halo with no characteristic peak of MFA. The results of XRD were in accordance to the DSC results and confirmed that crystalline MFA had completely converted into amorphous form (78,79).

Figure 25: MFA-EPO (20% w/w) ASDs prepared using hot melt extrusion at a screw speed of 150 rpm and 100 rpm and vacuum compression molding (VCM) prepared at 150 °C. The drug-polymer blends processed in HME at a screw speed of 50 rpm had high torque and were unable to form filaments.

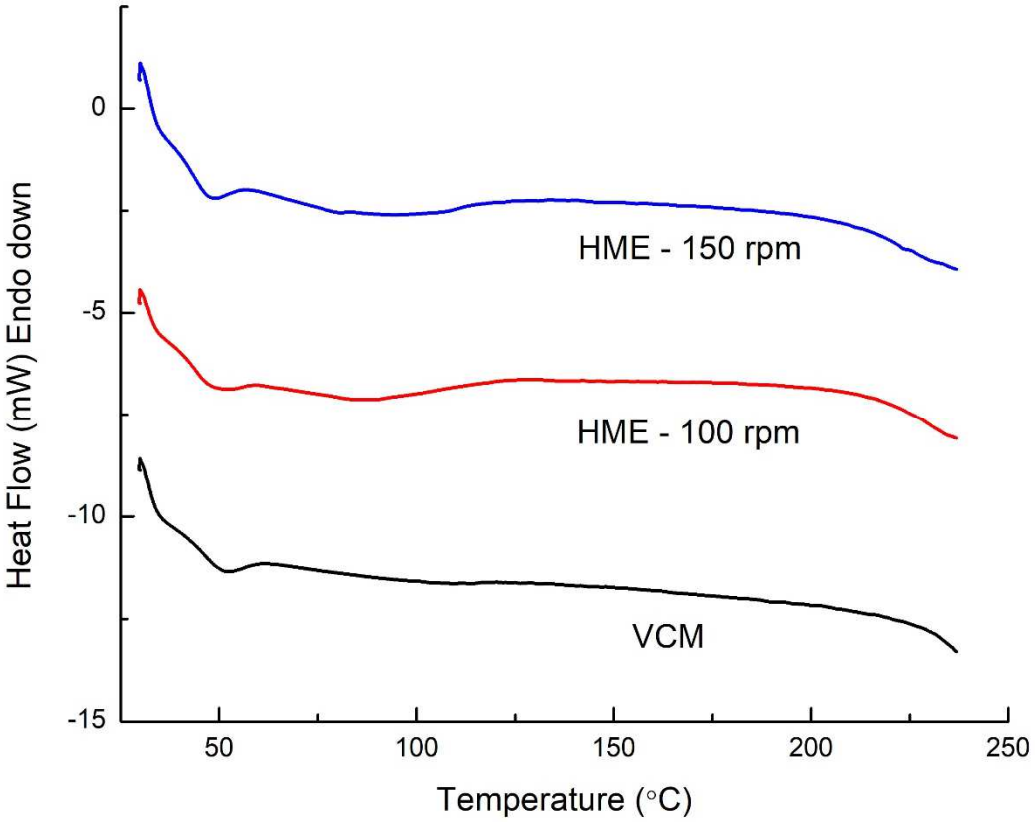

Figure 26: DSC thermograms of 20% w/w drug loaded MFA-EPO dispersions prepared using HME and VCM. A single glass transition temperature was observed in all the samples at around 50 °C indicating that MFA and EPO formed a monophasic system.

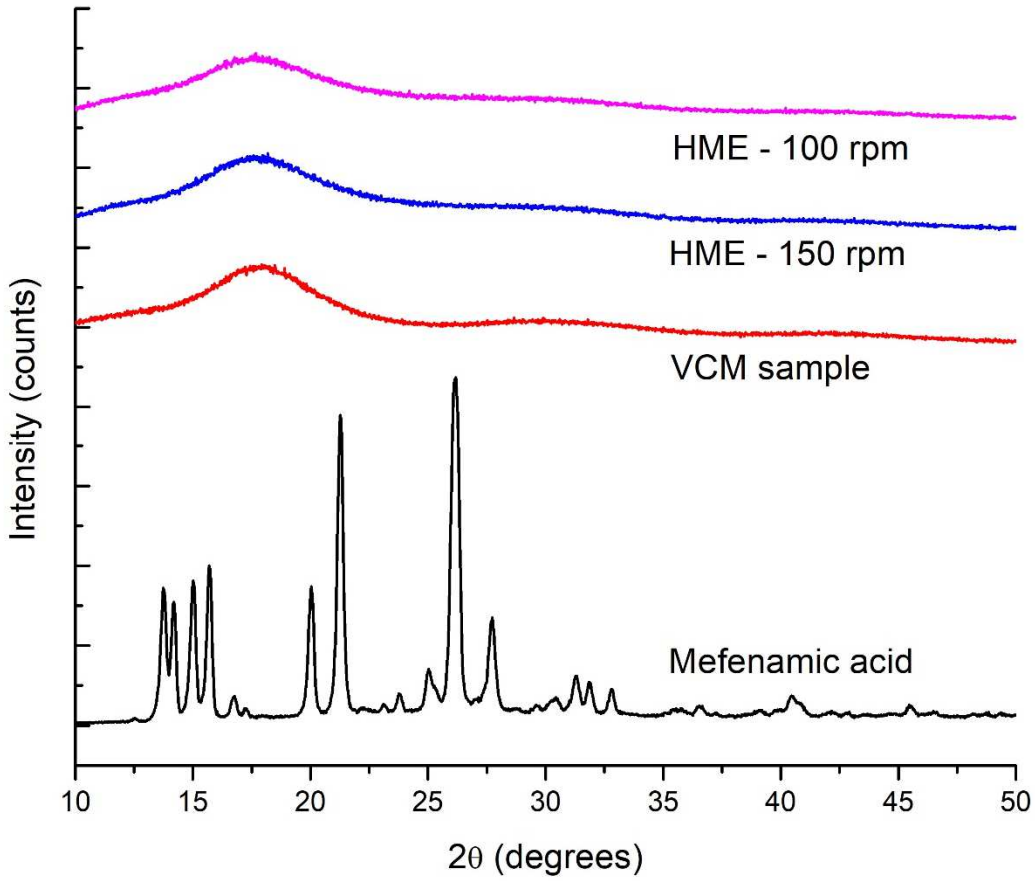

Figure 27: Powder X-ray diffraction scans of pure mefenamic acid, vacuum compression molding (VCM) sample, and hot-melt extrusion (HME) filaments processed at screw speeds of 100 rpm and 150 rpm

Table 11: Residual crystallinity and drug degradation of VCM and HME samples

Sample	**Residual Crystallinity (%)**	**Degradation (%)**
VCM	NA	5.0
HME – 100 rpm	NA	7.51
HME – 150 rpm	NA	NA

* NA indicate that no residual crystallinity/ drug degradation was observed in the samples studied

4.9. Effect of Temperature and Relative Humidity on Recrystalization

4.9.1. Determination of Recrystallization using DSC

The samples prepared using the heat molding method were analyzed using DSC (DSC 6000, Perkin Elmer, USA) to ensure that crystalline MFA was completely converted into an amorphous form. There was no endothermic peak observed in the DSC scans indicating that the MFA crystals were completely converted into amorphous form after the heat molding process. The samples were then stored at various temperature and relative humidity conditions and the DSC scans were performed at various time points. The DSC scans of 40% w/w drug loaded MFA-EPO solid dispersions at 40 °C and 75% RH are shown in Figure 28. It was observed that the value of heat of fusion increased with time indicating recrystallization. Figure 29 shows the rod shaped crystals of MFA observed under a microscope. This indicates that recrystallization of MFA takes place in a rod shaped with a dimensionality value, n=2. This helps to determine the recrystallization rate constant, k, using the non-linear regression analysis.

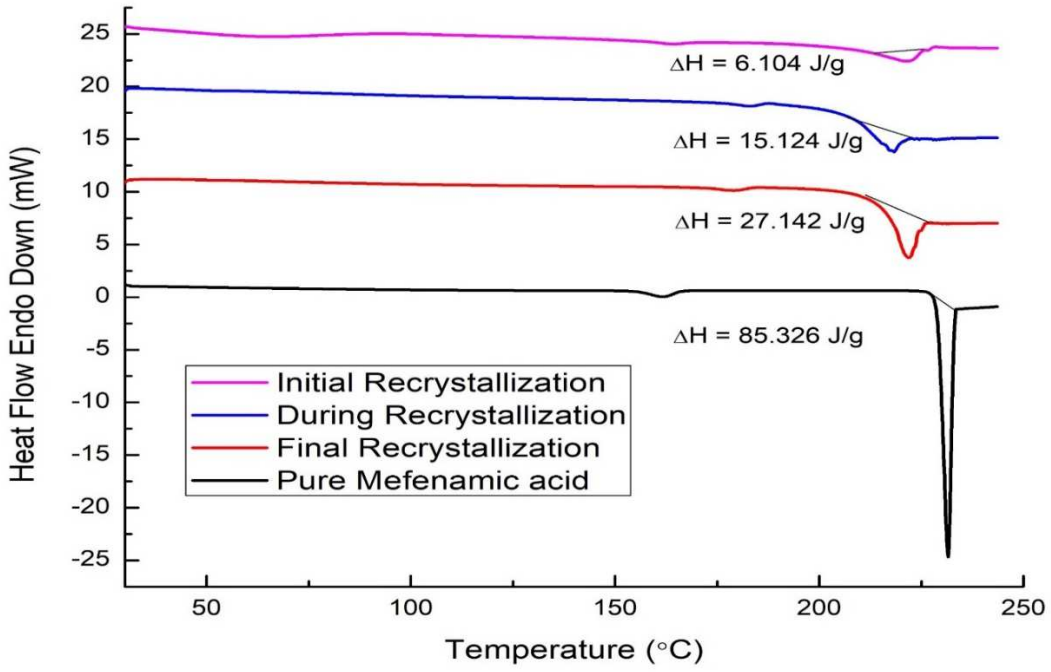

Figure 28: DSC thermograms showing the recrystallization of MFA over the period of time evident from the increase in the heat of fusion (ΔH) values.

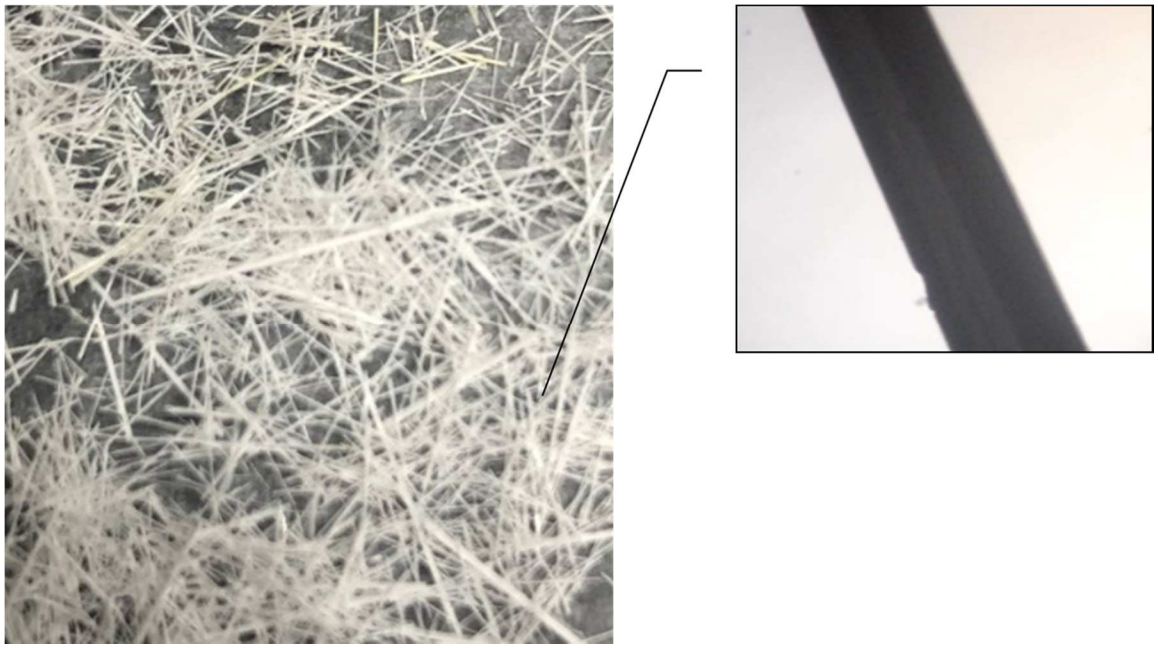

Figure 29: Rod shaped crystals of MFA recrystallized from acetone. The magnified image shows the perfect rod-shaped crystal of MFA under a microscope (10X).

4.9.2. Effect of Temperature on Recrystallization of MFA in EPO Matrix

The heat of fusion values (ΔH_f) of MFA observed at various time points at various temperatures and a constant relative humidity of 75% RH are shown in Table 12. The plots between the relative crystallinity and time at 75% RH and various temperatures are shown in Figure 30. At all the studied temperature ranges, it was observed that the relative crystallinity increased rapidly and then became constant. Earlier publications have reported a characteristic 'S' shaped curve for recrystallization of drugs in which the recrystallization rate was low initially, due to nucleation, then rapid recrystallization due to an increase in the nucleation sites and crystal growth followed by a flat phase that corresponds to the decrease in the nucleation sites. However, in the present study, initial nucleation sites were not observed. This could be due to the non-glass forming ability of MFA which undergoes recrystallization when the samples are cooled. This resulted in the formation of nucleation sites before the set experimental timelines (8 hr). However, rapid recrystallization was observed at a later stage due to an increase in the nucleation sites. The values of recrystallization rate, *k*, and the dimensionality constant, *n*, determined at 75% RH and various temperatures are given in Table 13. A plot of recrystallization rate constant, k and temperature is shown in Figure 31. When $n>0$, the value of *k* at 25 °C, 40 °C and 60 °C was observed as 3.58×10^{-3} hr^{-n}, 3.59×10^{-3} hr^{-n} and 6.47×10^{-3} hr^{-n}, respectively. However, at 70° and 80 °C, the values increased to 21.05×10^{-3} hr^{-n} and 44.04×10^{-3} hr^{-n}, respectively. This exponential increase in the value of *k* can again be attributed to an increase in the molecular mobility above the glass transition temperature, T_g. When non-linear regression analysis was performed at $n=2$, the value of *k* at 25 °C, 40 °C, 60 °C, 70 °C and 80 °C was observed as 0.22×10^{-3} hr^{-n}, 0.18×10^{-3} hr^{-n}, 0.71×10^{-3} hr^{-n},

2.50×10^{-3} hr^{-n} and 7.25×10^{3} hr^{-n}, respectively. By comparing the values of *k* from both the analysis, it can be inferred that the rate of recrystallization is low at lower temperature and increases exponentially above the T_g of the drug-polymer dispersions. Using non-linear regression analysis, higher values of recrystallization rate constant, *k*, were predicted using the dimensionality constant, *n*, as >0 as compared to the values obtained when *n* was fixed as 2. This was due to the flip-flop effect observed during non-linear regression analysis (80). The average value of n predicted when $n>0$ was found to be 1.44 which is close to 2. This indicates that MFA recrystallizes as rod shaped crystals inside the MFA polymeric matrix.

Table 12: Values of heat of fusion of MFA recrystallized from the samples at various temperatures and 75% RH.

Time (hr)	Heat of Fusion (ΔH_f) J/g				
	25 °C/ 75% RH	**40 °C/ 75% RH**	**60 °C/ 75% RH**	**70 °C/ 75% RH**	**80 °C/ 75% RH**
8	-	-	9.85 ± 0.45	14.69 ± 1.85	16.40 ± 1.77
12	-	6.57 ± 0.56	11.09 ± 2.90	15.18 ± 2.40	22.43 ± 0.52
18	6.8 ± 0.58	7.49 ± 0.37	12.26 ± 3.45	24.49 ± 3.39	25.16 ± 2.19
24	7.1 ± 0.70	7.76 ± 0.30	16.46 ± 1.17	30.73 ± 1.90	36.23 ± 9.12
48	9.95 ± 0.88	8.95 ± 0.54	24.67 ± 2.88	38.50 ± 2.68	35.28 ± 6.44
72	13.40 ± 1.77	10.73 ± 0.85	31.33 ± 1.09	44.75 ± 2.60	40.05 ± 4.46
96	14.58 ± 1.04	13.92 ± 0.86	39.60 ± 1.29	46.83 ± 1.20	40.60 ± 5.99
120	17.04 ± 0.86	17.98 ± 1.46	40.20 ± 2.58	48.25 ± 2.68	40.65 ± 2.54
144	17.81 ± 1.97	20.95 ± 1.43	43.24 ± 0.90	48.31 ± 3.79	40.83 ± 2.66
168	21.90 ± 1.25	21.13 ± 0.79	44.74 ± 0.90	50.94 ± 4.31	41.22 ± 2.45
192	23.32 ± 1.06	21.98 ± 0.13	45.96 ± 5.13	51.16 ± 4.26	41.70 ± 2.06
216	24.01 ± 1.54	25.68 ± 1.16	45.59 ± 2.57	51.01 ± 2.70	42.15 ± 3.52
240	23.94 ± 1.54	26.28 ± 0.94	46.10 ± 3.98	52.09 ± 2.08	42.17 ± 3.25
264	24.53 ± 1.34	26.56 ± 1.02	45.98 ± 2.96	51.83 ± 1.84	41.45 ± 2.42
288	24.72 ± 1.47	26.86 ± 1.16	46.73 ± 3.88	52.96 ± 2.36	42.07 ± 2.25

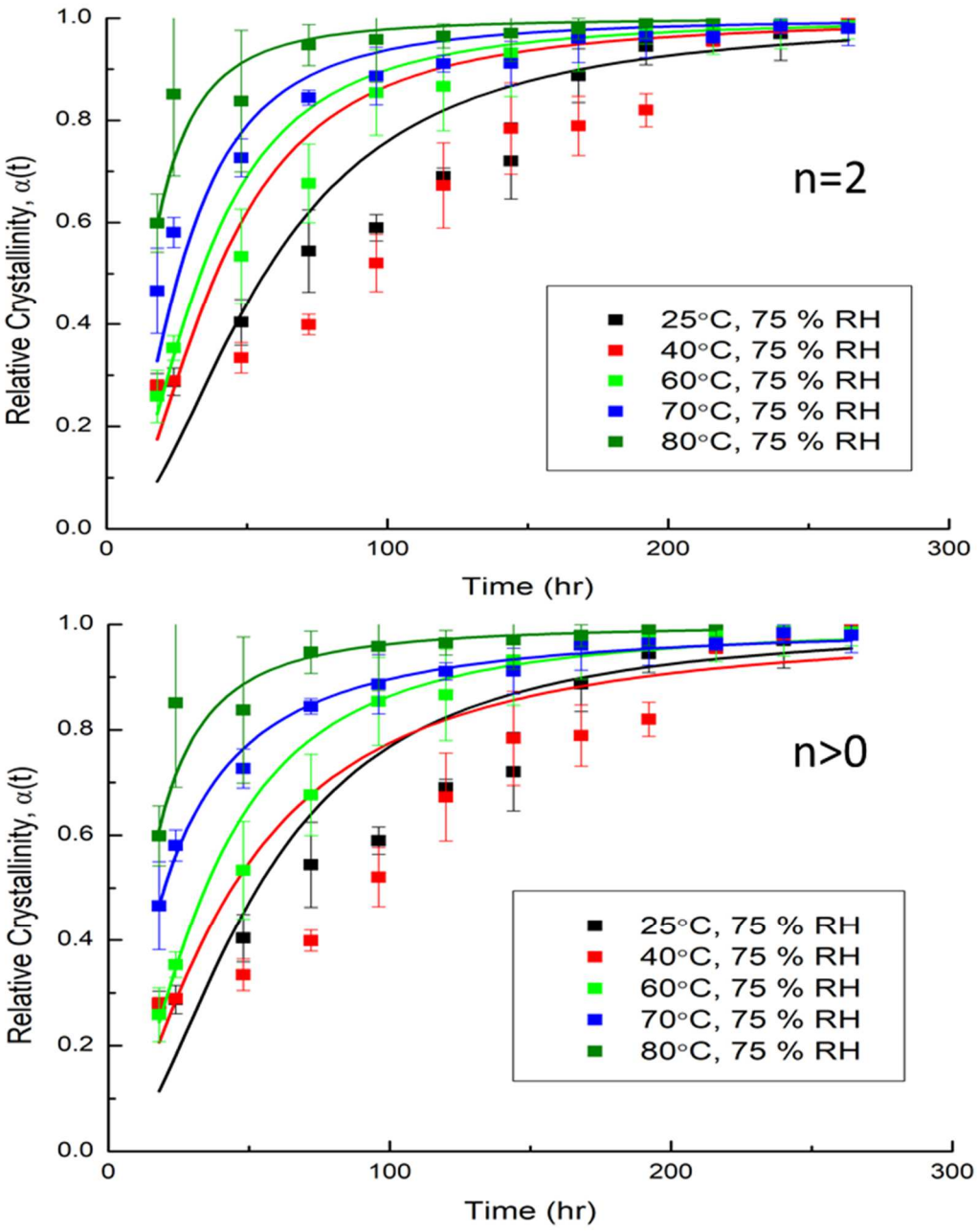

Figure 30: Relative crystallinity, α(t) as a function of time for 40% w/w drug loaded MFA-EPO dispersions stored at various temperatures and 75% RH.

Table 13: The values of recrystallization rate constant, *k* and dimensionality constant, *n* of MFA at various temperatures and 75% RH.

Stability conditions	***n* > 0**			***n* = 2**	
	$k \times 10^3$ (hr^{-n})	***n***	R^2	$k \times 10^3$ (hr^{-n})	R^2
25 °C / 75% RH	0.54 ± 0.89	1.89 ± 0.35	0.9225	0.31 ± 0.08	0.9139
40 °C / 75% RH	3.75 ± 2.56	1.47 ± 0.19	0.9452	0.66 ± 0.10	0.9348
60 °C / 75% RH	8.70 ± 4.10	1.37 ± 0.14	0.9689	1.10 ± 0.20	0.9522
70 °C / 75% RH	23.99 ± 3.73	1.27 ± 0.04	0.9792	2.04 ± 0.45	0.9257
80 °C / 75% RH	31.64 ± 6.97	1.43 ± 0.08	0.9738	7.65 ± 0.76	0.9268

The data are presented as mean±SE (standard error of fit)

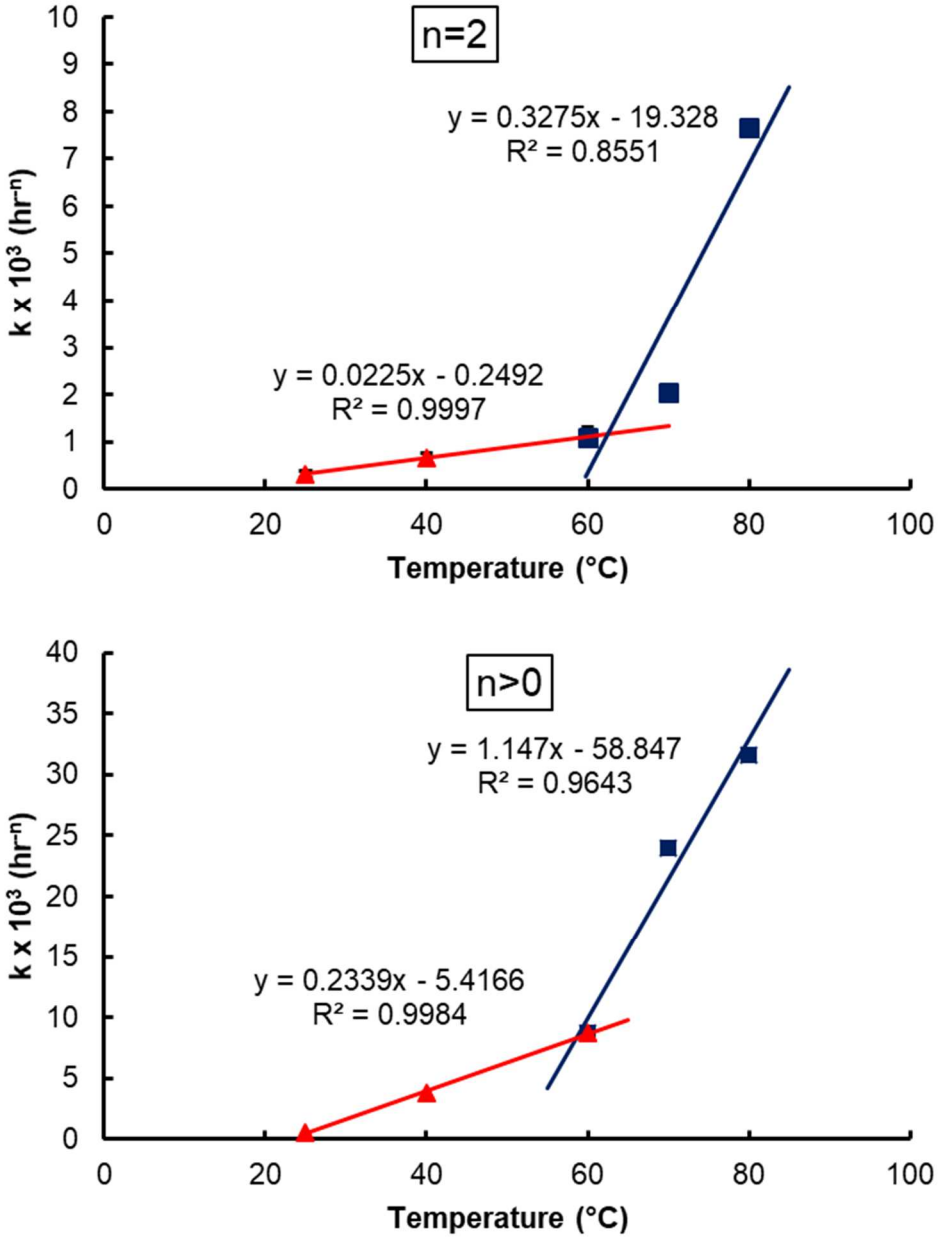

Figure 31: Relationship between the recrystallization rate constant, *k*, and temperature at a dimentionality value of $n = 2$ and $n > 0$.

4.9.3. Arrhenius Plot of Recrystallization as a Function of Temperature

The Arrhenius plot was constructed by ploting the values of log *k* vs 1/T that revealed that the crystallization rate increased exponentially with temperature, T, within the temperature range studied implying that the Arrhenius equation expresses the temperature dependence of recrystallization rate (Fig. 32). The recrystallization activation energy, ΔE_a, was determined from the slope of the linear regression of ln *k* and 1/T. The activation energy allows the prediction of recrystallization kinetics at temperature outside the experimental range. The value of activation coefficient, ΔE_a, was found to be 63,024 J/mol (15.06 Kcal/mol) when $n>0$ and 44,828 J/mol (10.74 Kcal/mol) when $n=2$. This value of activation energy, ΔE_a, can be used to determine the recrystallization rate at various temperatures.

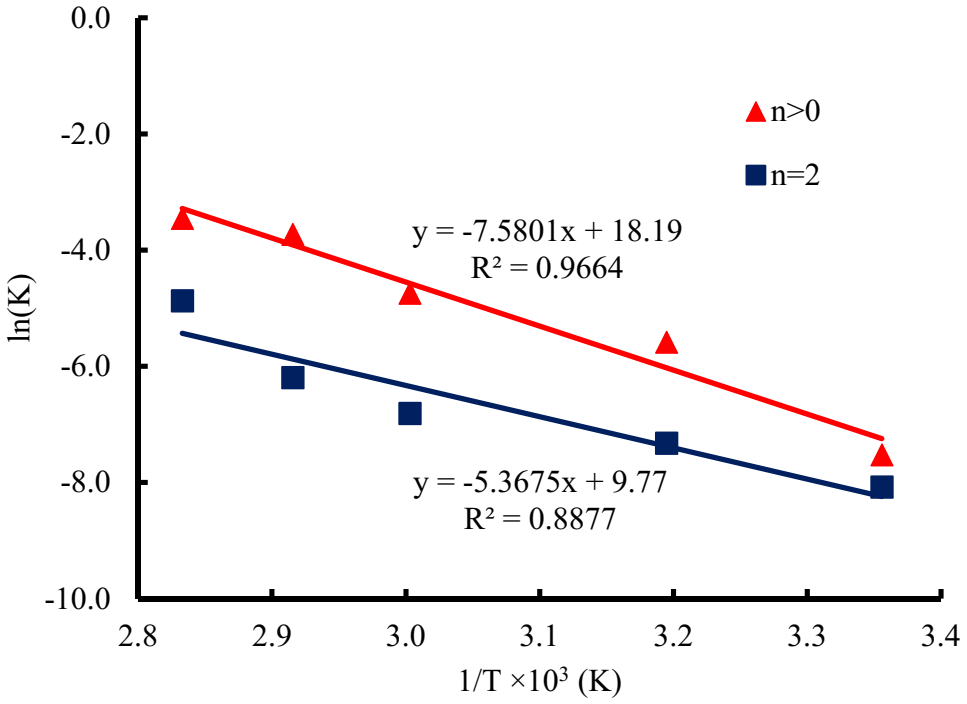

Figure 32: Arrhenius plot of crystallization rate constant, *k*, as a function of inverse of temperature, 1/T for 40% w/w drug loaded MFA-EPO dispersions.

4.9.4. Effect of Relative Humidity on Recrystallization of MFA in EPO Matrix

The values of heat of fusion, ΔH_f, of MFA observed at various time points at various relative humidity conditions and a constant temperature of 60 °C are shown in Table 14. The plots between the relative crystallinity and time at 60 °C and various relative humidity conditions are shown in Figure 33. At the relative humidity range studied, it was observed that the relative crystallinity increased rapidly and then became constant. The experimental values correlated well with the kinetic model at all the relative humidity conditions except at 11% RH where the kinetic model overpredicted the relative crystallinity (black squares as outliers in Fig. 33). Similar to the effect of temperature, no nucleation sites were observed in the samples stored at various relative humidity conditions. The values of recrystallization rate, k, and the dimensionality constant, n, determined at 60 °C and various relative humidity conditions are given in Table 15. A plot of recrystallization rate constant, *k*, and temperature is shown in Fig. 34. When non-linear regression analysis was performed at $n>0$, the values of *k* at 11% RH, 22% RH, 32% RH, 60% RH and 75% RH were 2.02×10^{-3} hr^{-n}, 4.98×10^{-3} hr^{-n}, 5.03×10^{-3} hr^{-n}, 5.58×10^{-3} hr^{-n} and 6.47×10^{-3} hr^{-n}, respectively. When non-linear regression analysis was performed at $n=2$, the values of *k* at 25 °C, 40 °C, 60 °C, 70 °C and 80 °C were 0.19×10^{-3} hr^{-n}, 0.53×10^{-3} hr^{-n}, 0.74×10^{-3} hr^{-n}, 0.75×10^{-3} hr^{-n} and 0.71×10^{-3} hr^{-n}, respectively. Upon comparing the values of k by both the analyses, it can be inferred that the rate of recrystallization was low at 11% RH and increased at 32%RH, 60% RH and 75% RH conditions. As described earlier, the experimental data at 11% RH did not fit well with the kinetic model used in this study.

Table 14: Values of heat of fusion of MFA recrystallized from the samples at 60 °C temperature and various relative humidities

Time (hr)	60 °C/11% RH	60 °C/22% RH	60 °C/32% RH	60 °C/60% RH	60 °C/75% RH
8	6.7 ± 0.5	11.9 ± 2.0	8.1 ± 0.8	9.13 ± 1.64	9.85 ± 0.45
12	7.7 ± 0.5	11.6 ± 1.2	7.5 ± 0.2	10.00 ± 0.34	11.09 ± 2.90
18	10.1 ± 1.3	12.3 ± 1.6	8.0 ± 1.1	11.03 ± 1.30	12.26 ± 3.45
24	10.1 ± 0.8	14.7 ± 1.3	18.0 ± 1.4	15.09 ± 1.66	16.46 ± 1.17
48	15.1 ± 2.7	28.6 ± 3.6	26.3 ± 2.6	22.81 ± 0.99	24.67 ± 2.88
72	20.6 ± 2.4	35.6 ± 4.7	29.7 ± 0.1	28.96 ± 0.84	31.33 ± 1.09
96	22.2 ± 0.8	36.6 ± 2.9	34.7 ± 2.9	36.51 ± 1.99	39.60 ± 1.29
120	29.3 ± 1.4	38.1 ± 4.2	37.4 ± 1.4	37.15 ± 0.83	40.20 ± 2.58
144	30.7 ± 0.7	38.4 ± 2.7	39.2 ± 2.2	40.00 ± 1.09	43.24 ± 0.90
168	37.4 ± 0.5	40.9 ± 3.9	40.9 ± 2.4	41.40 ± 4.41	44.74 ± 0.90
192	42.2 ± 2.8	43.7 ± 4.0	41.5 ± 3.6	42.12 ± 1.55	45.96 ± 5.13
216	43.7 ± 0.9	43.7 ± 3.1	42.3 ± 2.7	42.02 ± 2.32	45.59 ± 2.57
240	44.1 ± 4.5	45.3 ± 3.9	42.9 ± 1.8	42.32 ± 1.25	46.10 ± 3.98
264	44.4 ± 3.3	44.8 ± 4.8	43.2 ± 4.2	42.30 ± 1.40	45.98 ± 2.96
288	43.2 ± 4.2	45.5 ± 3.2	43.9 ± 3.9	42.94 ± 2.04	46.73 ± 3.88

*All the experiments were performed in triplicate and the values are represented as mean ± SD (n=3)

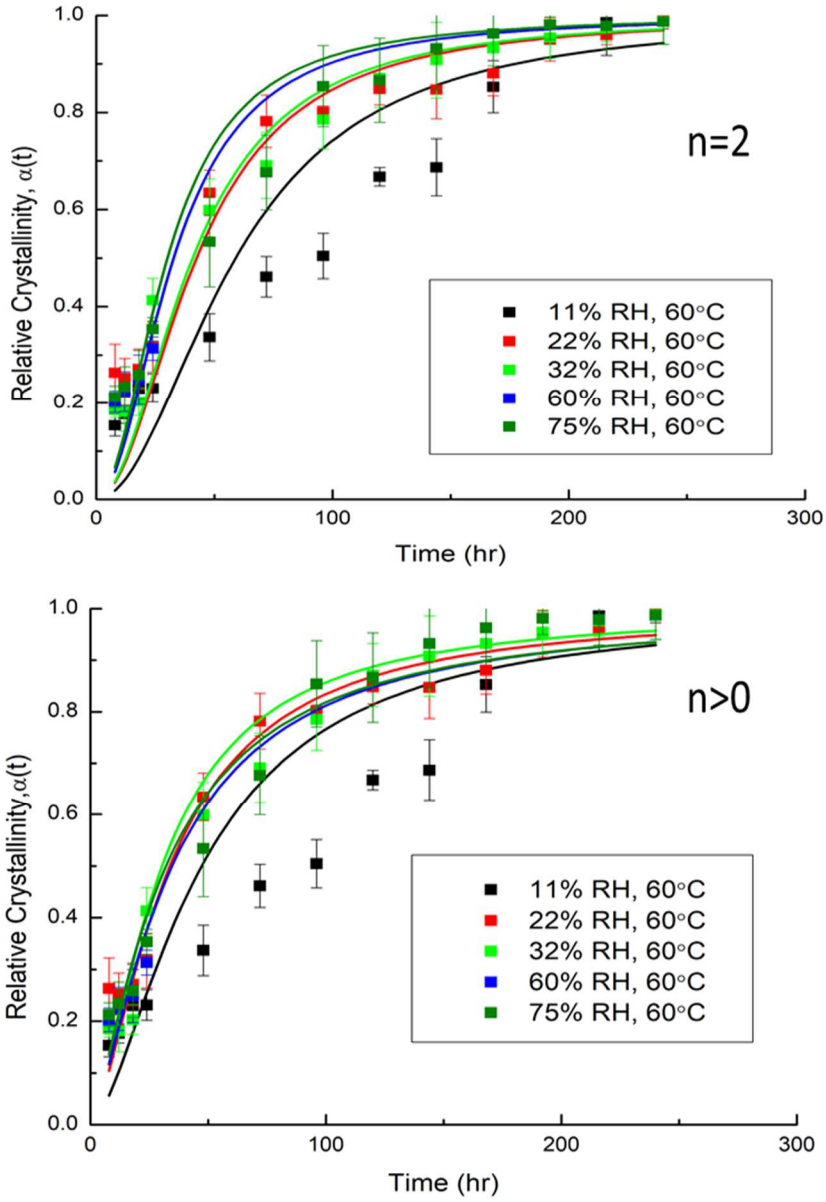

Figure 33: Relative crystallinity, α(t), as a function of time for 40% w/w MFA-EPO dispersions at 60 °C temperature and various relative humidities.

Table 15: Values of recrystallization rate constant, *k*, and dimensionality constant, *n*, of MFA at 60 °C temperature and various relative humidities

Stability conditions	$n > 0$			$n = 2$	
	$k \times 10^3$ (hr^{-n})	n	R^2	$k \times 10^3$ (hr^{-n})	R^2
11% RH/ 60 °C	5.06 ± 4.87	1.29 ± 0.20	0.8588	0.16 ± 0.03	0.8322
22% RH/ 60 °C	5.12 ± 2.89	1.49 ± 0.13	0.9045	0.55 ± 0.08	0.8751
32% RH/ 60 °C	5.77 ± 1.94	1.51 ± 0.07	0.9286	0.60 ± 0.11	0.8732
60% RH/ 60 °C	6.41 ± 3.45	1.43 ± 0.16	0.9694	0.93 ± 0.17	0.9130
75% RH/ 60 °C	8.70 ± 4.10	1.37 ± 0.14	0.9690	1.10 ± 0.20	0.9522

The data are presented as mean±SE (standard error of fit)

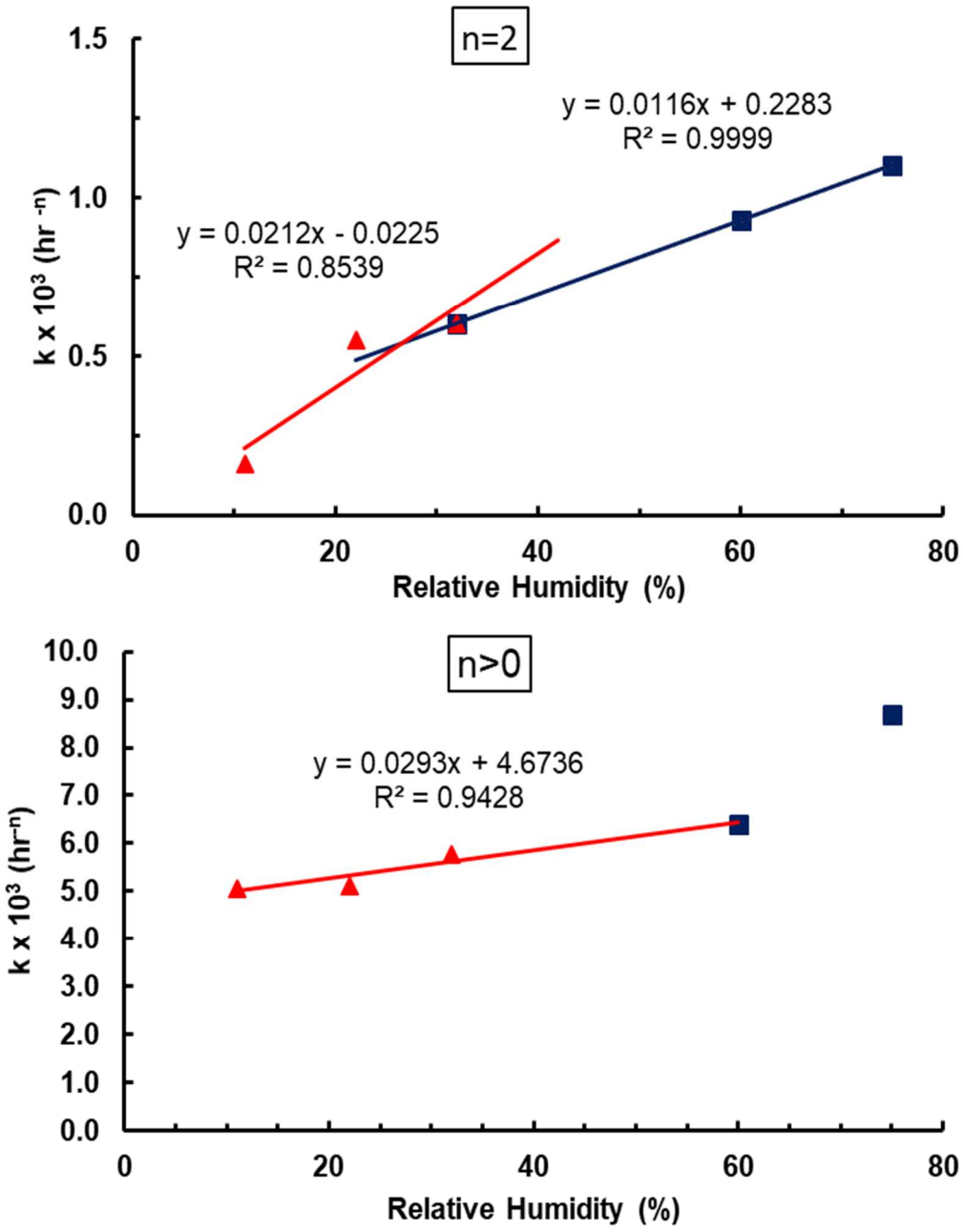

Figure 34: Plot showing relationship between the recrystallization rate constant, *k*, and relative humidity at a dimentionality value of $n = 2$ and $n > 0$ at 60 °C.

4.9.5. Effect of Relative Humidity on Recrystallization of MFA in EPO Matrix at Room Temperature

To understand the effect of relative humidity on recrystallization of MFA at room temperature, 25° C, the MFA-EPO (40% w/w) dispersions were further stored at 32±5% RH and 75±5% RH and a temperature of 25±2 °C. The amount of MFA recrystallized from the drug-polymer dispersions at different time points was determined using DSC and the recrystallization rate constant was estimated using modified Avarami equation. The heat of fusion (ΔH_f) values of MFA recrystallized at different relative humidities of 11%, 32% and 75% and temperature of 25 °C were given in Table 16. By comparing the heat of fusion values at room temperature and at 60 °C, it can be observed that after 288 hrs, the values of ΔH_f at 25 °C are significantly lower than that observed at 60 °C. This shows that recrystallization of MFA at room temperature is slower than that observed at 60 °C, which is close to the glass transition temperature of the drug-polymer system. The rate of recrystallization was calculated using non-linear regression analysis. The relationship between the reltive crystallinity and time is show in Figure 35. It can be observed that the relative crystallinity, α(t), was observed to be increasing linearly rather than exhibiting the characteristic 'S' shaped curve that was observed at higher temperatures. This show that the rate of recrystallization is slow and the drug-polymer system did not undergo nucleation, followed by crystal growth. In such cases, the data used to estimate the recrystallization rate will not fit the modified Avarami model. This is evident from the values of rate of recrystallization, *k* observed at various relative humidty and at room temperature as shown in Table 17 and Figure 36. The overestimated values at 11% and 32% RH is due to incomplete recrystallization of MFA in EPO matrix.

Table 16: Values of heat of fusion of MFA recrystallized from the samples stored at 25 °C temperature and various relative humidities

Time (hr)	11% RH/ 25 °C	32% RH/ 25 °C	75% RH/ 25 °C
8	7.47 ± 1.04	11.00 ± 2.58	NA
12	8.10 ± 0.83	13.85 ± 2.60	NA
18	9.86 ± 1.57	13.57 ± 4.18	6.83 ± 0.58
24	10.51 ± 0.40	16.34 ± 4.05	7.09 ± 0.70
48	11.67 ± 2.95	17.03 ± 3.69	9.95 ± 0.88
72	16.80 ± 2.58	16.97 ± 4.70	13.40 ± 1.77
96	17.54 ± 2.37	17.60 ± 4.71	14.58 ± 1.04
120	15.87 ± 1.43	19.51 ± 2.79	17.04 ± 0.86
144	17.94 ± 2.69	17.96 ± 2.05	17.81 ± 1.97
168	15.31 ± 1.65	20.26 ± 2.11	21.90 ± 1.25
192	15.45 ± 2.19	19.65 ± 0.94	23.32 ± 1.06
216	16.14 ± 1.89	21.19 ± 1.51	24.01 ± 1.54
240	17.08 ± 1.25	20.66 ± 1.35	23.94 ± 1.59
264	16.67 ± 1.11	20.19 ± 1.27	24.53 ± 1.34
288	18.22 ± 0.71	20.69 ± 1.41	24.72 ± 1.47

All the experiments were performed in triplicate and the values are represented as mean ± SD (n=3)

NA - No melting endotherm was observed

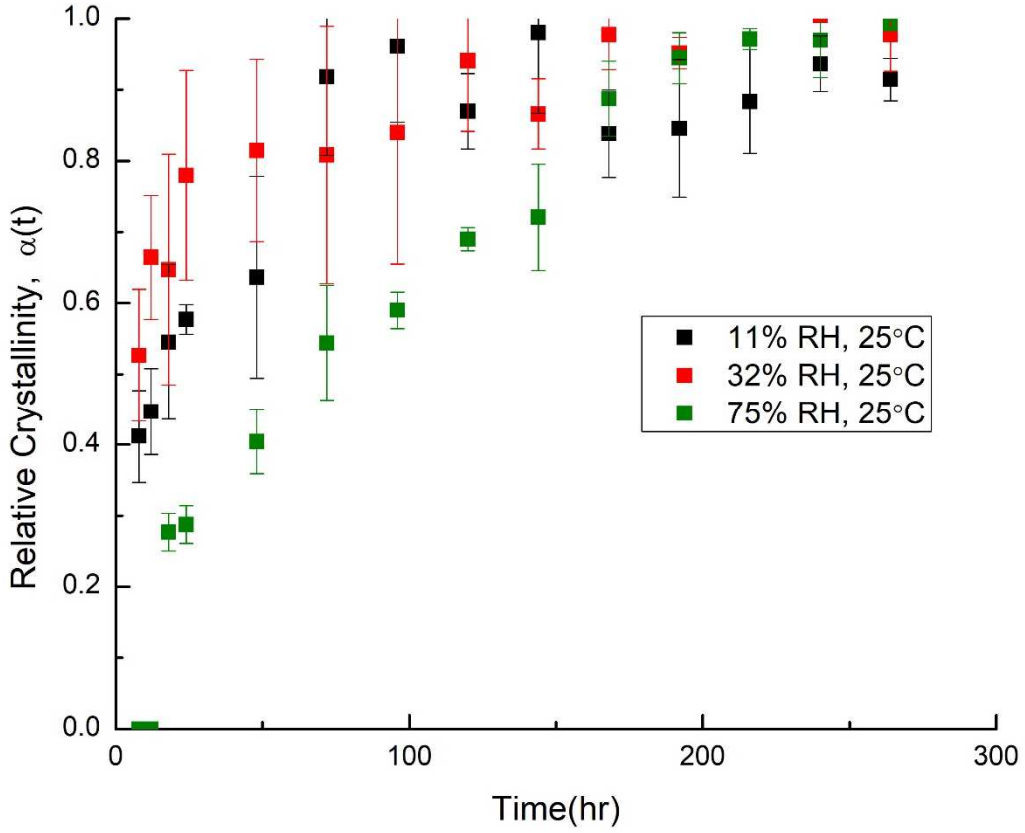

Figure 35: Plot of relative crystallinity, α(t), as a function of time for 40% w/w drug loaded MFA-EPO dispersions at 25 °C temperature and various relative humidity conditions

Table 17: The values of recrystallization rate constant, *k*, and dimensionality constant, *n*, of MFA at 25 °C temperature and various relative humidity conditions

Stability conditions	$n > 0$			$n = 2$	
	$k \times 10^3$ (hr^{-n})	n	R^2	$k \times 10^3$ (hr^{-n})	R^2
11% RH/ 25 °C	90.94 ± 21.4	0.86 ± 0.07	0.9652	0.16 ± 0.03	0.7301
32% RH/ 25 °C	94.69 ± 65.14	1.17 ± 0.23	0.7584	0.60 ± 0.11	0.6685
75% RH/ 25 °C	8.70 ± 4.10	1.37 ± 0.14	0.9690	1.10 ± 0.20	0.9522

The data are presented as represent mean ± SE (standard error of fit)

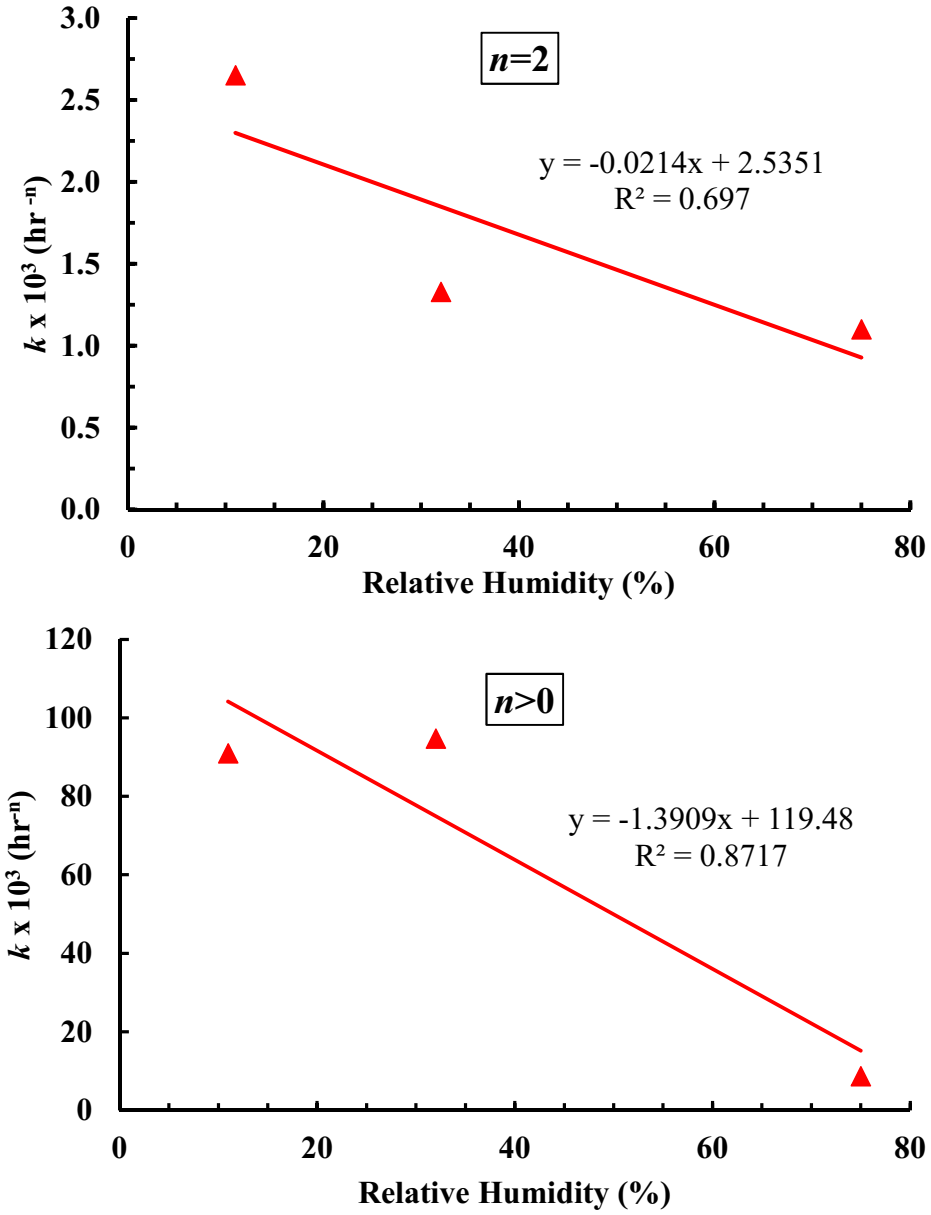

Figure 36: Relationship between the recrystallization rate constant, *k* and relative humidity at a dimentionality value of $n = 2$ and $n > 0$ at a temperature of 25 °C.

4.9.6. Effect of Drug Loading on Recrystallization at 40 °C and 75% RH

In earlier studies, the intermolecular interaction between the carboxylic acid of MFA and the aminoalkyl group of EPO was reported. Based on this, it is speculated that a stable system of MFA and EPO occurs within a stochiometric ratio; and when the drug loading is more than the stochiometric ratio, changes in the temperature and relative humidity cause phase separation. To test this hypothesis, the absolute amount of MFA recrystallized from the samples at various RH conditions was calculated. It was found that ~50% of the drug loading (40% w/w) recrystallized out irrespective of the RH conditions. That means, only 20% of MFA remained kinetically stable in the samples even at high relative humidity conditions. This value is close to the miscibility value of MFA in EPO predicted using thermodynamic phase diagrams. To further test this hypothesis, 30% MFA-EPO and 50% MFA-EPO samples were prepared and stored at 40 °C and 75% RH. The enthalpy values were determined, and the extent of recrystallization were calculated for 45 day (Fig. 37). The % drug miscible in the polymeric matrix at various drug loading was calculated and it was observed that irrespective of the drug loading, around 25% of MFA was miscible in EPO matrix even when subjected to extreme climatic conditions of 40 °C and 75% RH (Fig. 38).

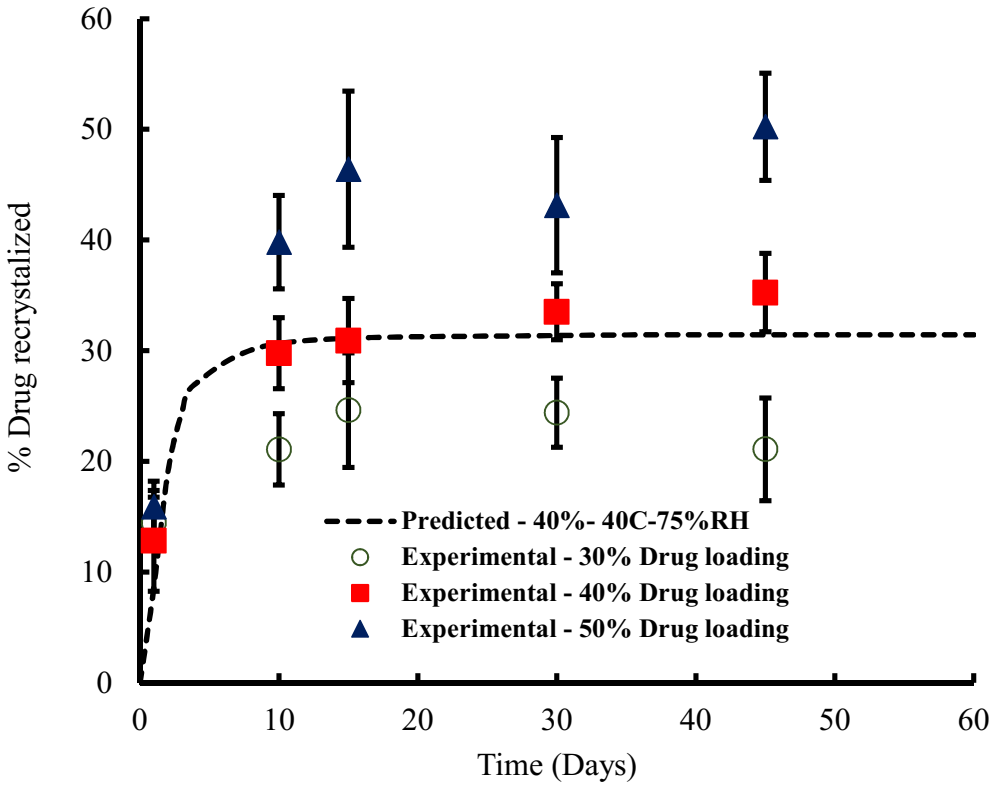

Figure 37: Plot demonstrating relationship between the % drug recrystallization and time at various drug loading of 30%, 40% and 50% w/w of MFA and EPO.

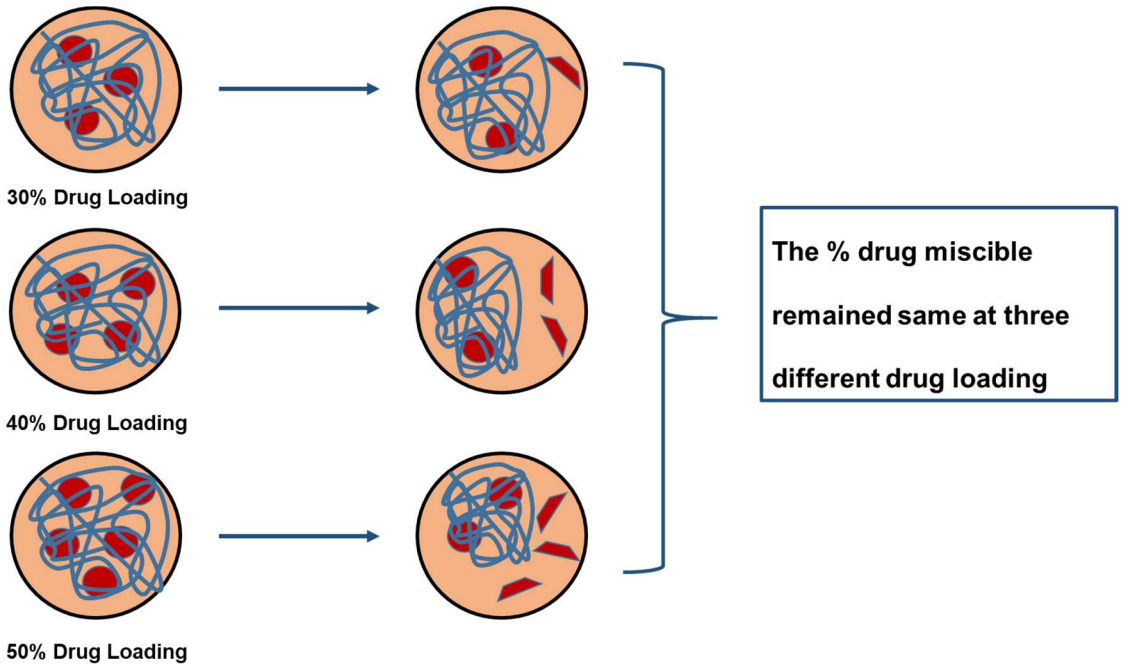

Figure 38: Effect of drug loading on drug miscibility. The red circles represent amorphous drug and the polygons represent the recrystallized drug.

5. Summary and Conclusions

The determination of ideal drug-loading and processing temperature for hot-melt extrusion to develop amorphous solid dispersions (ASDs) is challenging and often requires extensive experimentation. While theoretical concepts of solubility parameters are reportedly used for initial screening of polymeric excipients for such formulations, their applicability is limited only to some drug-polymer combinations. In the present investigations, therefore, thermodynamic aspects of mixing a non-glass forming drug, mefenamic acid (MFA), in four chemically distinct polymeric excipients with close values of Hansen and Hildebrand solubility parameters were studied. The rank order miscibility of MFA in the four polymeric carriers studied was estimated based on the difference in the values of solubility parameters, $\Delta\delta$, between the drug and the polymer. Based on the difference in the values of the solubility parameters, $\Delta\delta$, it was deduced that MFA will be miscible in all the four polymers studied. However, the values of interaction parameters, χ, calculated from the melting point depression data suggested that while MFA would have good miscibility in EPO, SLP, and VA64, it would have poor miscibility in F68 despite a difference in the value of solubility parameter, $\Delta\delta$, less than 7 $MPa^{0.5}$; a value of $\Delta\delta < 7$ $MPa^{0.5}$ is considered to suggest good drug-polymer miscibility. This suggests that the values of solubility parameters can lead to an overestimation of the degree of miscibility of the drugs and the polymeric excipients, and a difference in the value of solubility parameter, $\Delta\delta$, less than 7 $MPa^{0.5}$ does not necessarily always indicate good drug-polymer miscibility. Further, a systematic approach for the construction of thermodynamic phase diagrams and Gibbs free energy plots using the melting point depression data was also conducted. The Berghmans point

in the thermodynamic phase diagrams of MFA with various polymeric carriers studied showed that the predicted miscibility of MFA in both EPO and SLP was ~13% w/w, and in VA64 and F68 it was less than 5% w/w. The upper critical solution temperature (UCST) of drug-polymer mixtures predicted from the Gibbs free energy plots showed that MFA will be miscible in EPO and SLP in all proportions at a processing temperature above 140 °C; in the case of VA64 and F68, the upper critical solution temperature (UCST) was above 200 °C. The observations from the initial investigations thus lead to the conclusion that theoretical approaches, such as estimation of Hildebrand and Hansen solubility parameters and construction of the Bagley plot, should be used with caution in the assessment of drug-polymer miscibility, and the results from the thermodynamic phase diagrams and the Gibbs free energy plots will provide a better assessment tool for the selection of the ideal drug-loading and processing temperature for hot-melt extrusion process thereby reducing the total time and material required for the product and the process development.

To determine the ideal processing conditions required for HME and to understand the relationship between the processing parameters, i.e. drug loading, residence time and the processing temperature, a material sparing DSC method was developed. In this work, the residual crystallinity and degradation of MFA in EPO polymeric matrix as a function of drug loading, DSC heating rate and DSC heating temperature was examined using Box-Behnken experimental design. The results showed that the studied process parameters had significant effect on the residual crystallinity and drug degradation. A quadratic relationship was obtained between the studied independent parameters and the dependent parameters. In general, it was found that an increase in drug load resulted in an

increase in residual crystallinity, while an increase in temperature resulted in decrease in residual crystallinity. An increase in the temperature and decrease in the heating rate increased the drug degradation. Numerical and graphical optimization were used to predict the design space of the processing conditions which result in minimum residual crystallinity and minimum drug degradation. It was found that when a drug load of 20% w/w was processed at a heating rate of 5.5 °C/min and temperature of 146 °C, the resulting product had residual crystallinity of 13.6% and drug degradation of 3.8%. Based on the design space obtained from the experimental design, 20% w/w drug loaded MFA-EPO dispersions were prepared using HME and VCM. The drug-polymer dispersions obtained using both HME and VCM did not show any signs of residual crystallinity of MFA. However, degradation of MFA was observed in VCM sample and the HME filaments processed at 100 rpm, but not at 150 rpm. This reiterates the significance of adjusting the screw speed during HME process.

Once the optimized ASDs were obtained, their physical stability was determined by storing at accelerated conditions of 40 °C and 75% RH for three months. In practice, if recrystallization of the amorphous drug is observed after three months, the whole optimization process is performed again, resulting in loss of valuable time. Therefore, in the present investigation, a modified Avarami model was used to determine the physical stability of ASDs within an experimentally feasible time-frame. The rate of recrystallization calculated using the modified Avarami equation showed that temperature had a significant effect on the rate of recrystallization as compared to the relative humidity. The absolute crystallinity of MFA observed at three different drug loadings (30%, 40% and 50% w/w) was found to be similar after storing at 40 °C/75%

RH. This showed that the amount of drug that was miscible in the polymeric carrier remained in the amorphous form even after subjecting to accelerated stability conditions.

A work flow chart illustrating the formulation development process of ASDs using HME is shown in Figure 39. In summary, selection of the ideal polymer and the processing temperature can be first determined using thermodynamic phase diagrams and Gibbs free energy plots. Once the ideal polymer and the miscibility of the drug in the polymer is determind, the HME process can first be designed using a DSC to determine the ideal drug-loading and processing temperature (i.e., the design space). Once the design space is identified, the optimization of screw configuration and screw speed can be performed by either *in silico* simulations and/or by conducting a few HME experiments. Finally, the physical stability of the optimized ASDs can be determined at various temperatures and relative humidity conditions using the modified Avarami equation, thereby predict the shelf life of the ASDs. This approach significantly reduces the total number of experiments required to setup the HME process, thereby making the whole product development cost efficient.

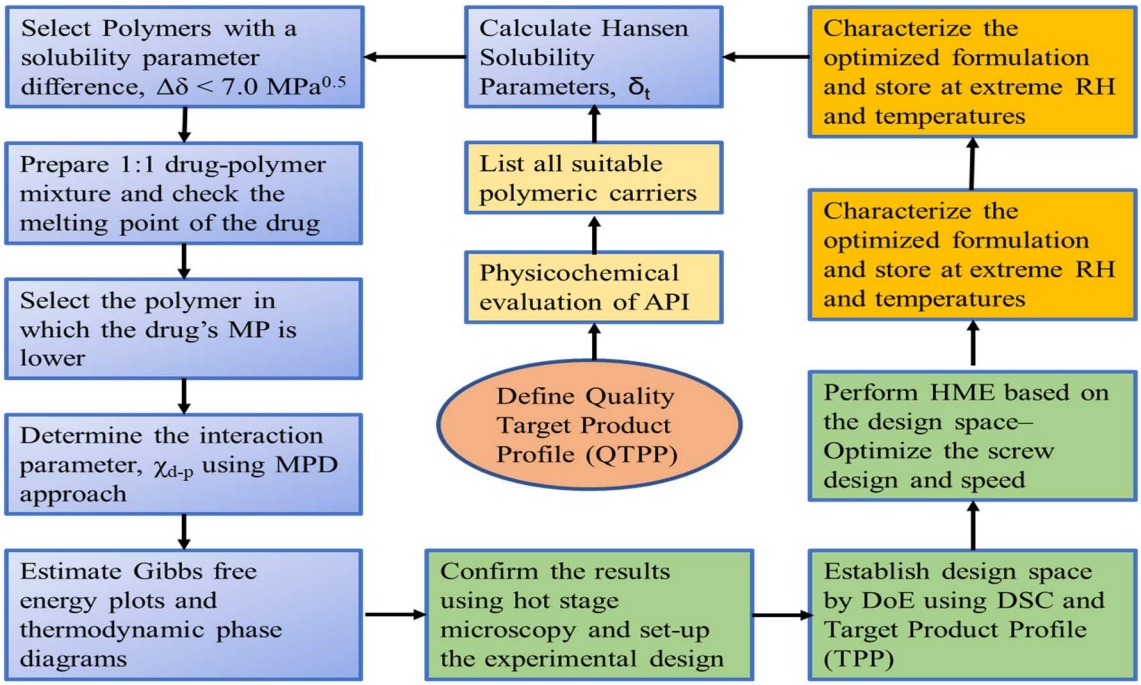

Figure 39: Flow chart summarizing the material-sparing approach for the formulation development of ASDs using HME

References

1. Sekiguchi K, Obi N. Studies on Absorption of Eutectic Mixture. I. A Comparison of the Behavior of Eutectic Mixture of Sulfathiazole and that of Ordinary Sulfathiazole in Man. Chemical and Pharmaceutical Bulletin. 1961;9(11):866–72.

2. Janssens S, Van den Mooter G. Physical chemistry of solid dispersions. Journal of Pharmacy and Pharmacology. 2009;61(12):1571–86.

3. Kawakami K, Pikal MJ. Calorimetric investigation of the structural relaxation of amorphous materials: Evaluating validity of the methodologies. Journal of pharmaceutical sciences. 2005;94(5):948–65.

4. Crowley KJ, Zografi G. The use of thermal methods for predicting glass-former fragility. Thermochimica Acta. 2001 Dec 14;380(2):79–93.

5. Kadajji VG, Betageri GV. Water soluble polymers for pharmaceutical applications. Polymers. 2011;3(4):1972–2009.

6. Kawakami K. Theory and practice of supersaturatable formulations for poorly soluble drugs. Therapeutic Delivery. 2015;6(3):339–52.

7. Surwase SA, Itkonen L, Aaltonen J, Saville D, Rades T, Peltonen L, et al. Polymer incorporation method affects the physical stability of amorphous indomethacin in aqueous suspension. European Journal of Pharmaceutics and Biopharmaceutics. 2015;96:32–43.

8. Luk E, Sandoval AJ, Cova A, Müller AJ. Anti-plasticization of cassava starch by complexing fatty acids. Carbohydrate polymers. 2013;98(1):659–64.

9. Sathigari SK, Radhakrishnan VK, Davis VA, Parsons DL, Babu RJ. Amorphous-state characterization of efavirenz—polymer hot-melt extrusion systems for dissolution enhancement. Journal of pharmaceutical sciences. 2012;101(9):3456–64.

10. Paudel A, Worku ZA, Meeus J, Guns S, Van den Mooter G. Manufacturing of solid dispersions of poorly water soluble drugs by spray drying: formulation and process considerations. International journal of pharmaceutics. 2013;453(1):253–84.

11. Khougaz K, Clas S-D. Crystallization inhibition in solid dispersions of MK-0591 and poly (vinylpyrrolidone) polymers. Journal of pharmaceutical sciences. 2000;89(10):1325–34.

12. Meng F, Trivino A, Prasad D, Chauhan H. Investigation and correlation of drug polymer miscibility and molecular interactions by various approaches for the preparation of amorphous solid dispersions. European Journal of Pharmaceutical Sciences. 2015;71:12–24.

13. Maniruzzaman M, Morgan DJ, Mendham AP, Pang J, Snowden MJ, Douroumis D. Drug–polymer intermolecular interactions in hot-melt extruded solid dispersions. International journal of pharmaceutics. 2013;443(1–2):199–208.

14. Knapik J, Wojnarowska Z, Grzybowska K, Hawelek L, Sawicki W, Wlodarski K, et al. Physical stability of the amorphous anticholesterol agent (ezetimibe): the role of molecular mobility. Molecular pharmaceutics. 2014;11(11):4280–90.

15. Kothari K, Ragoonanan V, Suryanarayanan R. The role of polymer concentration on the molecular mobility and physical stability of nifedipine solid dispersions. Molecular pharmaceutics. 2015;12(5):1477–84.

16. Wilson M, Williams MA, Jones DS, Andrews GP. Hot-melt extrusion technology and pharmaceutical application. Therapeutic delivery. 2012;3(6):787–97.

17. Crowley MM, Zhang F, Repka MA, Thumma S, Upadhye SB, Kumar Battu S, et al. Pharmaceutical applications of hot-melt extrusion: part I. Drug development and industrial pharmacy. 2007;33(9):909–26.

18. Li M, Gogos CG, Ioannidis N. Improving the API dissolution rate during pharmaceutical hot-melt extrusion I: Effect of the API particle size, and the co-rotating, twin-screw extruder screw configuration on the API dissolution rate. International journal of pharmaceutics. 2015;478(1):103–12.

19. Edueng K, Mahlin D, Bergström CA. The need for restructuring the disordered science of amorphous drug formulations. Pharmaceutical research. 2017;34(9):1754–72.

20. De Robertis S, Bonferoni MC, Elviri L, Sandri G, Caramella C, Bettini R. Advances in oral controlled drug delivery: the role of drug–polymer and interpolymer non-covalent interactions. Expert opinion on drug delivery. 2015;12(3):441–53.

21. Van Krevelen DW, Te Nijenhuis K. Properties of polymers: their correlation with chemical structure; their numerical estimation and prediction from additive group contributions. Elsevier; 2009.

22. Marsac PJ, Li T, Taylor LS. Estimation of drug–polymer miscibility and solubility in amorphous solid dispersions using experimentally determined interaction parameters. Pharmaceutical research. 2009;26(1):139.

23. Just S, Sievert F, Thommes M, Breitkreutz J. Improved group contribution parameter set for the application of solubility parameters to melt extrusion. European Journal of Pharmaceutics and Biopharmaceutics. 2013;85(3):1191–9.

24. Wlodarski K, Zhang F, Liu T, Sawicki W, Kipping T. Synergistic effect of polyvinyl alcohol and copovidone in itraconazole amorphous solid dispersions. Pharmaceutical Research. 2018;35(1):16.

25. Pawar J, Suryawanshi D, Moravkar K, Aware R, Shetty V, Maniruzzaman M, et al. Study the influence of formulation process parameters on solubility and dissolution enhancement of efavirenz solid solutions prepared by hot-melt extrusion: a QbD methodology. Drug Delivery and Translational Research. 2018;8(6):1644–57.

26. Turpin ER, Taresco V, Al-Hachami WA, Booth J, Treacher K, Tomasi S, et al. In silico screening for solid dispersions: The trouble with solubility parameters and χFH. Molecular pharmaceutics. 2018;15(10):4654–67.

27. Zhao Y, Inbar P, Chokshi HP, Malick AW, Choi DS. Prediction of the thermal phase diagram of amorphous solid dispersions by Flory–Huggins theory. Journal of pharmaceutical sciences. 2011;100(8):3196–207.

28. Tian Y, Booth J, Meehan E, Jones DS, Li S, Andrews GP. Construction of drug–polymer thermodynamic phase diagrams using Flory–Huggins interaction theory: identifying the relevance of temperature and drug weight fraction to phase separation within solid dispersions. Molecular pharmaceutics. 2013;10(1):236–48.

29. Lehmkemper K, Kyerematen SO, Heinzerling O, Degenhardt M, Sadowski G. Long-term physical stability of PVP-and PVPVA-amorphous solid dispersions. Molecular pharmaceutics. 2017;14(1):157–71.

30. Unga J, Tajarobi F, Norder O, Frenning G, Larsson A. Relating solubility data of parabens in liquid PEG 400 to the behaviour of PEG 4000-parabens solid dispersions. European journal of pharmaceutics and biopharmaceutics. 2009;73(2):260–8.

31. Weuts I, Kempen D, Decorte A, Verreck G, Peeters J, Brewster M, et al. Phase behaviour analysis of solid dispersions of loperamide and two structurally related compounds with the polymers PVP-K30 and PVP-VA64. European journal of pharmaceutical sciences. 2004;22(5):375–85.

32. Boersen N, Brown C, DiNunzio J, Johnson D, Marsac P, Meyer R, et al. Hot-melt extrusion: the process-product-performance interplay. In: Discovering and Developing Molecules with Optimal Drug-Like Properties. Springer; 2015. p. 345–81.

33. Mamidi HK, Palekar S, Nukala PK, Mishra SM, Patki M, Fu Y, et al. Process Optimization of Twin-Screw Melt Granulation of Fenofibrate Using Design of Experiment (DoE). International Journal of Pharmaceutics. 2020;120101.

34. Chokshi RJ, Sandhu HK, Iyer RM, Shah NH, Malick AW, Zia H. Characterization of physico-mechanical properties of indomethacin and polymers to assess their suitability for hot-melt extrusion processs as a means to manufacture solid dispersion/solution. Journal of pharmaceutical sciences. 2005;94(11):2463–74.

35. DiNunzio JC, Brough C, Hughey JR, Miller DA, Williams III RO, McGinity JW. Fusion production of solid dispersions containing a heat-sensitive active ingredient

by hot melt extrusion and Kinetisol® dispersing. European journal of pharmaceutics and biopharmaceutics. 2010;74(2):340–51.

36. Baird JA, Taylor LS. Evaluation of amorphous solid dispersion properties using thermal analysis techniques. Advanced drug delivery reviews. 2012;64(5):396–421.

37. Hancock BC, Shamblin SL, Zografi G. Molecular mobility of amorphous pharmaceutical solids below their glass transition temperatures. Pharmaceutical research. 1995;12(6):799–806.

38. Haser A, Cao T, Lubach J, Listro T, Acquarulo L, Zhang F. Melt extrusion vs. spray drying: The effect of processing methods on crystalline content of naproxen-povidone formulations. European Journal of Pharmaceutical Sciences. 2017;102:115–25.

39. Mistry P, Amponsah-Efah KK, Suryanarayanan R. Rapid assessment of the physical stability of amorphous solid dispersions. Crystal Growth & Design. 2017;17(5):2478–85.

40. Mishra SM, Rohera BD. An integrated, quality by design (QbD) approach for design, development and optimization of orally disintegrating tablet formulation of carbamazepine. Pharmaceutical development and technology. 2017;22(7):889–903.

41. Clas S-D, Cotton M, Moran E, Spagnoli S, Zografi G, Vadas EB. Assessment of the physical stability of lyophilized MK-0591 by differential scanning calorimetry. Thermochimica acta. 1996;288(1–2):83–96.

42. Marsac PJ, Shamblin SL, Taylor LS. Theoretical and practical approaches for prediction of drug–polymer miscibility and solubility. Pharmaceutical research. 2006;23(10):2417.

43. Wu T, Yu L. Surface crystallization of indomethacin below T g. Pharmaceutical research. 2006;23(10):2350–5.

44. Avrami M. Kinetics of phase change. I General theory. The Journal of chemical physics. 1939;7(12):1103–12.

45. Avrami M. Kinetics of phase change. II transformation-time relations for random distribution of nuclei. The Journal of chemical physics. 1940;8(2):212–24.

46. Prout EG, Tompkins FC. The thermal decomposition of potassium permanganate. Transactions of the Faraday Society. 1944;40:488–98.

47. Sheridan AK, Anwar J. Kinetics of the solid-state phase transformation of form β to γ of sulfanilamide using time-resolved energy-dispersive X-ray diffraction. Chemistry of materials. 1996;8(5):1042–51.

48. Supaphol P, Spruiell JE. Isothermal melt-and cold-crystallization kinetics and subsequent melting behavior in syndiotactic polypropylene: a differential scanning calorimetry study. Polymer. 2001;42(2):699–712.

49. Wellen RMR, Rabello MS. The kinetics of isothermal cold crystallization and tensile properties of poly (ethylene terephthalate). Journal of materials science. 2005;40(23):6099–104.

50. Yang J, Grey K, Doney J. An improved kinetics approach to describe the physical stability of amorphous solid dispersions. International journal of pharmaceutics. 2010;384(1–2):24–31.

51. Wyttenbach N, Janas C, Siam M, Lauer ME, Jacob L, Scheubel E, et al. Miniaturized screening of polymers for amorphous drug stabilization (SPADS): rapid assessment of solid dispersion systems. European Journal of Pharmaceutics and Biopharmaceutics. 2013;84(3):583–98.

52. Sotthivirat S, McKelvey C, Moser J, Rege B, Xu W, Zhang D. Development of amorphous solid dispersion formulations of a poorly water-soluble drug, MK-0364. International journal of pharmaceutics. 2013;452(1–2):73–81.

53. Shanbhag A, Rabel S, Nauka E, Casadevall G, Shivanand P, Eichenbaum G, et al. Method for screening of solid dispersion formulations of low-solubility compounds—miniaturization and automation of solvent casting and dissolution testing. International journal of pharmaceutics. 2008;351(1–2):209–18.

54. Auch C, Harms M, Mäder K. Melt-based screening method with improved predictability regarding polymer selection for amorphous solid dispersions. European Journal of Pharmaceutical Sciences. 2018;124:339–48.

55. SeethaLekshmi S, Guru Row TN. Conformational polymorphism in a non-steroidal anti-inflammatory drug, mefenamic acid. Crystal growth & design. 2012;12(8):4283–9.

56. Mamidi HK. Establishment of Design Space for Direct Compression of PEG (400) Loaded Neusilin® US2 by Modified SeDeM Expert System [PhD Thesis]. St. John's University; 2017.

57. Mamidi HK, Mishra SM, Rohera BD. Determination of maximum flowable liquid-loading potential of Neusilin® US2 and investigation of compressibility and compactibility of its liquisolid blends with PEG (400). Journal of Drug Delivery Science and Technology. 2019 Dec 1;54:101285.

58. Mamidi HK, Mishra SM, Rohera BD. Application of modified SeDeM expert diagram system for selection of direct compression excipient for liquisolid formulation of Neusilin® US2. Journal of Drug Delivery Science and Technology. 2021 Aug 1;64:102506.

59. Mamidi HK, Mishra SM, Rohera BD. Application of SeDeM diagram to improve the mechanical properties of powdered solutions. In CRS; 2017 [cited 2021 Sep 18]. Available from: https://crs.confex.com/crs/2017/meetingapp.cgi/Paper/3181

60. Fedors RF. A method for estimating both the solubility parameters and molar volumes of liquids. Polymer Engineering & Science. 1974;14(2):147–54.

61. Hoftyzer PJ, Van Krevelen DW. Properties of polymers: correlations with chemical structure. Elsevier Amsterdam; 1972.

62. Bagley EB, Nelson TP, Scigliano JM. Three-dimensional solubility parameters and their relationship to internal pressure measurements in polar and hydrogen bonding solvents. Journal of paint technology. 1971;43(555):35–42.

63. Nukala PK, Palekar S, Patki M, Fu Y, Patel K. Multi-dose oral abuse deterrent formulation of loperamide using hot melt extrusion. International journal of pharmaceutics. 2019;569:118629.

64. Aslan N, Cebeci Y. Application of Box–Behnken design and response surface methodology for modeling of some Turkish coals. Fuel. 2007;86(1–2):90–7.

65. Nukala PK, Palekar S, Patki M, Patel K. Abuse Deterrent Immediate Release Egg-Shaped Tablet (Egglets)Using 3D Printing Technology: Quality by Design to Optimize Drug Release andExtraction. AAPS PharmSciTech. 2019 Feb;20(2):80.

66. Shadambikar G, Kipping T, Di-Gallo N, Elia A-G, Knüttel A-N, Treffer D, et al. Vacuum Compression Molding as a Screening Tool to Investigate Carrier Suitability for Hot-Melt Extrusion Formulations. Pharmaceutics. 2020 Nov;12(11):1019.

67. Zhou W, Gilpin RK. Rapid ESI–MS method for examining the thermal decomposition of pharmaceuticals. Journal of pharmaceutical sciences. 2004;93(6):1545–56.

68. Greenhalgh DJ, Williams AC, Timmins P, York P. Solubility parameters as predictors of miscibility in solid dispersions. Journal of pharmaceutical sciences. 1999;88(11):1182–90.

69. Djuris J, Nikolakakis I, Ibric S, Djuric Z, Kachrimanis K. Preparation of carbamazepine–Soluplus® solid dispersions by hot-melt extrusion, and prediction of drug–polymer miscibility by thermodynamic model fitting. European Journal of Pharmaceutics and Biopharmaceutics. 2013;84(1):228–37.

70. Sun YE, Tao J, Zhang GG, Yu L. Solubilities of crystalline drugs in polymers: an improved analytical method and comparison of solubilities of indomethacin and nifedipine in PVP, PVP/VA, and PVAc. Journal of pharmaceutical sciences. 2010;99(9):4023–31.

71. Frank TC, Gupta SK. Quickly screen solvents for organic solids. Chemical Engineering Progress. 1999;95(12):41–61.

72. Arnauts J, Berghmans H. Amorphous thermoreversible gebs of atadic polystyrene. Polymer communications (Guildford). 1987;28(3):66-8 [Internet]. [cited 2020 Aug 6]. Available from: https://scholar.google.com/scholar_lookup?title=Amorphous%20thermoreversible%20gels%20of%20atactic%20polystyrene&publication_year=1987&author=J.%20Arnauts&author=H.%20Berghmans

73. Alshehri SM, Park J-B, Alsulays BB, Tiwari RV, Almutairy B, Alshetaili AS, et al. Mefenamic acid taste-masked oral disintegrating tablets with enhanced solubility via molecular interaction produced by hot melt extrusion technology. Journal of Drug Delivery Science and Technology. 2015 Jun 1;27:18–27.

74. Kojima T, Higashi K, Suzuki T, Tomono K, Moribe K, Yamamoto K. Stabilization of a supersaturated solution of mefenamic acid from a solid dispersion with EUDRAGIT® EPO. Pharmaceutical research. 2012;29(10):2777–91.

75. Mamidi HK, Rohera BD. Application of Thermodynamic Phase Diagrams and Gibbs Free Energy of Mixing for Screening of Polymers for Their Use in Amorphous Solid Dispersion Formulation of a Non-Glass-Forming Drug. Journal of Pharmaceutical Sciences. 2021 Jul 1;110(7):2703–17.

76. Moseson DE, Taylor LS. The application of temperature-composition phase diagrams for hot melt extrusion processing of amorphous solid dispersions to prevent residual crystallinity. International journal of pharmaceutics. 2018;553(1–2):454–66.

77. Otsuka M, Nishizawa J-I, Shibata J, Ito M. Quantitative Evaluation of Mefenamic Acid Polymorphs by Terahertz-Chemometrics. Journal of Pharmaceutical Sciences. 2010 Sep 1;99(9):4048–53.

78. Nukala PK, Palekar S, Solanki N, Fu Y, Patki M, Shohatee AA, et al. Investigating the application of FDM 3D printing pattern in preparation of patient-tailored dosage forms. Journal of 3D Printing in Medicine. 2019 Feb 1;3(1):23–37.

79. Mamidi HK, Rohera BD. Material-sparing Approach Using Differential Scanning Calorimeter and Response Surface Methodology for Process Optimization of Hot-Melt Extrusion. Journal of Pharmaceutical Sciences [Internet]. 2021 Aug 29 [cited 2021 Sep 18]; Available from: https://www.sciencedirect.com/science/article/pii/S0022354921004640

80. Mishra SM, Rohera BD. Mechanics of tablet formation: a comparative evaluation of percolation theory with classical concepts. Pharmaceutical Development and Technology. 2019 Sep 14;24(8):954–66.

Vita

Name	*Hemanth k. Mamidi*
Masters Degree	*Master of Science*, *St. John's University, New York* *Major:Industrial Pharmacy*
Date Graduated	*June, 2017*
Other Degrees and Certificates	*Bachelor of Pharmacy, Jawaharlal Nehru Technological University, Hyderabad,* *Major: Pharmacy*
Date Graduated	*April, 2011*